COMBUSTION SYNTHESIS OF ADVANCED MATERIALS: PRINCIPLES AND APPLICATIONS

Arvind Varma, Alexander S. Rogachev[1], Alexander S. Mukasyan, and Stephen Hwang

Department of Chemical Engineering
University of Notre Dame
Notre Dame, Indiana 46556

[1] Permanent address: Institute of Structural Macrokinetics, Russian Academy of Sciences, Chernogolovka, 142 432 Russia.

ADVANCES IN CHEMICAL ENGINEERING, VOL. 24

Copyright © 1998 by Academic Press
All rights of reproduction in any form reserved.

0065-2377/98 $25.00

Combustion synthesis is an attractive technique to synthesize a wide variety of advanced materials including powders and near-net shape products of ceramics, intermetallics, composites, and functionally graded materials. This method was discovered in the former Soviet Union by Merzhanov et al. *(1971). The development of this technique by Merzhanov and coworkers led to the appearance of a new scientific direction that incorporates both aspects of combustion and materials science. At about the same time, some work concerning the combustion aspects of this method was also done in the United States (Booth, 1953; Walton and Poulos, 1959; Hardt and Phung, 1973). However, the full potential of combustion synthesis in the production of advanced materials was not utilized. The scientific and technological activity in the field picked up in the United States during the 1980s. The significant results of combustion synthesis have been described in a number of review articles (e.g., Munir and Anselmi-Tamburini, 1989; Merzhanov, 1990a; Holt and Dunmead, 1991; Rice, 1991; Varma and Lebrat, 1992; Merzhanov, 1993b; Moore and Feng, 1995). At the present time, scientists and engineers in many other countries are also involved in research and further development of combustion synthesis, and interesting theoretical, experimental, and technological results have been reported from various parts of the world (see SHS Bibliography, 1996).*

This review article summarizes the state of the art in combustion synthesis, from both the scientific and technological points of view. In this context, we discuss wide-ranging topics including theory, phenomenology, and mechanisms of product structure formation, as well as types and properties of product synthesized, and methods for large-scale materials production by combustion synthesis technique.

I. Introduction

Combustion synthesis (CS) can occur by two modes: *self-propagating high-temperature synthesis* (SHS) and *volume combustion synthesis* (VCS). A schematic diagram of these modes is shown in Fig. 1. In both cases, reactants may be pressed into a pellet, typically cylindrical in shape. The samples are then heated by an external source (e.g., tungsten coil, laser) either locally (SHS) or uniformly (VCS) to initiate an exothermic reaction.

The characteristic feature of the SHS mode is, after initiation locally, the self-sustained propagation of a reaction wave through the heterogeneous mixture of reactants. The temperature of the wavefront can reach quite high values (2000–4000 K). In principle, if the physicochemical parameters of the medium, along with the instantaneous spatial distributions of temperature and concentration are known, we can calculate the combustion velocity and reaction rate throughout the mixture. Thus, the SHS mode of reaction can be considered to be a well-organized wavelike propagation of the exothermic chemical reaction through a heterogeneous medium, followed by the synthesis of desired condensed products.

During volume combustion synthesis, the entire sample is heated uniformly in a controlled manner until the reaction occurs essentially simultaneously through-

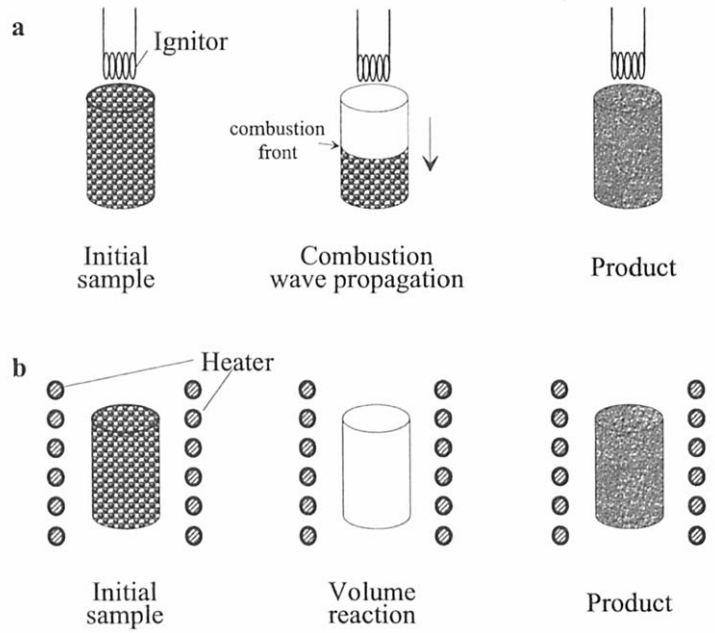

FIG. 1. The modes of combustion synthesis : (a) SHS; (b) VCS.

out the volume. This mode of synthesis is more appropriate for weakly exothermic reactions that require preheating prior to ignition, and is sometimes referred to as the *thermal explosion* mode. However, the term *explosion* used in this context refers to the rapid rise in temperature after the reaction has been initiated, and not the destructive process usually associated with detonation or shock waves. For this reason, volume combustion synthesis is perhaps a more appropriate name for this mode of synthesis.

From the viewpoint of chemical nature, three main types of CS processes can be distinguished. The first, *gasless combustion synthesis from elements,* is described by the equation

$$\sum_{i=1}^{n} X_i^{(s)} = \sum_{j=1}^{m} P_j^{(s,l)} + Q, \tag{1}$$

where $X_i^{(s)}$ are elemental reactant powders (metals or nonmetals), $P_j^{(s,l)}$ are products, Q is the heat of reaction, and the superscripts (s) and (l) indicate solid and liquid states, respectively. Perhaps the most popular example of this type of reaction is carbidization of titanium:

$$\mathrm{Ti} + \mathrm{C} = \mathrm{TiC} + 230\ \mathrm{kJ/mol}.$$

The second type, called *gas–solid combustion synthesis,* involves at least one gaseous reagent in the main combustion reaction:

$$\sum_{i=1}^{n-p} X_i^{(s)} + \sum_{i=1}^{p} Y_i^{(g)} = \sum_{j=1}^{m} P_j^{(s,l)} + Q, \tag{2}$$

where $Y_i^{(g)}$ represents the gaseous reactants (e.g., N_2, O_2, H_2, CO), which, in some cases, penetrate the sample by infiltration through its pores. This type of CS is also called *infiltration* (or *filtration*) *combustion synthesis.* Nitridation of titanium and silicon are common examples:

$$\mathrm{Ti}^{(s)} + 0.5\mathrm{N_2}^{(g)} = \mathrm{TiN}^{(s)} + 335\ \mathrm{kJ/mol},$$

$$3\mathrm{Si}^{(s)} + 2\mathrm{N_2}^{(g)} = \mathrm{Si_3N_4}^{(s)} + 750\ \mathrm{kJ/mol}.$$

The third main type of CS is *reduction combustion synthesis,* described by the formula

$$\sum_{i=1}^{n-q-r} (MO_x)_i^{(s)} + \sum_{i=1}^{r} Z_i^{(s)} + \sum_{i=1}^{q} X_i^{(s)} = \sum_{j=1}^{m-k} P_j^{(s,l)} + \sum_{j=1}^{k} (ZO_y)_j^{(s,l)} + Q, \tag{3}$$

where $(MO_x)_i^{(s)}$ is an oxide that reacts with a reducing metal $Z_i^{(s)}$ (e.g., Al, Mg, Zr, Ti), resulting in the appearance of another, more stable oxide $(ZO_y)_j^{(s,l)}$, and reduced metal $M_i^{(s,l)}$. This reaction may be followed by the interaction of $M_i^{(s,l)}$ with other elemental reactants $X_i^{(s)}$ to produce desired products $P_j^{(s,l)}$. Thus, in general,

the reduction combustion synthesis can be considered to be a two-step process, where the first step is a *thermite* reaction:

$$\sum_{i=1}^{n-q-r} (MO_x)_i^{(s)} + \sum_{i=1}^{r} Z_i^{(s)} = \sum_{j=1}^{k} (ZO_y)_j^{(s,l)} + \sum_{j=1}^{l} M_j^{(s,l)} + Q_1, \qquad (4a)$$

while the second step is the synthesis from elements similar to scheme (1):

$$\sum_{j=1}^{l} M_i^{(s,l)} + \sum_{i=1}^{q} X_i^{(s)} = \sum_{j=1}^{m-1} P_j^{(s,l)} + Q_2, \qquad (4b)$$

with the total heat release, $Q = Q_1 + Q_2$. An example of this type of CS is

$$B_2O_3{}^{(s)} + 2Al^{(s)} + Ti^{(s)} = Al_2O_3{}^{(l)} + TiB_2{}^{(s,l)} + 700 \text{ kJ/mol},$$

where TiB_2 is the desired product and Al_2O_3 can be removed (e.g., by centrifugal separation) and used separately or a ceramic composite material ($Al_2O_3 + TiB_2$) can be produced. In some cases, the reducing reactant (Z_i) is the same as that used for the synthesis (X_i), for example,

$$2B_2O_3{}^{(s)} + 5Ti^{(s)} = 3TiO_2{}^{(s)} + 2TiB_2{}^{(s)} + 140 \text{ kJ/mol}.$$

Historically, combustion synthesis (both SHS and VCS) is a direct descendant of classic works on combustion and thermal explosion (e.g., Mallard and Le Chatelier, 1883; Semenov, 1929; Zeldovich and Frank-Kamenetskii, 1938; Williams, 1965; Glassman, 1977); see Hlavacek (1991) and Merzhanov (1995) for additional comments in this regard. We discuss later in Section IV how the theory of SHS grew directly from these works. The progress in combustion science made it possible to organize self-sustained exothermic reactions in powder mixtures that were controllable and predictable, hence avoiding the uncontrollable evolution of the reaction that is commonly associated with the terms *combustion, fire,* and *explosion.*

The number of products synthesized by CS increased rapidly during the 1970s and 1980s, and currently exceeds 400 different compounds (see Section III). Specifically, these materials include carbides (TiC, ZrC, SiC, B_4C, etc.), borides (TiB_2, ZrB_2, MoB_2, etc.), silicides (Ti_5Si_3, $TiSi_2$, $MoSi_2$, etc.), nitrides (TiN, ZrN, Si_3N_4, BN, AlN), and intermetallics (NiAl, Ni_3Al, TiNi, TiAl, CoAl, etc.). The methods used for production are described in Section II and the major products are presented in Section III. The theory of CS is discussed in Section IV, where we emphasize the physical basis of the theoretical approaches. The simplifying assumptions in the existing theories are also discussed in order to illustrate their limitations. The effects of different experimental conditions, including the role of gravity, for controlling the synthesis process to obtain desired products are presented in Section V. The unique aspects of CS, such as extremely high temperatures, fast heating rates, and short reaction times, cause certain problems for

control of product microstructure. Thus it is necessary to develop ways of tailoring the microstructure of the product, based on the study of synthesis mechanisms and structure-forming processes in the combustion wave. This aspect of the problem is considered in Section VI, where two important features of the synthesis, product structure formation and combustion wave microstructure, are discussed.

Throughout this work, more emphasis is placed on the SHS mode of synthesis rather than the VCS mode because more information is available for SHS. Also, note that in this review, we do not consider production of powders by gas-phase combustion synthesis processes (e.g., Calcote *et al.,* 1990; Davis *et al.,* 1991).

II. Methods for Laboratory and Large-Scale Synthesis

In this section, we discuss the laboratory techniques and production technologies used for the combustion synthesis process. The laboratory studies reveal details of the CS process itself, while the technologies may also include other processing, such as densification of the product by external forces. In both cases, it is necessary to control the green mixture characteristics as well as the reaction conditions. For the production technologies, however, optimization of parameters related to external postcombustion treatment is also necessary in order to produce materials with desired properties.

The main characteristics of the green mixture used to control the CS process include mean reactant particle sizes, d_i; morphologies and size distribution of the reactant particles; reactant stoichiometry, ν_i; initial density, ρ_0; size of the sample, D; initial temperature, T_0; dilution, b, that is, fraction of the inert diluent in the initial mixture; and reactant or inert gas pressure, p. In general, the combustion front propagation velocity, U, and the temperature–time profile of the synthesis process, $T(t)$, depend on all of these parameters. The most commonly used characteristic of the temperature history is the maximum combustion temperature, T_c. In the case of negligible heat losses and complete conversion of reactants, this temperature equals the thermodynamically determined adiabatic temperature T_c^{ad} (see also Section V,A). However, heat losses can be significant and the reaction may be incomplete. In these cases, the maximum combustion temperature also depends on the experimental parameters noted earlier.

A. Laboratory Techniques

Laboratory studies in combustion synthesis are generally designed to determine the dependencies of U, $T(t)$, and T_c on the process parameters. A schematic diagram of the apparatus commonly used is shown Fig. 2 (cf. Lebrat *et al.,* 1992, for de-

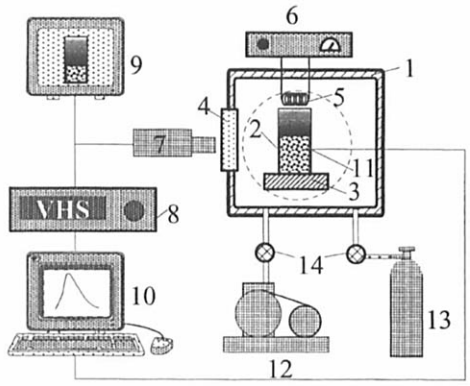

FIG. 2. Laboratory setup for combustion synthesis. 1–reaction chamber; 2–sample; 3–base; 4–quartz window; 5–tungsten coil; 6–power supply; 7–video camera; 8–video cassette recorder; 9–video monitor; 10–computer with data acquisition board; 11–thermocouple; 12–vacuum pump; 13–inert or reactant gas; 14–valve.

tails). The operating pressure in the reaction chamber varies from 150 atm to a vacuum of 10^{-2} torr. The reactant powders are dried, mixed in the appropriate amounts, and pressed to the desired green (i.e., initial) density. The sample is ignited typically by an electrically heated tungsten coil, and once initiated, the combustion wave self-propagates through the sample. The temperature is measured by a pyrometer or by thermocouples imbedded in the sample, while a video or movie camera is used to monitor the propagation of the combustion wave. The main features of the laboratory apparatus have remained essentially unchanged during the last 20 years, with the exception of significant improvements in data acquisition, control, and analysis by the use of computers and imaging by video techniques.

Owing to the large number of experimental parameters, it is not easy to determine the functional dependencies of U, $T(t)$ and T_c. Thus, a full description of these relationships has not been obtained for any system produced by combustion synthesis. Generally, experimental investigations have identified the combustion velocity, U, and temperature, T_c, dependencies on a single parameter (e.g., density, reactant particle size, dilution), while maintaining other parameters fixed. Merzhanov (1983) and later Rice (1991) generalized a large number of experimental results in order to extract some trends of combustion velocity and temperature variations on different experimental parameters.

Based on their analyses, and incorporation of additional details, we have outlined some general relationships for gasless combustion synthesis of materials from elements (type 1), as shown schematically in Fig. 3. Both characteristic features of the process, the combustion wave propagation velocity and maximum temperature, have maximum values when the composition of the green mixture corresponds to the most exothermic reaction for a given system (Fig. 3a). In gen-

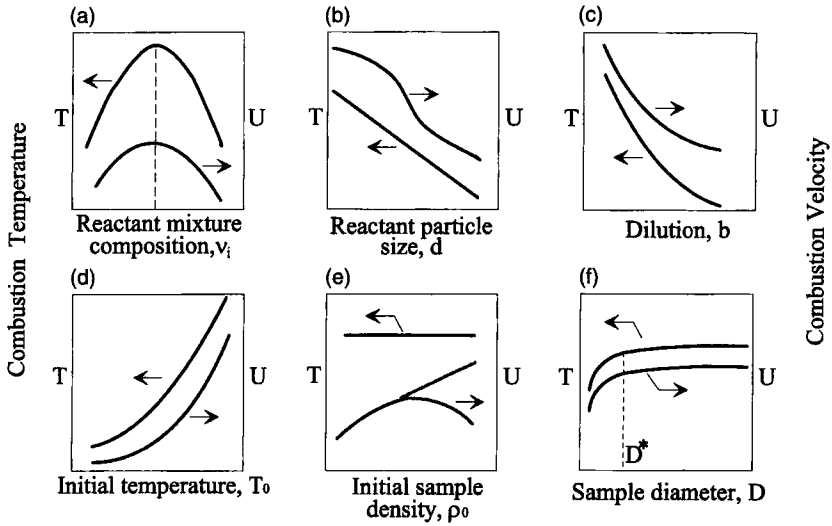

FIG. 3. Dependencies of combustion velocity, U, and maximum combustion temperature T_c on various CS parameters.

eral, U and T_c decrease with increasing initial reactant particle size, and with addition of an inert (nonreactive) diluent to the green mixture (Figs. 3b and c), while increasing significantly with increasing initial sample temperature (Fig. 3d). Different trends have been observed when the initial sample density is varied. With increasing ρ_0, the combustion front velocity either increases monotonically or goes through a maximum, while the combustion temperature generally remains constant (Fig. 3e). A decrease in the sample size (e.g., sample diameter, D) does not influence U and T_c when the size is larger than a critical value D^*, since heat losses are negligible compared to heat release from the chemical reaction. Below the critical sample size, both the combustion velocity and temperature decrease due to significant heat losses (Fig. 3f). Note that many exceptions to the dependencies discussed have been observed, even for the simplest case of gasless combustion synthesis from elements. The combustion wave behavior becomes more complicated in gas–solid and reduction type reactions. All of these effects are discussed in greater detail in Section V.

Within the region of optimal experimental parameters, the combustion wave velocity remains constant and the temperature profile $T(t)$ has the same form at each point of the reaction medium. This regime is called *steady propagation* of the combustion synthesis wave, or *steady SHS process.* As the reaction conditions move away from the optimum, where the heat evolution decreases and/or heat losses increase, different types of *unsteady propagation* regimes have been observed. These include the appearance of an *oscillating combustion synthesis*

regime, where macroscopic oscillations of the combustion velocity and temperature occur. The reaction may also propagate in the form of a hot-spot, which, for example, may move along a spiral pattern in cylindrical samples, and is called the *spin combustion* regime of CS. The combustion regime has great importance in the production of materials, because it influences the product microstructure and properties.

B. Production Technologies

In general, methods for the large-scale production of advanced materials by combustion synthesis consist of three main steps: (1) preparation of the green mixture, (2) high-temperature synthesis, and (3) postsynthesis treatment. A schematic diagram of these steps is presented in Fig. 4. The first step is similar to

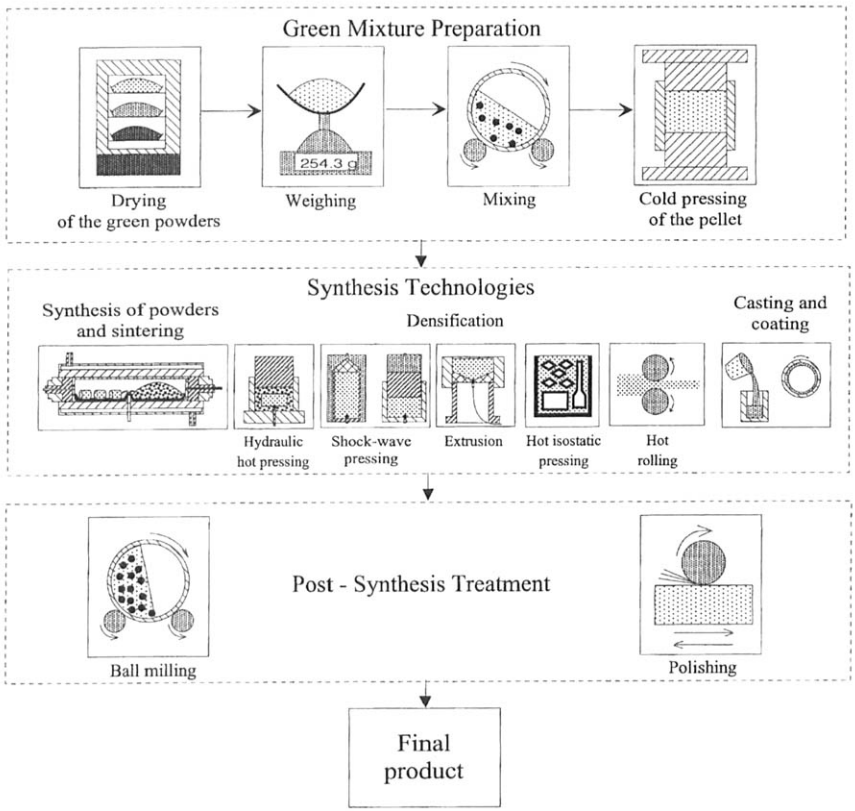

FIG. 4. Generalized schematic diagram of CS technologies.

the procedures commonly used in powder metallurgy, where the reactant powders are dried (e.g., under vacuum at 80–100°C), weighed into the appropriate amounts, and mixed (e.g., by ball mixing). For some applications, cold pressing of the green mixture is necessary, especially for the production of low porosity or poreless materials. Typically, no plasticizer is used, and the porosity of the cold-pressed compacts varies from 40 to 80% of the theoretical density for metal–nonmetal mixtures, and up to 90% for metal–metal mixtures. The final procedure in sample preparation determines the type of product to be synthesized: a powder product results from uncompacted powder reactants, while sintered products are yielded from cold-pressed compacts. Pressing the green mixture into special molds or machining pressed initial compacts yields complex-shaped articles.

The main production technologies of combustion synthesis are presented in the second block of Fig. 4. Following Merzhanov (1990a), they may be classified into several major types: powder production and sintering, densification, and casting and coating.

The volume combustion synthesis mode is used primarily for the synthesis of weakly exothermic systems. Various types of heaters, mostly commercially available furnaces, in addition to spiral coil and foil heaters, are used to preheat the sample up to the ignition point. To date, VCS synthesized materials have been produced only in laboratories, and no industrial or pilot production by this mode of synthesis has been reported.

The third main step of combustion synthesis technologies is postsynthesis treatment. This step is optional, since not all products require additional processing after synthesis. Powder milling and sieving are used to yield powders with a desired particle size distribution. Annealing at elevated temperatures (800–1200°C) removes residual thermal stress in brittle products. The synthesized materials and articles may also be machined into specified shapes and surface finishes.

1. Powder Production and Sintering

The design of a typical commercial reactor for large-scale production of materials is similar to the laboratory setup, except that the capacity of the former is larger, up to 30 liters. Since the synthesis of materials produced commercially is well understood, most reactors are not equipped with optical windows to monitor the process. A schematic diagram of such a reactor is shown in Fig. 5. Typically, it is a thick-walled stainless steel cylinder that can be water cooled (Borovinskaya *et al.,* 1991). The green mixture or pressed compacts are loaded inside the vessel, which is then sealed and evacuated by a vacuum pump. After this, the reactor is filled with inert or reactive gas (Ar, He, N_2, O_2, CO, CO_2). Alternatively, a constant flow of gas can also be supplied at a rate such that it permeates the porous reactant mixture. The inner surface of the reactor is lined with an inert material to

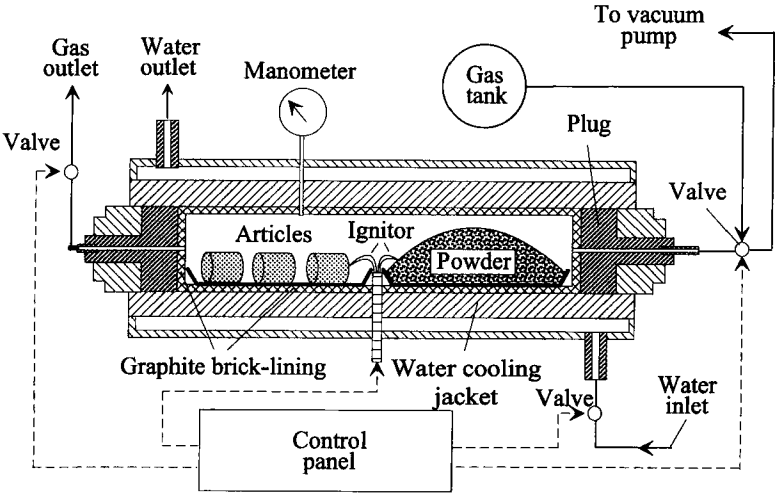

FIG. 5. Schematic diagram of an SHS reactor.

protect the vessel from the extreme reaction temperatures. Graphite is typically used for lining during carbide, boride, or silicide synthesis, while boron nitride and silicon nitride provide protection during nitride synthesis.

Two different types of reactors are used depending on the product synthesized. The first type can maintain pressures up to 150 atm, and is widely used for production of powders in gasless and gas–solid systems. Carbides, borides, silicides, intermetallics, chalcogenides, phosphides, and nitrides are usually produced in this type of reactor. The second type, a high-pressure reactor (up to 2000 atm), is used for the production of nitride-based articles and materials, since higher initial sample densities require elevated reactant gas pressures for full conversion. For example, well-sintered pure BN ceramic with a porosity of about 20–35% was synthesized at 100 to 5000-atm nitrogen pressure (Merzhanov, 1992). Additional examples are discussed in Section III.

2. *SHS with Densification*

The application of an external force during or after combustion is generally required to produce a fully dense (i.e., poreless) material. A variety of techniques for applying the external force, such as static, dynamic, and shock-wave loading have been investigated.

The oldest method uses relatively slow (static) loading provided by a hydraulic press along with a specially designed die (Borovinskaya *et al.*, 1975b; Miyamoto *et al.*, 1984; Adachi *et al.*, 1989; Zavitsanos *et al.*, 1990; Dunmead *et al.*, 1990a). Owing to the high temperature of the combustion products being densified, several approaches have been used to isolate the reacting sample from the die. One

possible solution is the use of steel dies lined with graphite or BN ceramics (Nishida and Urabe, 1992). Another possibility is to use a pressure-transmitting medium such as SiO_2 (sand) or Al_2O_3, as shown in Fig. 6a (Merzhanov *et al.*, 1981).

In this technique, pressure is applied immediately after the combustion process, or after a short time delay (typically a few seconds). The duration of this time delay is extremely important for achieving maximum density. The period of time before application of pressure should be long enough to allow the expulsion of gases from the sample, but shorter than the cooling time. An example of this critical time is given in Fig. 7a, which shows the dependence of residual porosity on the pressing delay time for TiC-Cr_2C_3-Ni cemented carbide synthesis. The effect of applied pressure on residual porosity is clearly important, and is illustrated for TiC-(Ni,Al) material in Fig. 7b. Essentially poreless (porosity less

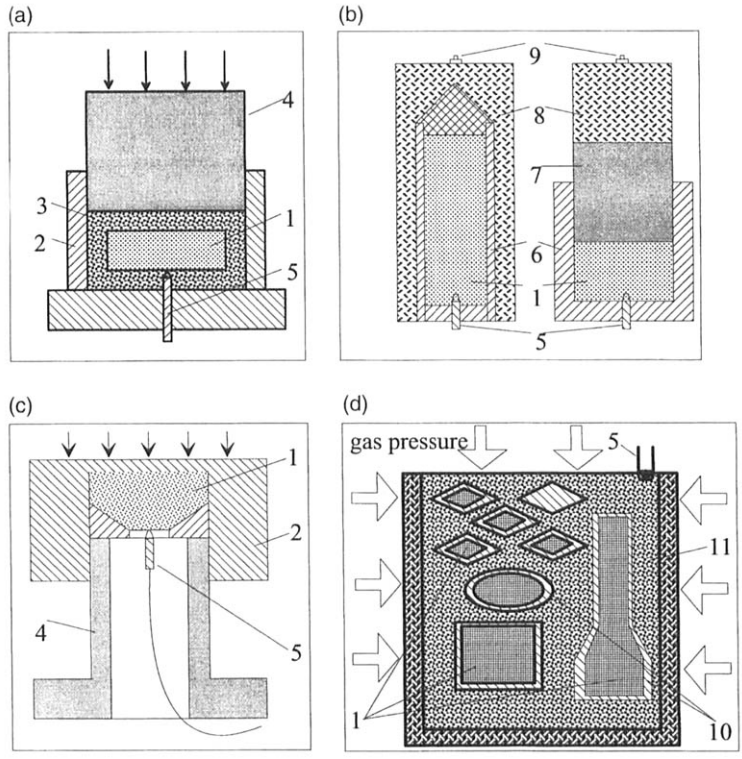

FIG. 6. Schemes for SHS densification. 1–sample; 2–press die; 3–pressure-transmitting medium; 4–pressing body; 5–ignitor; 6–metal container; 7–massive piston; 8–explosive; 9–electric fuse; 10–glass containers; 11–"chemical furnace" mixture.

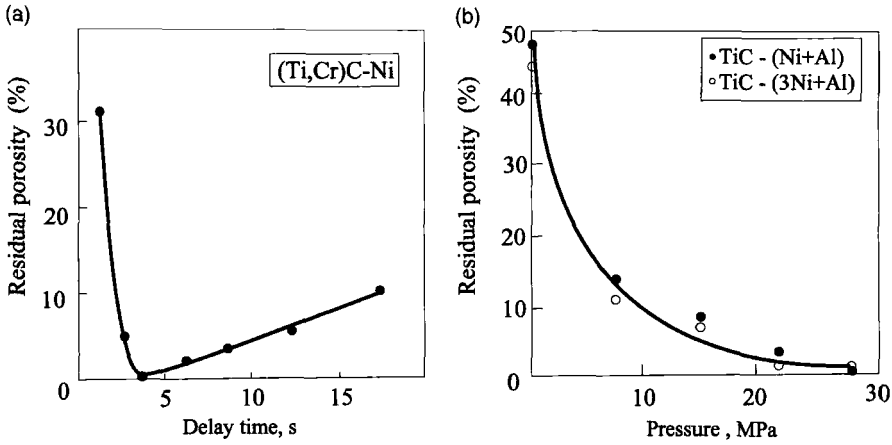

FIG. 7. Residual porosity for different samples as a function of (a) pressing delay time (Merzhanov, 1990a), (b) applied pressure (Adapted from Dunmead *et al.*, 1990a).

than 1%) and large-scale (up to 1 m in diameter) ceramic and metal–ceramic composite materials can be produced by SHS using the static pressing method (Kvanin *et al.*, 1993).

Another method of SHS densification involves high-speed loading by an explosion shock wave or by a fast-moving solid body. Two possible schemes for high-speed loading by shock waves are presented in Fig. 6b; the first method provides axial and the other radial densification. The dynamic axial densification method has been used to synthesize dense materials including TiC, TiB_2, and HfC (Kecskes *et al.*, 1990; Grebe *et al.*, 1992; Rabin *et al.*, 1992a; Adadurov *et al.*, 1992). The radial shock-wave densification technique was applied to produce several materials, including dense high-temperature ceramic superconductor $YBa_2Cu_3O_{7-x}$ (Gordopolov and Merzhanov, 1991; Fedorov *et al.*, 1992).

The pressing body can also be accelerated by gas pressure and mechanical or electromagnetic forces. High gas pressures driving a mechanical piston have been applied in a number of SHS systems (Hoke *et al.*, 1992; LaSalvia *et al.*, 1994). In this case, the sample under combustion is impacted by a massive piston moving at a speed of ~10 m/s. Based on the magnitude of this speed, this method of compaction is between static pressing (~0.1 m/s) and shock-wave pressing (~1000 m/s). Materials produced by this method include ceramics (TiC, TiB_2), ceramic composites ($TiB_2+Al_2O_3$, TiB_2+BN, TiB_2+SiC), ceramic–metal composites (TiC+Ni, TiB_2+Ni), and intermetallics (TiNi, Ti_3Al). Electromagnetic forced pressing was designed for the pulse densification of cermets with a uniform or gradient distribution of the binder metal (Matsuzaki *et al.*, 1990).

In the techniques just described, combustion synthesis was first initiated, and then dynamic loading was applied, to the hot product immediately after the combustion front propagated through the sample. Alternatively, shock compression applied to the reaction mixture may result in a rapid increase in temperature, initiating the chemical reaction with supersonic propagation rates. This approach, called *shock-induced synthesis,* has recently been developed (Work *et al.,* 1990; Vecchio *et al.,* 1994; Meyers *et al.,* 1994). A variety of dense silicides (e.g., $MoSi_2$, $NbSi_2$, Ti_5Si_3, $TiSi_2$) and aluminides (NiAl, $NiAl_3$) have been synthesized using this method. Although the boundary between combustion and shock-induced synthesis is not well defined, the difference between them is addressed in a review article that describes different shock-induced methods to synthesize materials (Thadani, 1993).

Another method used for the production of fully dense materials by combustion synthesis is SHS with extrusion, shown schematically in Fig. 6c (Podlesov *et al.,* 1992a,b). In this case, a powder compact of the reaction mixture is placed in the mold, and the process is initiated locally by a heated tungsten wire. After the combustion wave has propagated through the sample, relatively low pressure ($<$1000 MPa) is applied to the plunger, extruding the products through the hole of the conic die. A high plasticity at the elevated reaction temperature allows the formation of long rods of refractory materials. The form and size of the die hole determine the extruded product configuration. The most developed application of SHS extrusion to date is the production of TiC-based cermet electrodes used for electric spark alloying (Podlesov *et al.,* 1992b).

A promising method for densification of combustion-synthesized products is a combination of SHS with hot isostatic pressing (HIP). This idea was first applied to the synthesis of TiB_2 ceramics under a pressure of 3 GPa, which was provided by a cubic anvil press, resulting in 95% dense material (Miyamoto *et al.,* 1984; Yamada *et al.,* 1987). The relatively low exothermic reaction of SiC from elemental powders was also carried out under these conditions (Yamada *et al.,* 1985), and 96% conversion to β-SiC was achieved as compared to 36% conversion when the reaction was initiated locally.

Another approach is to use high gas pressure for densification of the product *simultaneously* with combustion synthesis. The method of SHS+HIP with pressing by gas has been developed by using a so-called *chemical furnace.* A schematic drawing of this *gas pressure combustion sintering* method is shown in Fig. 6d (Miyamoto *et al.,* 1984; Koizumi and Miyamoto, 1990). The green mixture is placed in evacuated glass containers, which are surrounded by a highly combustible mixture (e.g., Ti+C) that is enveloped by high-pressure gas (e.g., Ar at 100 MPa). After ignition, the combustible mixture acts as a chemical furnace, which heats the samples in the containers up to their ignition point. The heat evolved from the chemical furnace also heats the glass to its softening temperature, where it becomes plastic and easily deformable. Thus the material synthesized inside the containers is then pressed isostatically by the surrounding high

gas pressure to zero porosity. A variety of ceramics, cermets, and functionally graded materials (FGMs) have been produced using this method, including TiC, TiB_2, TiB_2-Ni FGM (Miyamoto *et al.*, 1990a,b), $MoSi_2$-SiC/TiAl FGM (Matsuzaki *et al.*, 1990), and Cr_3C_2-Ni (Tanihata *et al.*, 1992).

Along with the various methods of combustion product densification, the hot rolling technique has been investigated (Rice *et al.*, 1986; Osipov *et al.*, 1992). It was shown that simultaneous synthesis and hot rolling of intermetallic and ceramic materials (e.g., TiAl, $TiC_{0.47}$, TiC_xN_{1-x}-Ni) under vacuum yields articles with porosity in the range of 5 to 50% (Osipov *et al.*, 1992). We expect that with further development of this technique, thin sheets and foils of combustion synthesized materials could be produced in the future.

3. SHS with Casting

During combustion synthesis, highly exothermic reactions (typically reduction-type) result in completely molten products, which may be processed using common metallurgical methods. Casting of CS products under inert gas pressure or centrifugal casting has been used to synthesize cermet ingots, corrosion- and wear-resistant coatings, and ceramic-lined pipes.

Casting under gas pressure is similar to conventional SHS production (see Section II,B,1). The reduction-type initial mixture (e.g., CrO_3+Al+C,WO_3+ Al+C) is placed in a casting die and the reaction initiated under an inert gas pressure (0.1–5 MPa) to prevent product sputtering by gas evolution from the thermite reaction (Merzhanov *et al.*, 1980; Yukhvid, 1992). Increased gas pressure was shown to decrease sputtering significantly, and subsequent product loss (see Fig. 8).

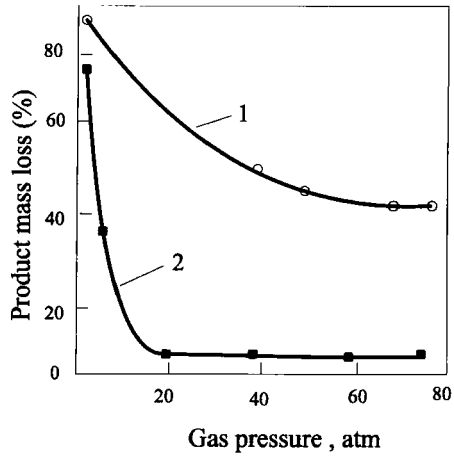

FIG. 8. The product mass loss as a function of Ar gas pressure. 1–CrO_3-Al-C; 2–WO_3-CoO-Al-C (Adapted from Yukhvid *et al.*, 1983).

In some cases, the molten product may consist of two immiscible phases, either molten oxides (e.g., Al_2O_3, MgO) with dispersed nonoxides (e.g., metals carbides or borides) or molten metals with dispersed ceramic droplets. Owing to the difference in densities, the two phases may separate. By controlling the characteristic times of cooling (t_{cool}) and phase separation (t_{ps}), different distributions of phases may result. Thus, it is possible to obtain cermets with uniform ($t_{cool} << t_{ps}$), gradient ($t_{cool} \sim t_{ps}$), and layered ($t_{cool} >> t_{ps}$) products.

Centrifugal casting allows for greater control of the distribution of phases, by controlling the time of separation. The two types of centrifugal casting equipment are shown in Fig. 9. For *radial centrifuges* (Fig. 9a), the sample is placed at a

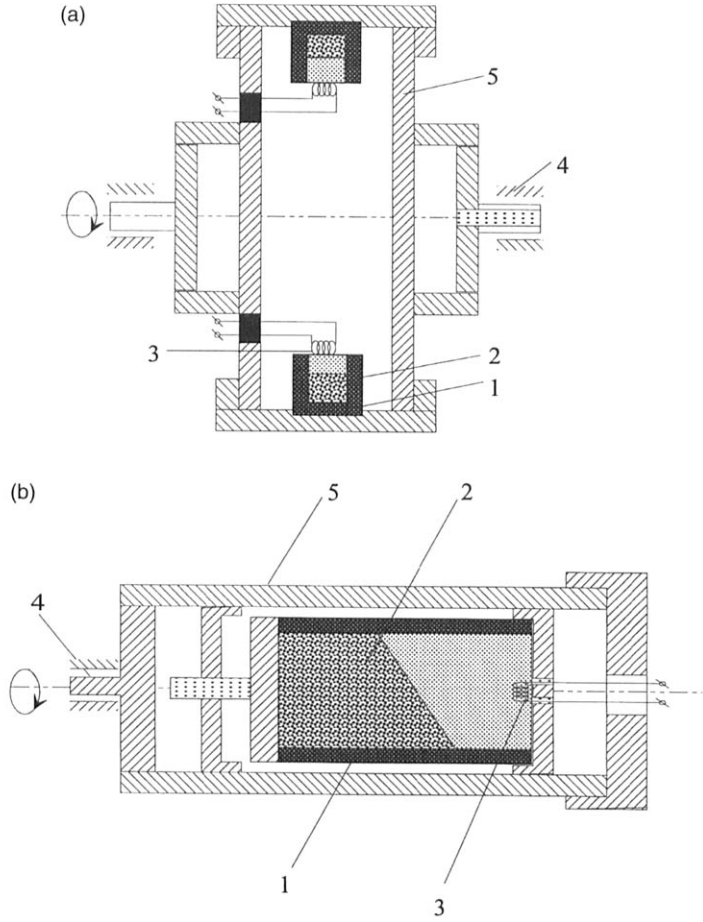

FIG. 9. Scheme of SHS+centrifugal casting: (a) radial centrifuge; (b) axial centrifuge. 1–sample container; 2–reactant mixture; 3–ignitor; 4–axle; 5–reactor. (Adapted from Merzhanov and Yukhvid, 1990)

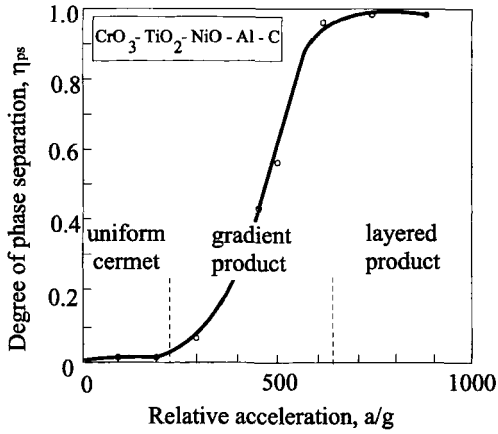

FIG. 10. The degree of phase separation as a function of centrifugal acceleration, a, where g is acceleration due to gravity (Adapted from Merzhanov and Yukhvid, 1990).

fixed radial position from the axis of rotation, and the applied centrifugal force is parallel to the direction of propagation. The influence of centrifugal acceleration on the degree of phase separation, η_{ps}, is shown in Fig. 10. This parameter characterizes the phase distribution in the final product:

$$\eta_{ps} = m_s/m_t,$$

where m_s is mass of the nonoxide phase (e.g., metal, carbide, boride) fully separated from the oxide matrix, and m_t is the total mass of this phase produced by the reaction. Thus, $\eta_{ps} = 0$ for the cermet product with uniformly distributed oxide and nonoxide phases, while $\eta_{ps} = 1$ for multilayer materials or when the metal-type ingot is totally separated from the oxide slag layer. Finally, the ingots have a gradient distribution of phases when $0 < \eta_{ps} < 1$ (see Fig. 10).

The second type of centrifugal casting apparatus, called an *axial centrifuge* (Fig. 9b) is used for production of ceramic, cermet, or ceramic-lined pipes. The axial centrifuge casting method was developed further for production of long pipes with multilayer ceramic inner coatings (Odawara and Ikeuchi, 1986; Odawara, 1992). In this process, a thermite-type SHS mixture (e.g., $Fe_2O_3/2Al$) is placed inside a rotating pipe, and ignited locally. A reduction-type combustion reaction propagates through the mixture, and the centrifugal force results in separate layers of metal and ceramic oxide, with the latter forming the innermost layer. The process is carried out in air under normal pressure, and pipes up to 5.5 m long have been obtained.

III. Classes and Properties of Synthesized Materials

The synthesis of several hundred materials, by both the SHS and VCS modes, has been reported in the literature. The types of compounds produced include carbides, borides, intermetallics, silicides, aluminides, composites, nitrides, hydrides, and oxides. The purpose of this section is to provide a description of the synthesized compounds, as well as the materials (i.e., powders, poreless materials, and functionally graded materials) and articles produced. The practical applications of experimental and technological methods are also described.

A. Gasless Combustion Synthesis from Elements

1. Carbides

a. Group IV Metal Carbides. Group IVa transition metal carbides (TiC, ZrC, HfC) were among the first compounds synthesized by the SHS method (Merzhanov and Borovinskaya, 1972). With high melting points, hardness, and chemical stability, these materials can be used as abrasives (economical substitutes for diamond powders and pastes) or as components of cermet and ceramic materials (Storms, 1967; Samsonov, 1964).

These compounds have relatively high heats of formation (e.g., -185 kJ/mol for TiC and -198 kJ/mol for ZrC). The heat evolved upon initiation of the reaction allows the materials to be synthesized in the SHS mode, with a high degree of conversion. For example, the amount of unreacted carbon has been reported to be as low as 0.09 wt % for TiC and 0.01 wt % for ZrC and HfC (Merzhanov and Borovinskaya, 1972). Emission spectrochemical analysis of the powders (Holt and Munir, 1986) confirmed the high purity of the combustion synthesized TiC, where the largest impurity constituents were Al (up to 2000 ppm), Ar (300 ppm), Si (100 ppm), Fe (100 ppm), B (80 ppm), and Ca (30 ppm). With the exception of Fe, impurities in the product were two to seven times *lower* than in the initial mixture. Owing to the high temperature of combustion, the material *self-purifies* by purging any volatile impurities from the reaction mixture.

In particular, the Ti-C system has been used commonly in numerous investigations to understand the influence of various process parameters (see Section V), as well as the mechanisms of combustion and product structure formation (see Section VI). In Table I, some properties of TiC powders are presented. While many of the problems associated with producing TiC powders with tailored phase composition and purity have been addressed, this system continues to be investigated further. Recent work confirms and augments earlier results exploring the synthesis of pure TiC during combustion (Chang *et al.*, 1991; Lee and Chung, 1992; Chang *et al.*, 1995).

TABLE I
SOME CHARACTERISTICS OF SHS POWDERS[a]

Powder	Chemical Composition (wt %)	Main Impurities (wt %)	Average Particle Size (μm) or Specific Surface Area (m^2/g)
TiC	C_{fixed} = 19.2–19.5	C_{free} < 0.8	3–5 μm
TiC	Ti = 77.0–79.5	C_{free} < 0.2–2.0	polydispersed
(titanium carbide abrasive)	C_{fixed} = 18.0–19.8	Mg = 0.06 Fe = 0.1	1–200 μm
NbC	C_{total} = 11.0	C_{free} < 0.1 O < 0.2	1–100 μm polydispersed
SiC (β-phase)	C_{total} = 27.0–27.8	C_{free} < 0.3–0.8 O < 1.0 Fe < 0.2	8–10 m^2/g
BC_4	B_{total} = 74 C_{total} = 20.0	B_2O_3 < 0.5 Mg < 0.5	3.9 m^2/g
TiB_2 (polydispersed)	Ti = 69.6 B_{total} = 29.2	O < 0.5	1–200
TiB_2 (finely dispersed)	Ti = 66.7 B_{total} = 30.5	B_2O_3 < 0.2 Mg < 0.3	1–10
$MoSi_2$	Mo = 61.9–62.5 Si_{total} = 35.5–36.5	Si_{free} < 0.3 O < 0.3 Fe < 0.1	1–50
$TiSi_2$	Ti = 44.3 Si_{total} = 52.0	O < 0.1 Fe < 0.1	1–100

[a]Data from Borovinskaya *et al.*, (1991) and Merzhanov (1992).

In addition, the high heat formation of titanium carbide and specific features of the Ti-C phase diagram make it possible to produce, by CS, *nonstoichiometric* carbides, TiC_x (x=0.38–1.0) (Shkiro and Borovinskaya, 1975); *self-binding* materials, which consist of nonstoichiometric titanium carbide and titanium located along the carbide grain boundaries; and *cemented* carbides (Borovinskaya *et al.*, 1992b). A wide variety of metal additives have been investigated to produce dense cemented carbides, where combustion-synthesized TiC grains are joined by metal (e.g., up to 60 wt % of Ni or Fe) or intermetallic binders.

Static pressing of hot TiC_x immediately after synthesis yields dense ceramic or cermet (self-binded carbide) materials, with product densities as high as 99% of theoretical (Merzhanov *et al.*, 1981; Holt and Munir, 1986; Borovinskaya *et al.*, 1992b). Dense self-binded TiC_x-Ti cermets with residual porosity ~1% were also produced by pseudo HIP (Borovinskaya, 1992; Raman *et al.*, 1995). Applying SHS with isostatic pressing to a Ti+0.42C green mixture, dense (4.54 g/cm^3) cermets with high hardness (86–87 HRA) and bending strength (652 MPa) were synthesized.

The production of TiC-based materials with different binders has been reported: TiC+Ni (Rogachev *et al.*, 1987; Fu *et al.*, 1993b), TiC+(Ni-Al) (Dunmead *et al.*, 1990b; Tabachenko and Kryuchkova, 1993; Mei *et al.*, 1994), TiC+(Ni-Mo) (Borovinskaya *et al.*, 1992b; LaSalvia and Meyers, 1995), TiC+(Ni-Mo-Cu) and (TiC-Cr_3C_2)+Ni (Borovinskaya *et al.*, 1992b), (TiC-Cr_3C_2)+steel and (TiC-TiN)+(Ni-Mo) (Merzhanov, 1992), TiC+(Ti-Al) (Maupin and Rawers, 1993), and TiC-Al (without pressing) (Choi and Rhee, 1993). Some properties of combustion-synthesized and static pressed cemented carbides are listed in Table II.

Dynamic densification has also been used to obtain dense TiC ceramics (Niiler *et al.*, 1990; Meyers *et al.*, 1991; Vecchio *et al.*, 1992; Grebe *et al.*, 1992; Kecskes *et al.*, 1993; Wang *et al.*, 1994a), TiC-Ni (LaSalvia *et al.*, 1994), and (TiC-Cr_3C_2)+Ni cermets (Adadurov *et al.*, 1992). Other densification methods applied to TiC and TiC-based cermets include SHS+HIP (Koizumi and Miyamoto, 1990; Choi *et al.*, 1992), SHS+extrusion (Shishkina *et al.*, 1992) and hot rolling (Rice *et al.*, 1986). The synthesis of TiC and TiC-Fe in the volume combustion mode was also reported (Saidi *et al.*, 1994). Dense ceramic materials of Cr_3C_2 and Cr_3C_2-TiC composites were obtained by the gas-pressure combustion sintering method, with a density of more than 99% of theoretical and flexural strength 625 MPa (Xiangfeng *et al.*, 1992).

TABLE II
SOME PROPERTIES OF SHS CERMET ALLOYS[a]

Cemented Carbide Alloy	Basic Composition	Density (g/cm^3)	Average Grain Size (μm)	Hardness (HRA)	Ultimate Flex Strength (kg/mm^2)	Application
STIM-1B/3	TiC/TiB_2+Cu	4.94	5–7	93.5	70–80	Cutting edges, targets
STIM-2	TiC+Ni	5.50	5–7	90.0	100–120	Wear-resistant coatings
STIM-2A	TiC+(Ni-Mo)	6.40	1–2	87.0	160–180	Press tools
STIM 3B/3	TiC-Cr_3C_2+Ni	5.37	3–4	92.5	80–100	Cutting edges
STIM-3B	TiC-Cr_3C_2+steel	5.40	2–4	92.5	100–120	Corrosion-resistant articles
STIM-4	TiB+Ti	4.20	1–2	86.0	100–120	Thermal shock-resistant articles
STIM-5	TiC-TiN+Ni-Mo	5.0	1–2	91.0	120–140	Cutting edges

[a]Data from Borovinskaya *et al.* (1991).

b. Group Va Carbides. To a lesser extent, combustion synthesis from elements of transition (Group Va) metal carbides has also been investigated, especially for TaC (Shkiro *et al.*, 1978, 1979) and NbC (Martynenko and Borovinskaya, 1975). Some properties of reaction-synthesized NbC powders are presented in Table I.

c. Nonmetal Carbides. Among nonmetallic carbides, SiC synthesized from elemental Si and C powders has attracted the most attention. Silicon carbide has a relatively low heat of formation (69 kJ/mol), and additional heat input is required for combustion to occur. For example, locally igniting pressed Si+C samples, placed on a ribbon heater, yielded ~64% conversion to β-SiC, while increasing the area of ignition with a specially designed carbon-sleeve heater improved the conversion to ~99% (Yamada *et al.*, 1986). Dense SiC ceramics were produced by using the carbon-sleeve heater, combined with hot pressing (Yamada *et al.*, 1985). Another method of heating and ignition is to pass an electric current through the sample, yielding fine stoichiometric SiC powders (Yamada *et al.*, 1987). Fine-grained powders (0.2–0.5 μm) with high specific surface area (6.2 m^2/g) were synthesized in the VCS mode by inductively preheating the Si+C mixture to 1300°C (Pampuch *et al.*, 1987, 1989). Solid SiC and SiC-C blocks were also produced by infiltration of arc-melted silicon into porous carbon, during which the SHS reaction occurred (Ikeda *et al.*, 1990). Some properties of SiC powder synthesized by the SHS method are presented in Table I.

An interesting variation of passing electrical current through the reactant mixture has been reported (Feng and Munir, 1994). In this study, the gradient of the applied electric field was normal to the direction of the combustion front propagation. Since the reaction zone (containing molten silicon) has high electrical conductivity, the orientation of the electric field led to more intense Joule heating in this zone. It was demonstrated that the application of relatively low voltage (9.5–25 V) across samples of height 1.4 cm resulted in about a 10-fold increase in the combustion velocity (from 0.1 to ~1 cm/s).

Kharatyan and Nersisyan (1994) reported an alternative method of activating the reaction between Si and C without preheating. Potassium nitrate (KNO_3) is used as an activating agent. With this method, fine (<1-μm) SiC powders containing 28–29 wt % bound and 0.5 wt % free carbon were produced.

2. *Borides*

It has been demonstrated that most of the transition metal borides can be synthesized in the SHS mode (Holt *et al.*, 1985; Rice *et al.*, 1987; Mei *et al.*, 1992; Fu *et al.*, 1993a; Li, 1995). Early works reported synthesis of relatively pure (with residual unreacted boron less than 0.3 wt %) ZrB_2, TiB_2, HfB_2, and MoB (Merzhanov and Borovinskaya, 1972; Hardt and Holsinger, 1973). Combustion-

synthesized borides also include TiB, TaB_2, LaB_6, and NbB_2 (Holt and Dunmead, 1991). Similar to TiC for carbides, the combustion synthesis of transition metal borides from elements has focused primarily on TiB_2. Some properties of TiB_2 powders obtained by the SHS method are listed in Table I.

The high heat of formation for these borides (e.g., −279 kJ/mol for TiB_2 and −160 kJ/mol for TiB) makes it possible to add chemically inert metals and alloys (or weakly exothermic mixtures) to the metal–boron system. The subsequent plasticity of the products at the combustion temperature allows for various methods of densification to be applied, yielding poreless boride ceramics or boride-based cermets. For example, dense TiB-Ti self-binding borides (Borovinskaya *et al.*, 1992b; Shcherbakov *et al.*, 1992) and TiB_2 ceramics with 95% theoretical densities (Zavitsanos *et al.*, 1990) have been formed by hydraulic pseudo isostatic pressing and uniaxial pressing in a graphite-lined die, respectively. Dynamic compaction is considered to be another promising method for obtaining TiB_2-based ceramics (Niiler *et al.*, 1990; Meyers *et al.*, 1991; Wang *et al.*, 1994a). Other dense boride-based materials were produced by hydraulic pressing of TiB_2-Fe immediately after synthesis (Fu *et al.*, 1993a) and by reaction hot pressing of TiB_2-Al and TiB_2-Ni (DeAngelis, 1990). The hydrostatic pressing method was also applied to synthesize TiB_2-TiNi composites with 93% relative density and molar content of TiNi ranging from 0 to 95% (Yanagisawa *et al.*, 1990). Dense TiB_2 ceramic materials were formed by high-pressure combustion sintering under 3 GPa in a cubic anvil press (Miyamoto *et al.*, 1984), as well as by gas HIP at 100 MPa using a chemical furnace (Urabe *et al.*, 1990). Synthesis of composite products, such as TiB_2-Al (Taneoka *et al.*, 1989) and TiB_2-Fe (Fu *et al.*, 1993a), has been reported. Mechanical testing of combustion-synthesized TiB_2-Fe composites demonstrates promising properties at elevated temperatures (Andrievski and Baiman, 1992).

3. *TiC-TiB_2 Composite Ceramics*

In some cases, several refractory compounds can result from two or more parallel reactions occurring simultaneously in the combustion wave. A typical example of this type is the Ti-C-B system, where both the Ti+C and Ti+2B reactions affect the combustion synthesis and structure formation processes (Shcherbakov and Pityulin, 1983). By adjusting the contents of carbon and boron powders in the reactant mixture, either carbide- or boride-based ceramics can be obtained.

The Ti-C-B system was used for a series of ceramic poreless composites produced by the SHS+HIP method (Borovinskaya *et al.*, 1992b). Near-eutectic 40TiC-60TiB_2 (wt %) compositions were primarily investigated, while various metal additives were tested (e.g., Co, Cu) as the binder phase, with contents varying from 0 to 12 wt %. The materials demonstrated good mechanical properties (Table II) and may be used for cutting tools. Note that material with higher TiC content (80 wt %) possess higher bending strength.

4. Silicides

Compounds of metals with silicon were synthesized from elements by both the SHS (Sarkisyan *et al.,* 1978; Azatyan *et al.,* 1979; Deevi, 1991, 1992) and VCS modes (Trambukis and Munir, 1990; Subrahmanyam, 1994). Powders and sintered samples of various chemical compositions were obtained, including Ti_5Si_3, TiSi, $TiSi_2$, Mo_3Si, Mo_5Si_3, $MoSi_2$, Zr_2Si, Zr_5Si_3, ZrSi, and $ZrSi_2$. Among them, titanium and molybdenum silicides have received the most attention, due to their high melting points, excellent oxidation resistance, relatively low density, and high electrical and thermal conductivities (Samsonov and Vinitskii, 1980; Rozenkranz *et al.,* 1992; Shah *et al.,* 1992). The properties of some silicide powders are shown in Table I.

Combustion-synthesized $MoSi_2$ powders have been used to produce high-temperature heating elements (Merzhanov, 1990a). The application of the SHS+extrusion method for one-step production of $MoSi_2$ heaters has also been reported (Podlesov *et al.,* 1992a). Further, combustion synthesis of molybdenum alumosilicide (Mo-Al-Si) was demonstrated (Hakobian and Dolukhanyan, 1994).

5. Aluminides

Combustion synthesis of nickel aluminides in the VCS mode was first demonstrated during sintering of a Ni-Al mixture (Naiborodenko *et al.,* 1968). Shortly thereafter, the SHS mode of combustion synthesis was reported for a variety of aluminides, including those of Ni, Zr, Ti, Cr, Co, Mo, and Cu (Naiborodenko *et al.,* 1970, 1982; Naiborodenko and Itin, 1975a,b; Maslov *et al.,* 1976, 1979; Itin *et al.,* 1980).

In this class, most attention has been paid to nickel aluminides (Philpot *et al.,* 1987; Rabin *et al.,* 1990; Lebrat and Varma, 1992a; Lebrat *et al.,* 1992, 1994; Rogachev *et al.,* 1993; Wenning *et al.,* 1994; Alman, 1994) and titanium aluminides (Kuroki and Yamaguchi, 1990; Kaieda *et al.,* 1990a; Ho-Yi *et al.,* 1992; Kachelmyer *et al.,* 1993; Lee *et al.,* 1995; Hahn and Song, 1995). However, synthesis of other aluminides has also been investigated, including aluminides of iron (Rabin and Wright, 1991, 1992; Rabin *et al.,* 1992b), niobium (Maslov *et al.,* 1979; Kachelmyer and Varma, 1994; Kachelmyer *et al.,* 1995), and copper (Wang *et al.,* 1990).

As discussed earlier, aluminides have been used as binders for carbide- and boride-based cermets, for example, by adding Ni and Al powders to exothermic mixtures of Ti with C or B. On the other hand, some intermetallic compounds (e.g., NiAl, Ni_3Al, TiAl) possess high enough heats of formation so that composites with intermetallic matrices can be produced either in the VCS or SHS regimes. The ceramic components are added either in the green mixture or synthesized *in situ* during the reaction.

For example, Ni_3Al matrix composites reinforced by Al_2O_3, SiC, or B_4C whiskers have been formed in the SHS mode (Lebrat *et al.*, 1992, 1994). Also, the reinforcement of combustion-synthesized Ni_3Al with TiC particles was investigated for two types of particles: commercially available TiC powders added in the reaction mixture and *in situ* synthesized TiC grains (Mei *et al.*, 1993). The NiAl matrix composite reinforced with TiB_2 particles (10 and 30 wt %) was synthesized using SHS+hot pressing (Wang *et al.*, 1993). The TiAl matrix was formed in the SHS mode, while reinforcing SiC particles were added in the initial Ti+Al mixture (Rawers *et al.*, 1990). Also, Al, and $TiAl_3$ matrix composites, reinforced by TiC, TiB_2, and TiC+TiB_2 particles synthesized *in situ,* have been fabricated in the SHS regime (Gotman *et al.*, 1994).

Owing to their high plasticity at the combustion temperature, poreless aluminides can be produced using various methods of densification. Dense titanium aluminide materials were obtained in the VCS regime with pseudo HIP (Shingu *et al.*, 1990), while hydraulic hot pressing combined with SHS was used to form NiAl matrix composites with porosities of 1% or less (Wang *et al.*, 1993). Hot rolling under vacuum was applied to form combustion-synthesized TiAl (Osipov *et al.*, 1992). Other materials were synthesized by the extrusion of Ni-rich NiAl (Alman, 1994). Shock-induced synthesis with dynamic densification was reported for titanium, niobium, and nickel aluminides (Work *et al.*, 1990; Ferreira *et al.*, 1992; Strutt *et al.*, 1994). Densification of iron aluminides and Fe_3Al matrix composites reinforced with Al_2O_3 particles was performed by pressing in graphite-lined dies at 10–70 MPa (Rabin and Wright, 1991), as well as by HIP and pseudo HIP techniques (Rabin *et al.*, 1992b). It was shown recently that a 99.7% dense Fe_3Al-Nb alloy billet could be prepared by SHS, followed by superplastic consolidation (Dutta, 1995).

6. *Compounds of Ti with Ni, Co, and Fe*

While intermetallic Ti-(Ni, Co, Fe) compounds cannot be synthesized from elemental powders without preheating, a relatively low increase above room temperature is generally sufficient to initiate a self-sustained reaction. Almost all compounds of the Ti-Ni, Ti-Co, and Ti-Fe systems have been produced by this method (Itin *et al.*, 1977, 1983; Bratchikov *et al.*, 1980; Itin and Naiborodenko, 1989; Yi and Moore, 1989, 1990; Kaieda *et al.*, 1990b; Zhang *et al.*, 1995). Intermetallic TiNi compounds are especially attractive for their shape memory characteristics. Combustion-synthesized Ti-Ni powders and materials have been used in the industrial production of sheets, tubes, and wires with shape memory in Russia (Itin and Naiborodenko, 1989) and in Japan (Kaieda *et al.*, 1990b). Cold-deformed binary alloys have retained up to 90% of their original shape, while 99.5% of the original shape may be restored for ternary alloys (e.g., Ti-Ni-Fe and Ti-Ni-Al). A 70-kg coil of hot-rolled TiNi wire produced by the CS+HIP technique is shown in Fig. 11.

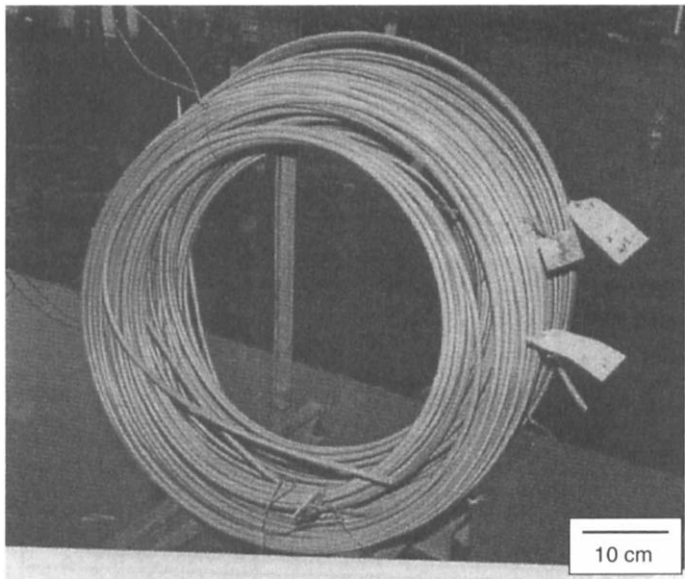

FIG. 11. Hot-rolled coil of TiNi wire after forging. The weight of the coil is 70 kg (Adapted from Kaieda *et al.*, 1990b).

7. *Diamond Composites*

At normal pressures, diamond is a metastable phase of carbon, which converts to graphite at temperatures higher than 1300 K (either in vacuum or inert gas). The rate of conversion is extremely rapid at temperatures higher than 2000 K (Howers, 1962; Evans and James, 1964). Thus, graphitization during sintering of diamond composites makes it difficult (if not impossible) to produce refractory matrix composite with diamond particles. Due to the short time of interaction, SHS is an attractive method for the production of diamond-containing composite materials with refractory and wear-resistant matrices. SHS combined with pressing (pseudo HIP) was used to obtain TiB-diamond composites from elemental Ti+B with up to 20 wt % synthetic diamond (Padyukov *et al.*, 1992a,c). By decreasing the combustion temperature from 2200 K to 1900 K, the extent of graphitization was reported to decrease from 6% to 0.5% (Padyukov *et al.*, 1992b). Further investigation of the combustion synthesis of TiB- and NiAl-matrix diamond-containing materials has shown that under certain conditions, diamond particles retain their shape, surface quality and mechanical properties after synthesis (Padyukov and Levashov, 1993; Levashov *et al.*, 1993). The characteristic microstructure of the diamond-containing portion of an Ni-Al/diamond composite synthesized by the SHS method is shown in Fig. 12.

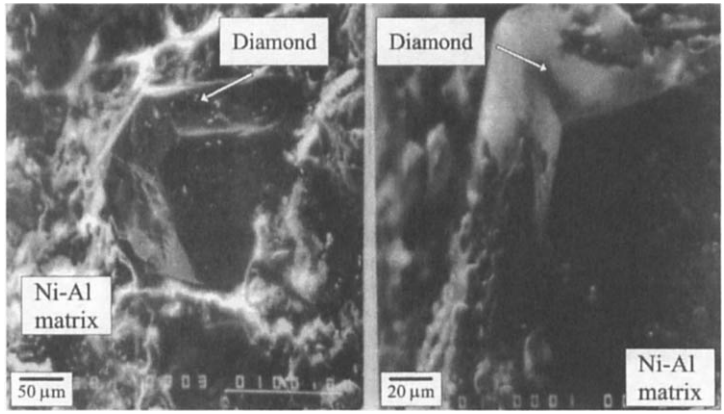

FIG. 12. Characteristic microstructure of the diamond-containing region in a Ni-Al diamond composite produced by the SHS method (Adapted from Levashov *et al.*, 1993).

8. *Functionally Graded Materials*

The concept of functionally graded materials (FGMs) is to tailor nonuniform distribution of components and phases in materials, and hence combine mechanical, thermal, electrical, chemical, and other properties that cannot be realized in uniform materials. For example, the material structure may have a smooth transition from a metal phase with good mechanical strength on one side, to a ceramic phase with high thermal resistance on the other side (see Fig. 13). With a gradual variation in composition, FGMs do not have the intermaterial boundaries found in multilayer materials, and hence they exhibit better resistance to thermal stress.

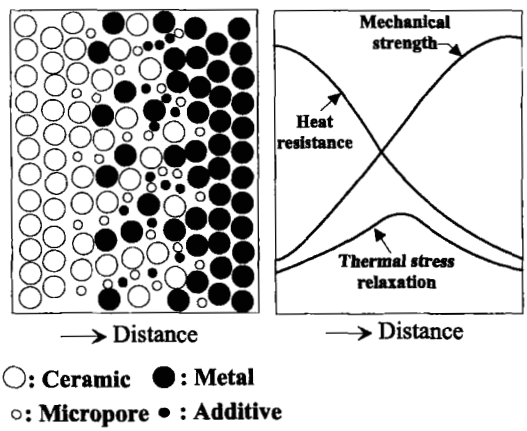

FIG. 13. The concept of functionally graded materials (Adapted from Sata *et al.*, 1990b).

Combustion synthesis was applied successfully in the production of TiB_2-Cu FGMs with the amount of TiB_2 varying from 0 (metal side) to 100% (ceramic side) for cylindrical samples, 30 mm in diameter and 5 mm thick (Sata *et al.*, 1990a,b; Sata, 1992). A predetermined distribution of elements in the green mixture was created using an automatic powder stacking apparatus. During synthesis, simultaneous densification by hydrostatic pressing was also applied. Similar methods were used to produce TiB_2-Cu FGM samples from cylindrical green compacts of 17 mm in diameter and 10 mm in height (Wang *et al.*, 1994b). However, other phases (Ti_3Cu_4, Cu_3Ti, $TiCu_4$, TiB, Ti_2B_5) appeared when the Cu content was increased. The method of gas-pressure combustion sintering was applied to produce TiC-Ni FGM (Miyamoto *et al.*, 1990a). The Vickers microhardness of this material gradually changed from 2 GPa at the nickel side to 23 GPa at the TiC side, where the TiC grain size decreased with increasing local Ni content. The microstructure of a Cr_3C_2/Ni FGM, consolidated from a green compact consisting of powder layers with different Cr-C-Ni compositions by the SHS+HIP method, is shown Fig. 14.

Another approach is to prepare a green mixture with relatively few (typically two or three) layers, while desired gradients in the product appear during the SHS process due to infiltration and migration of melts, diffusion, and other transport phenomena (Pityulin *et al.*, 1992, 1994). This approach was used to produce poreless functionally gradient cermets, including TiC-Ni and (Ti,Cr)C-Ni, by combining SHS with pseudo HIP. An example of a multilayer material synthesized by the CS+hot pressing method is the TiB_2-Al_2O_3-ZTA (zirconia toughened alumina) composite. The microstructure of this layered material is shown in Fig. 15 (DeAngelis and Weiss, 1990). We can see that the layers can have different thicknesses and are well bonded to one another. Recently, the production of diamond-containing FGMs was also reported (Levashov *et al.*, 1994), where properties

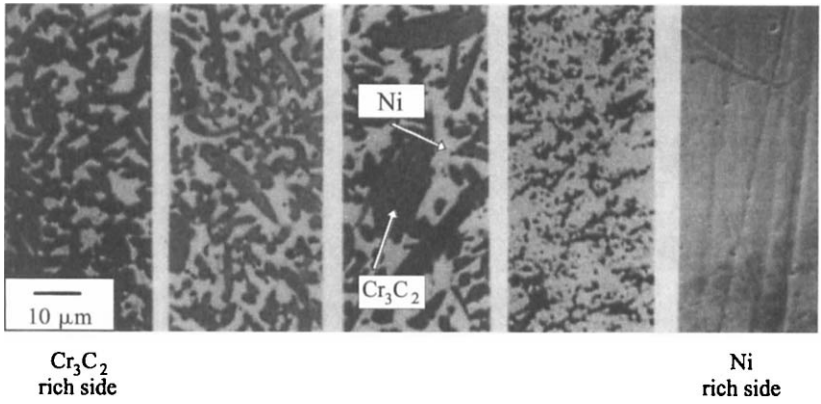

FIG. 14. SEM image of Cr_3C_2/Ni FGM microstructure (Adapted from Miyamoto *et al.*, 1992).

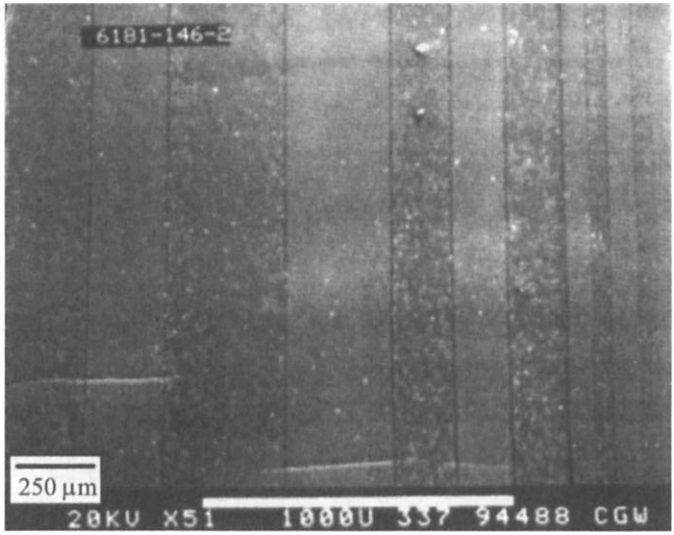

FIG. 15. Scanning electron microscope photomicrograph of multilayer TiB_2/Al_2O_3 with zirconia toughened alumina (Adapted from DeAngelis and Weiss, 1990).

of materials are determined by the gradient distribution of diamond in the combustion-synthesized matrix.

9. *Other Classes of Products*

Chalcogenides, including sulfides and selenides of Mg, Ti, Zr, Mo, and W, represent another group of compounds that can be synthesized from elements during the combustion process. Experimental synthesis of luminescent ZnS samples was also carried out (Molodetskaya *et al.,* 1992). Combustion reactions between chalcogenides and alkali metal compounds were applied to produce GaAs and GaP from solid-state precursors (Wiley and Kaner, 1992). In addition, compounds of metals (Ni, Cu, Zr, etc.) with phosphorus were obtained (Muchnik, 1984; Muchnik *et al.,* 1993). Also, phosphides of Al, Ga, and In were formed by direct combustion synthesis from elemental powders (Kanamaru and Odawara, 1994). An interesting example of the combustion synthesis of aluminum iodide Al_2I_6 from a mixture of Al powder with crystalline iodine was reported (Shtessel *et al.,* 1986). Note, however, that synthesis of chalcogenides, phosphides, and iodides represents a process intermediate between gasless and solid–gas processes due to intense vaporization of the nonmetal reactant during combustion.

Among intermetallic compounds not mentioned previously, Mg_2Ni is a promising material for storing hydrogen. It has been shown that the combustion synthesis of this material is feasible, in spite of a relatively low heat of reaction.

For example, high-purity Mg_2Ni was obtained in the SHS mode (Akiyama *et al.*, 1995).

B. Combustion Synthesis in Gas–Solid Systems

1. Nitrides and Nitride-Based Ceramics

a. Metallic Nitrides. A wide variety of metallic nitrides including TiN, ZrN, NbN, HfN, TaN, and VN have been produced by combustion synthesis. Among these, titanium and zirconium nitrides have been investigated more thoroughly. These nitride powders can be used to form refractory corrosion-resistant coatings and conducting materials in electronic applications (Borovinskaya *et al.*, 1991). Depending on the nitrogen pressure, titanium and zirconium nitrides with a wide range of nitrogen compositions have been synthesized, ranging from solid solutions with a minimum amount of nitrogen ($MeN_{0.1}$) to single-phase supersaturated solutions ($MeN_{0.34}$-$MeN_{0.45}$), as well as stoichiometric MeN (Borovinskaya and Loryan, 1976, 1978). Even when the porosity of the green mixture is optimal (40–45%), the degree of conversion from Ti to TiN may not exceed 60–70% (Eslamloo-Grami and Munir, 1990a,b). In a recent work, Brezinsky *et al.* (1996) achieved conversions up to 75% during nitridation of titanium in supercritical nitrogen. However, full conversion can be achieved by dilution of the initial Ti powder with 40–50 wt % of TiN (Borovinskaya and Loryan, 1978).

Other metallic nitrides have also been synthesized by combustion synthesis. Vanadium nitride was first produced by Maksimov *et al.* (1979), and is the basis of ferrovanadium (VN+Fe), a commonly used alloying agent for the manufacture of steels with low-temperature applications (Maksimov *et al.*, 1984). Also, a unique cubic structure of TaN, which has the highest microhardness among all transition metal nitrides (3200 kg/mm^2) and can be used as a hard alloy component, was formed during combustion of tantalum powder in liquid nitrogen (Borovinskaya *et al.*, 1970). Niobium nitride powders, with a transition temperature to superconductivity at 14.3 K, were synthesized by SHS. In addition to powders, thin superconducting plates and wires of NbN were obtained using a $Nb+NbN+N_2$ mixture, as a chemical furnace (Ohyanagi *et al.*, 1993). Recently, both the SHS and VCS modes were utilized for the synthesis of magnesium nitride, Mg_3N_2 (Li *et al.*, 1994). It was found that addition of Mg_3N_2 as diluent to the initial Mg powder is necessary for carrying out the SHS process, in order to provide high permeability of nitrogen in the sample after melting of magnesium.

It is worth noting that a large number of publications (see Sections V and VI) deal with fundamental studies of combustion in metal–nitrogen systems. However, only a relatively few describe the properties of these powders and materials.

TABLE III
SOME CHARACTERISTICS AND PROPERTIES OF METALLIC SHS NITRIDES[a]

Products	Chemical Composition (wt %)	Impurities (wt %)	Particle Size and Specific Surface Area	Other Properties: Microhardness, H, and Transition Temperature to Superconducting State, T_{sc}
Titanium nitride (cubic, a = 4.24)	Ti = 77.0–78.5 N = 20.3–21.5	O = 0.3–0.5 Fe < 0.2	1–200 μm, easily grindable	H = 1800 kg/mm^2
Hafnium nitride (cubic, a = 4.510)	Hf = 92.0–94.0 N = 5.9–6.0	O = 0.3–0.5	1–50 μm	T_{sc} = 6.6 K
Tantalum nitride (cubic, a = 4.323)	Ta = 91.7–92.2 N = 7.3–7.6	O = 0.1–0.3 C = 0.05–0.1	1–10 μm 0.06 m^2/g	H = 3200 kg/mm^2
Zirconium nitride (cubic, a = 4.576)	Zr = 87.3 N = 12.6	O = 0.3–0.5 Fe < 0.2	1–200 μm	H = 1570 kg/mm^2 T_{sc} = 9.6 K
Niobium nitride (cubic, a = 4.385)	Nb = 86.9 N = 6.1	O = 0.1–0.3 C = 0.05–0.1	1–50 μm	H = 1670 kg/mm^2 T_{sc} = 14.3 K

[a]Data from Merzhanov and Borovinskaya (1972) and Borovinskaya *et al.* (1991).

The characteristics and properties of some combustion-synthesized transition metal nitrides are presented in Table III.

b. Nonmetallic Nitrides. Nonmetallic nitrides, including Si_3N_4, BN, and AlN, have important applications as high-temperature structural ceramics. As discussed earlier (see Section I), two methods can be used to produce nitrides by CS: elemental ($Si+N_2$, $B+N_2$, $Al+N_2$) and reduction (e.g., $B_2O_3+Mg+N_2$) reactions. In Tables IV, V, and VI, a comparison of the chemical composition and spe-

TABLE IV
SOME CHARACTERISTICS AND PROPERTIES OF Si_3N_4 POWDERS[a]

Content (wt %)	SHS β-phase	SHS $\alpha+\beta$-phase, ($\alpha \geq 80\%$)
Basic compound, Si_3N_4	98–99	98–99
Nitrogen, N	38.5–39.0	38.5–39.0
Oxygen, O	0.5–1.0	0.5–1.0
Iron, Fe	0.1–0.3	<0.01–0.3
Carbon, C	<0.1	≤0.1
Silicon free, Si_{free}	<0.1	<0.1
Specific Surface, m^2/g	1–3	3–11

[a]Data from Merzhanov (1992).

TABLE V
SOME CHARACTERISTICS AND PROPERTIES OF BN POWDERS[a]

Content (wt %)	SHS Product Ultrapure	SHS Product Technically Pure	Furnace Product ORPAC GRADE 99	Furnace Product Denka (Japan)
Basic compound, BN	>99.5	97.3	98–99	>98
Nitrogen, N	>55.7	54.9	54–55	54.5
Oxygen, O	<0.5	1.5	1.5	1.5
Carbon, C	<0.01	0.3	—	—
Metal impurities (Mg, Fe)	<0.2	0.3	—	—
Specific Surface, m^2/g	11.0	8–14	10	—

[a]Data from Merzhanov (1992).

cific surface area of powders produced by CS and by conventional methods is presented. Powders synthesized by SHS have comparable, if not higher, nitrogen contents than those produced by conventional methods. The metal impurities (mainly Fe) are the consequence of either inappropriate mixing/grinding equipment or impure raw materials, both of which may be remedied.

The industrial ceramics produced by conventional sintering of β-phase Si_3N_4 powders synthesized by SHS (Petrovskii *et al.*, 1981) can be used as high-temperature articles with attractive dielectric properties ($\tan\delta = 4.4\ 10^{-3}$ at $f = 10^6$ Hz, and dielectric strength, $E_d = 9.2$ kV/mm). Also, silicon nitride powders with a relatively high α-phase content ($\geq 80\%$) have been used for the production of advanced structural ceramics with good mechanical properties ($\sigma_b = 900$ MPa, $K_{1c} = 6.7$–7.2 mN/$m^{3/2}$, and $H_V = 13.3$–14.2 GPa).

The dielectric materials produced by hot pressing SHS AlN powders have comparable thermal conductivities, but higher bending strengths than those produced in conventional furnaces (Gogotsi *et al.*, 1984). For this reason, they are suitable for fabrication of panels in the microelectronics industry. Also, aluminum

TABLE VI
SOME CHARACTERISTICS AND PROPERTIES OF ALN POWDERS[a]

Content (wt %)	SHS Product Ultrapure	SHS Product Technically Pure	Furnace Product ART USA A-100	Furnace Product Starck (Grade B) (Germany)
Basic compound, AlN	99.7	98.8	99.0	98.1
Nitrogen, N	33.9	32.7	33.0	33.3
Oxygen, O	0.3	0.6	1.0	2.3
Iron, Fe	0.07	0.12	0.005	100 ppm
Specific Surface, m^2/g	2.0–20	1.5	2.5–4.0	1.0–8.0

[a]Data from Merzhanov (1992).

nitride powders synthesized by SHS have been used as a heat-conducting component in silicon–organic adhesive sealants. Used successfully in Russia for electronic applications, this glue has a thermal conductivity about twice that of alternative adhesives (Merzhanov, 1992).

Combustion synthesis of boron nitride powder, BN, was reported in one of the earliest works on SHS (Merzhanov and Borovinskaya, 1972). The mechanisms of combustion and product structure formation from elements were later investigated (Mukasyan and Borovinskaya, 1992). More recently, finely dispersed hexagonal boron nitride powder has been obtained from reduction-type reactions (Borovinskaya *et al.*, 1991).

The high temperatures present in the CS process make it possible to not only produce powders, but also to sinter materials and form net-shape articles in the combustion wave (Merzhanov, 1993a). Several types of SHS nitrides and their applications are presented in Table VII.

Since their mechanical properties are maintained at high temperatures (up to 1700 K), silicon nitride-based materials are attractive for use in high-temperature structural applications in chemically aggressive environments. For example, several properties of a Si_3N_4-based ceramic (Si_3N_4+SiC+TiN), suitable for ceramic engines, are shown in Table VIII.

TABLE VII
SHS CERAMICS BASED ON NONMETALLIC NITRIDES[a]

Composition	Product Type	Applications
Si_3N_4	Bricks, plates, cylinders	Corrosion-resistant plugs for chemical pumps
Si_3N_4 + SiC + TiN (black ceramic)	Plates, rods, plugs, sleeves	Cylinders, plugs, and other parts for combustion engines
Si_3N_4 + SiC + BN + C	Plates, rods, balls	Friction pairs, ball bearings
SiAlON	Articles of complicated shape: turbine blades, honeycomb structures, etc.	Internal combustion engine parts for turbo-supercharges; catalyst supports for incineration of exhaust gases
SiAlON + BN	Bricks, plates	Parts for metallurgy
SiAlON + SiC + BN	Bricks, nozzle, turbine blades	Internal combustion engine parts; metallurgical tools
AlN	Cylinders, plates	Heat-conducting substrates
AlN + TiB_2	Bricks, plates, cylinders	Cathodes for coating by vacuum spraying
BN	Rods, bricks, plate, tubes, crucibles, rings, sleeves, bricks	Insulating sleeves; crucibles for pouring and tubes for flow of melted alloys
B + BN	Plugs	Nuclear safety
BN + SiO_2	Plates	Lining of MHD generator

[a]Data from Merzhanov (1993a).

TABLE VIII
SOME PROPERTIES OF SHS SILICON NITRIDE-BASED CERAMICS[a]

Property	Value
Density, g/m^3	3–3.4
Porosity, %	<1–15
Elastic modulus, Gpa	180–250
Rockwell hardness, HRA	85–93
Vickers hardness, GPa	6–14.5
Bend strength, MPa, T = 1750 K	270–650
Critical stress intensity factor, MN/m$^{3/2}$	2.5–5
Thermal conductivity (873–1371 K), W/m K	15–20

[a]Data from Merzhanov (1990a).

Aluminum nitride is most commonly used for its high thermal conductivity. Recently, a poreless composite material, TiAl-TiB_2-AlN, was obtained by reacting a Ti+(0.7–0.95)Al+(0.05–0.50)B mixture at 30- to 100-atm nitrogen pressure (Yamada, 1994). The use of high-pressure nitrogen gas was found to be effective for simultaneous synthesis and consolidation of nitride ceramics with dispersed intermetallic compounds (e.g., TiAl). Dense, crack-free products with uniform grains (approximately 10 mm in size) were obtained.

The main applications for boron nitride materials take advantage of their dielectric properties, which are maintained at high temperatures (even above 2000 K) in nonoxidizing atmospheres. Some properties of boron nitride-based materials are listed in Table IX, and some examples of the

TABLE IX
SOME PROPERTIES OF SHS BN-BASED CERAMICS[a]

Properties	BN	BN + SiO_2
Chemical composition, wt %	N = 55; O < 0.5; B_{free} < 0.5; B_2O_3 < 0.3; C < 0.5	BN = 74 SiO_2 = 26
Density, g/cm^3	1.5	1.85
Dielectric strength, kV/mm	25	19
Dielectric permeability	3.1	6.0
Tangent of dielectrical loss at 1 MHz	0.0034	0.036
Resistivity, Ω	2×10^8	1.3×10^8
Thermal conductivity, W/mK		
T = 400 K	20	
T = 900 K	8	8
Bend strength, MPa	25	50

[a]Data from Mukasyan *et al.* (1989).

various shapes and forms that can be produced from BN-based materials are shown in Fig. 16.

2. *Hydrides*

The heats of formation for transition metal hydrides are much lower than those for nitrides or oxides. However, the high diffusivity of hydrogen within the reaction medium makes it possible to organize self-sustained combustion (Dolukhanyan *et al.,* 1976, 1978). More than 30 hydrides and deuterides of scandium, titanium, vanadium, and the major lanthanide metals have been obtained by gas–solid combustion synthesis (Dolukhanyan *et al.,* 1992). Hydrides of the transition metal alloys and intermetallic compounds (e.g., $ZrNiH_3$, Ti_2CoH_3) were also obtained (Dolukhanyan *et al.,* 1981). The production of complex hydrocarbides and hydronitrides is of special interest (Agadzhanyan and Dolukhanyan, 1990). For example, multicomponent single-phase hydronitrides of the following compositions $Zr_{0.9}Nb_{0.1}C_xN_{1-x}H_{0.19}$, $Zr_{0.4}Nb_{0.6}C_xN_{1-x}H_{0.26}$ can be synthesized.

3. *Oxides*

Combustion synthesis has been used to produce complex oxide materials, such as ferrites and ferroelectric, piezoelectric, and superconducting materials. In these systems, the heat required for SHS is supplied by the heat released from the reac-

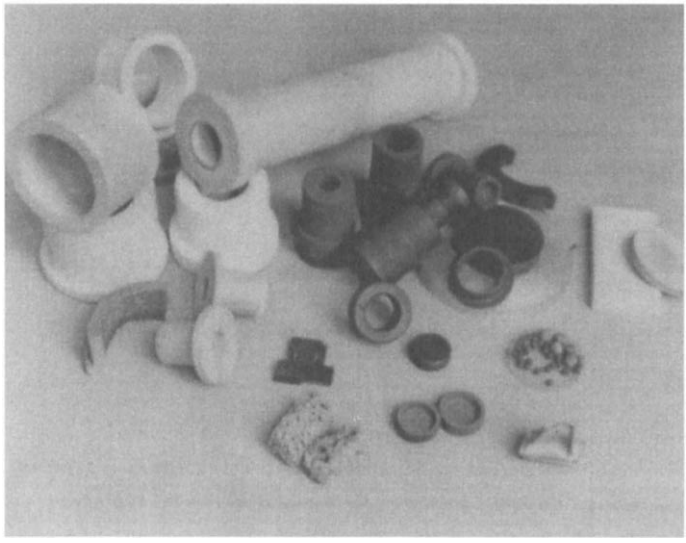

FIG. 16. Ceramic materials and net-shape articles produced by combustion synthesis. (Adapted from Mukasyan, 1986)

tion between oxygen and metal. Oxygen can be supplied to the reaction by either an external (oxygen gas) or an internal (e.g., reduction of oxides in the starting reaction mixture) source or by a combination of the two.

a. High-Temperature Superconductors. One of the promising oxide materials produced by SHS is the $YBa_2Cu_3O_{7-x}$ (Y_{123}) ceramic superconductor (Merzhanov, 1990a). This material has a number of applications, including targets for magnetron spraying, superconducting shields, wires, and cables. The compound is produced by SHS using the following reaction:

$$3Cu + 2BaO_2 + 1/2Y_2O_3 + (1.5\text{-}x)/2\ O_2 \rightarrow YBa_2Cu_3O_{7-x}\ (Y_{123}).$$

The effects of processing conditions, including green density, oxygen pressure, Cu, BaO_2, and Y_2O_3 particle sizes, as well as the use of Cu_2O and CuO as starting materials, have been investigated (Merzhanov, 1990b; Lebrat and Varma, 1992b; Lin *et al.*, 1994). The reaction mechanism has also been identified by the quenching technique (Merzhanov, 1990b; Lebrat and Varma, 1991). It was shown that oxidation of Cu metal by gas-phase oxygen initiates the reaction, while the subsequent decomposition of barium peroxide provides an internal source of oxygen.

A comparison of Y_{123} powders produced by SHS (SHS-J1 and SHS-J2) with those produced by furnace synthesis is shown in Table X. The oxygen content, transition temperature, orthorhombic phase Y_{123} content, basic impurities, and mean particle sizes of SHS powders compare favorably with those produced by furnace synthesis. However, the time of Y_{123} production for a conventional fur-

TABLE X
SOME CHARACTERISTICS AND PROPERTIES OF SUPERCONDUCTIVE POWDERS ($YBa_2Cu_3O_{7-x}$) PRODUCED BY CONVENTIONAL AND SHS METHODS[a]

Powder	Oxygen Content (7-x)	Transition Temperature, T_{sc} (K)	Percent Orthorhombic (Y_{123}) Phase	Basic Impurities	Average Particle Size (μm)
SC5-S[b]	6.92	93.5	98	CuO	40.0
SC5-P[b]	6.87	93.5	~99	CuO	8.2
SC5-6.5[b]	6.88	90.5	97	$BaCuO_2$	6.8
SC5-7[b]	6.85	92.5	~99	CuO	5.7
CPS A-1203[b]	6.85	92.0	~99	$BaCuO_2$	3.0
SSC 03-0065[b]	6.89	92.0	~99	—	6.5
SHS-J1[c]	6.90	92.0	97	CuO	9.0
SHS-J2[c]	6.92	93.5	~99	—	8.0

[a]Data from Merzhanov (1991).
[b]Conventional methods.
[c]Combustion synthesis.

nace is an order of magnitude longer than that for SHS. Recently, relatively high-density (~90%) items with superconducting transition temperature, T_{sc}=92 K, have been fabricated by SuperConco Co. (U.S.) by sintering SHS-J2 powders (Avakyan *et al.*, 1996). Also, thick films (1 mm) made from this powder exhibit a critical current density up to 10^6 A/cm^2. The materials of $Bi_2Sr_2CaCu_2Oy$ and $Tl_2Ba_2Ca_2Cu_3O_y$ compositions with T_{sc}=125 and 135 K, respectively, have also been synthesized by SHS (Merzhanov, 1990b).

b. Ferroelectric Materials. The properties of various ferroelectric materials produced by SHS have recently been reported (Avakyan *et al.*, 1996). It was noted that the properties of electronic ceramics produced by SHS, including chemical and phase compositions as well as electromagnetic properties, are strongly affected by the maximum combustion temperature. This feature suggests that the properties of the final product can be tailored for a specific application by changing the combustion temperature, which can be achieved by adjusting the processing conditions (see Section V).

Ferroelectric laminated bismuth compounds, which have application as high-temperature piezoelectrics and semiconductors, can be synthesized by SHS. In Table XI, the properties of several ferroelectric materials along with potential applications are presented. In addition, $LiNbO_3$ and $LiTaO_3$ can be obtained by SHS with densities two times higher than those produced by conventional methods, by varying the Li_2O/Me_2O_5 ratio in the product (Me is Nb or Ta). The formation of rare-earth (lithium and terbium) molybdate materials can also be achieved by SHS. All of the materials mentioned have electronic applications. During conven-

TABLE XI
SOME CHARACTERISTICS AND PROPERTIES OF SHS-PRODUCED FERROELECTRIC MATERIALS[a]

Composition	Resistivity, ρ (Ω · cm)	Dielectric Constant, ϵ	Dielectric Dispersion, tan δ	Applications
$Bi_4V_2O_{11}$	4.7×10^9	63	0.089	Gas sensor (ethanol, acetone)
$BiFeO_3$	4.2×10^9	46	0.169	Gas sensor (ethanol, acetone, gasoline)
$Bi_2Fe_4O_9$	6.0×10^9	10	0.004	Gas sensor (ethanol, acetone)
$Bi_4Fe_2O_9$	2.8×10^9	40	0.109	Temperature-sensitive resistance, gas sensor (ethanol, acetone, gasoline)
$BaBi_2Ta_2O_9$	4.0×10^{11}	49	0.0022	Gas sensor (ethanol, acetone, natural gas, H_2O
Bi_3TiNbO_9	1.9×10^{10}	70	0.0047	Moisture sensor
$BaBi_2Ni_2O_9$	3.5×10^{11}	92	0.0081	Moisture sensor
$Na_{0.5}Bi_{4.5}Ti_4O_{15}$	1.45×10^9	82	0.0059	Moisture sensor

[a]Data from Avakyan *et al.* (1996).

tional synthesis, difficulties arise when forming single crystals of lithium and terbium molybdates due to the high volatility of molybdenum oxide. This difficulty has been overcome by using SHS-produced stoichiometric powders, which are characterized by minimal losses during heating, melting, and crystallization.

C. Products of Thermite-Type SHS

It is impossible to describe, even briefly, all of the products obtained by thermite-type self-propagating reactions. Some examples were given previously in Section I, and some additional examples involving Mg metal are presented later in Table XX. The use of Mg leads to MgO product that can be easily leached, leaving behind the desired product composition in powder form. In this section, we consider some selected products reported in the literature, specifically those whose phase distribution and properties are controlled by gravitational or centrifugal forces. Owing to high heats of formation, the products are completely molten at the combustion temperature. As a result, gravity-induced processes of convection and buoyancy may affect phase separation and crystallization, as well as combustion wave propagation.

Centrifugal SHS casting (Section II,B,3) was used to produce oxide-carbide ceramics by the following reaction: $MO_x + Al + C \rightarrow MC_y + Al_2O_3$ (Yukhvid *et al.*, 1994). In general, titanium, chromium, molybdenum, and tungsten carbides are synthesized with an alumina melt in the combustion wave, for example, Cr_3C_2-Al_2O_3, WC-Al_2O_3, (Ti,Cr)C-Al_2O_3, and MoC-Al_2O_3. Also, addition of metal (Fe group) oxides (NiO, CoO, Fe_2O_3) results in formation of cermet composites containing a metal binder [e.g., (Ti,Cr)C-Ni] in addition to the carbide phase. The lighter oxide phase can be fully separated from the cermet by centrifugal acceleration. A centrifugal overload of 150 *g* is sufficient to separate MoC from Al_2O_3, while 300 and 1000 *g* are required to separate WC-Co cermet and WC, respectively, from the alumina melt (Merzhanov and Yukhvid, 1990). Lower centrifugal overloads result in incomplete separation and the formation of graded materials. This phenomenon has been used to obtain refractory and chemically stable protective coatings on various substrates, which possess relatively complex composition and structure (Grigor'ev and Merzhanov, 1992; Yukhvid, 1992).

An interesting application of a thermite-type SHS reaction with centrifugal overload is the fabrication of multilayered composite pipes (Odawara, 1982, 1990; Odawara and Ikeuchi, 1986; Kachin and Yukhvid, 1992). A simple and well-known composition, Fe_2O_3+2Al, was used to produce a two-layer lining inside the steel pipe; see Fig. 17 (Odawara, 1992). The iron outer layer provides good adhesion of the coating to the inner surface of the steel pipe, while the inner layer (Al_2O_3) provides protection from corrosion and abrasion. Separation of the layers was achieved by rotating the pipe (centrifugal acceleration between 50 and

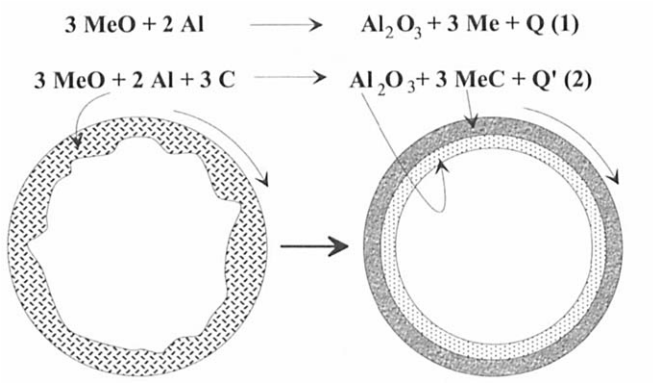

FIG. 17. The concept of centrifugal process for production of ceramic-lined steel pipes (Adapted from Odawara and Ikeuchi, 1986).

200 *g*). Some properties of the ceramic layer are presented in Table XII. The effects of adding SiO_2 and Al_2O_3 to the Fe_2O_3+2Al mixture, on the structure of pipe lining layer have been investigated (Orru' *et al.*, 1995). More complex structures were formed using multicomponent mixtures (Merzhanov and Yukhvid, 1990). For example, the Ti-C-Ni-Al-O reaction system yielded multiphase gradient layers, where the composition gradually changed from TiC-Ni cermet to the Al_2O_3+TiO_2 ceramic. The local density changed from 6.8 g/cm^3 at the cermet side, down to 3.9 g/cm^3 at the ceramic side. The production of steel pipes lined with a porous alumina–zirconia ceramic layer by reaction of Fe_2O_3+Al+Zr+additives has also been described (Li *et al.*, 1995).

TABLE XII
PROPERTIES OF THE ALUMINA-BASED CERAMIC LAYER PRODUCED BY THE CENTRIFUGAL THERMITE PROCESS[a]

Property	Value
Porosity	5.6%
Bulk density	3.86 g/cm^3
Linear expansion (293–1273 K)	8.57×10^{-6} K^{-1}
Thermal conductivity (at 293 K)	13.9 W m^{-1} K^{-1}
Resistivity (at 293 K)	2×10^7 Ω
Vickers hardness	1200 MPa
Compressive strength	>850 MPa
Bending strength	150 MPa
Bulk modulus	2.2×10^5 MPa

[a]Data from Odawara (1992).

D. Commercial Aspects

As the extent of fundamental research in the field increases, so does the feasibility of using CS technology either to produce novel materials or to replace existing commercial synthesis processes. In this section, we consider the technological and economic advantages of using CS to produce advanced materials, as well as describe some current commercial projects.

1. Technological Advantages

As noted in Section I, the CS process is characterized by high temperatures, fast heating rates, and short reaction times. These features make CS an attractive method for commercial synthesis, with the potential for new materials and lower costs, compared to conventional methods of furnace synthesis.

The typical production technologies for combustion synthesis were described in Section II. It is evident that apparatus needed for synthesis is relatively simple, especially since no additional equipment is needed for bulk heating of the material (e.g., furnaces, plasma generators, etc.). In addition, it has been reported that replacing conventional furnaces with a CS apparatus leads to significant reduction in workspace requirements (Merzhanov, 1992). Finally, owing to low power requirements, combustion synthesis technology is one of the few methods of materials synthesis that is feasible in outer space (Hunter and Moore, 1994).

In terms of operation, CS offers several advantages of production. The foremost is that the energy for synthesis is supplied solely by the heat of chemical reaction, instead of an external source. Further, when layer-by-layer combustion is organized, the heating of the reactant charge is uniform. On the other hand, heating materials by external sources results in temperature gradients during synthesis, which can lead to undesired nonuniformities in the product. This effect may be especially pronounced for large or irregular-shaped bodies. In some cases, the synthesis temperatures during CS may be higher than those attainable in conventional furnaces.

The time of production by CS methods is much shorter than that for conventional methods of powder metallurgy. Also, materials and articles can be produced directly in the combustion wave. Furthermore, a continuous mode of production may be realized, where reactants are fed at a rate equal to the combustion wave velocity.

The quality of the materials produced by CS is another important consideration. One of the attractive aspects of the process is its ability to produce materials of high purity, since the high temperatures purge the powders of any volatile impurities adsorbed on the reactants. Furthermore, the temperature gradients, combined with rapid cooling in the combustion wave, may form metastable phases and unique structures not possible by conventional methods.

TABLE XIII
COST BREAKDOWN FOR Si_3N_4 POWDER PRODUCTION[a]

Category	Conventional		SHS-based	
	Cost ($/kg)	% of Total	Cost ($/kg)	% of Total
Raw materials	9.4	27.8	9.4	33.6
Fixed costs	7.7	22.9	4.4	15.6
Utilities	0.8	2.2	0.7	2.4
Expendable materials	13.5	44.6	11.2	40.2
Labor	2.3	2.3	2.3	8.3
Total	33.7	100.0	28.0	100.0

[a]Data from Golubjatnikov *et al.* (1993).

2. *Economic Considerations*

Some comparisons of production costs by SHS and conventional processes have been reported. Analysis for Si_3N_4, AlN, and SiC materials has shown that combustion synthesis is economically favorable to existing technologies, as shown in Tables XIII, XIV, and XV (Golubjatnikov *et al.,* 1993). For all materials, the total cost per kilogram of material produced is lower for SHS-based processing than for conventional methods, with a major contribution to savings from reduced fixed costs (i.e., capital equipment costs). The significant difference in the raw material cost for SiC tiles occurs due to the use of Si+C powder mixtures in the SHS case, compared with SiC powder for conventional methods.

3. *Current Commercial Projects*

As noted recently, the scale-up of SHS reactors is nontrivial due to the extreme reaction conditions (Hlavacek and Puszynski, 1996). However, the existence of numerous manufacturing plants in the former Soviet Union demonstrates that the

TABLE XIV
COST BREAKDOWN FOR ALN TILE PRODUCTION[a]

Category	Conventional		SHS-based	
	Cost ($/kg)	% of Total	Cost ($/kg)	% of Total
Raw materials	8.2	32.0	8.2	34.9
Fixed costs	6.7	26.2	4.6	19.7
Utilities	1.9	7.2	1.8	7.7
Expendable materials	7.4	28.8	7.4	31.4
Labor	1.5	5.7	1.4	6.2
Total	25.5	100.0	23.4	100.0

[a]Data from Golubjatnikov *et al.* (1993).

TABLE XV
COST BREAKDOWN FOR SiC TILE PRODUCTION[a]

Category	Conventional		SHS-based	
	Cost ($/kg)	% of Total	Cost ($/kg)	% of Total
Raw materials	16.2	75.7	5.7	58.7
Fixed costs	2.1	10.0	0.8	8.5
Utilities	1.6	7.5	0.5	5.6
Expendable materials	0.3	1.1	0.4	4.4
Labor	1.2	5.7	2.2	22.9
Total	21.4	100.0	9.7	100.0

[a]Data from Golubjatnikov *et al.* (1993).

production of materials by SHS is feasible. To date, the following products have been manufactured commercially: powders of TiC, TiN, TiC-TiN, TiB_2, Cr_3C_2, TiC-Cr_3C_2, TiH_2, B, BN, AlN, β-Si_3N_4, nitrided ferovanadium, $MoSi_2$, ceramic insulators, lithium niobate, and nickel–zinc ferrites (Merzhanov, 1992).

The first commercial application of SHS technology was the production of $MoSi_2$ at the Kirovakan Plant (Armenia) of High-Temperature Heaters in 1979. Replacing induction furnaces with SHS technology resulted in improved productivity and product quality for this oxidation-resistant material used for high-temperature heating elements. Another example is the manufacture of abrasive TiC pastes (commercial-grade KT), which can be used for one-step grinding and polishing. The larger agglomerated TiC grains carry out the grinding, and then break up into smaller particles which polish the sample. In addition, large-scale production of articles and net-shape materials has been reported in Russia. Examples include BN-based ceramic bushings and STIM cutting inserts (Merzhanov, 1992).

In Japan, several commercial projects have been reported in the literature. For example, at the National Research Institute for Metals, the NiTi shape-memory alloy is produced by combustion synthesis from elemental powder for use as wires, tubes, and sheets. The mechanical properties and the shape-memory effect of the wires are similar to those produced conventionally (Kaieda *et al.*, 1990b). Also, the production of metal–ceramic composite pipes from the centrifugal-thermite process has been reported (Odawara, 1990; see also Section III,C,1).

In Spain, SHS Prometeus Espana AIE was created in 1993 as a joint venture between Tecnologia y Gestion de la Innovation (Spain), Empresa Nacional Santa Barbara (Spain), ISMAN (Russia), and United Technologies (USA). They have reported successful production of Si_3N_4, SiAlON, and AlN powders, as well as carbide-based composites (Cr_3C_2, Cr_3C_2-TiC) with or without a metal matrix (Borovinskaya *et al.*, 1995).

In the United States, a Georgia-based company has begun commercial production of improved high-performance titanium diboride-based materials using a

combustion synthesis process (*Chemical Engineering Progress,* 1995). This technology was developed by researchers at Georgia Institute of Technology and licensed to Advanced Engineered Materials (AEM), Woodstock, Georgia. Commercialization of the process has begun at AEM's plant, with a capacity of 1.6 million lb/yr of materials.

Currently, other U.S. companies have also acknowledged the economic benefits of combustion-synthesized materials and are involved in pilot-scale production. However, for proprietary reasons, the details are not available. It is likely that in the future, as materials produced by combustion synthesis demonstrate unique properties (e.g., nanophase and disordered materials) compared with conventional methods and its economical benefits become more evident, the technique will receive more attention.

IV. Theoretical Considerations

Progress is being made toward a theory of combustion synthesis. Much of the development to date has been based on classical combustion theory, where the emphasis is on the prediction of macroscopic characteristics, such as combustion front velocity and stability nature. Using this approach, a large number of impressive results have been obtained. However, the principal issues concerning the microstructural aspects of the process have not been resolved. In this section, we present a variety of theoretical results, as well as some remaining problems and possible ways to approach them.

A. Combustion Wave Propagation Theory in Gasless Systems

1. Combustion Wave Velocity

The application of combustion theory to gasless synthesis processes is based on a comparison of the mass and thermal diffusivities in the solid reactant mixture. In these types of systems, the Lewis number is very small:

$$\mathrm{Le} = \frac{\mathscr{D}}{\alpha} << 1 \tag{5}$$

where $\mathscr{D}$ and α are the mass and thermal diffusivities, respectively, indicating that heat conduction occurs much faster than mass diffusion. As a result, mass transfer by diffusion at the *macroscopic* scale may be neglected, and an average concentration of the reactants in any local region of the heterogeneous mixture may be used. Thus, the physical and thermal properties (e.g., density, thermal conductiv-

ity, heat capacity) are the average of reactant and product values. In this case, the combustion synthesis process is controlled only by heat evolution from the exothermic reaction and heat transfer from the reaction zone to the unreacted mixture. Thus, assuming a flat combustion wave, its propagation is described by the energy continuity equation with a heat source:

$$c_p\rho\frac{\partial T}{\partial t}=\frac{\partial}{\partial X}\left(\lambda\frac{\partial T}{\partial X}\right)+\sum_k \Phi_k(\eta,T), \tag{6}$$

where Φ_k represents a heat source or sink, and η denotes reactant conversion. For example, heat evolution from a single-stage chemical reaction, along with the chemical kinetic equation, would be presented as

$$\Phi_k = Q\rho\phi(\eta,T), \tag{7a}$$

$$\frac{\partial\eta}{\partial t}=\phi(T,\eta), \tag{7b}$$

where Q represents the heat of reaction.

Phase transformations with a significant thermal effect (e.g., melting, evaporation) are also sometimes included. For example, the effect of melting can be accounted for by introducing a negative heat source (Aldushin and Merzhanov, 1978):

$$\Phi_k = -\Delta H_{fus}\rho\delta(\Delta T)\zeta$$

$$\delta(\Delta T) = \delta(T - T_m) = \begin{cases} 0, & \text{if } T < T_m \text{ or } T > T_m \\ 1, & \text{if } T = T_m, \end{cases} \tag{8}$$

where ΔH_{fus} is the latent heat of fusion and ζ represents the fraction of reactant melted.

Similarly, heat losses from the combustion zone to the surroundings yield other types of negative sources. For convective heat losses,

$$\Phi_k = h\frac{S}{V}(T - T_a), \tag{9a}$$

where h is the convective heat transfer coefficient, S and V are the sample surface area and volume, respectively, and T_a is the temperature of the surroundings. Similarly, for heat losses by radiation,

$$\Phi_k = \epsilon_m\sigma\frac{S}{V}\left(T^4 - T_a^4\right), \tag{9b}$$

where ϵ_m is the emissivity of sample surface and σ is the Stefan–Boltzmann constant.

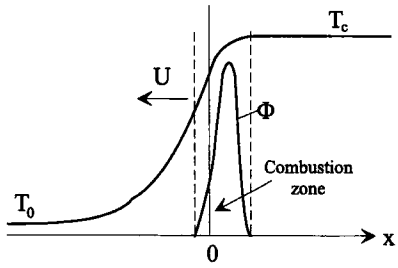

FIG. 18. Temperature and heat generation profiles in the combustion zone for a single reaction.

For a combustion wave that propagates through the reactant mixture with a velocity U, we can change to a coordinate system attached to the wave (see Fig. 18):

$$x = X + U \cdot t. \tag{10}$$

Substituting Eq. (10) into Eq. (6) yields

$$\rho c_p \frac{\partial T}{\partial t} + \rho c_p U \frac{\partial T}{\partial x} = \frac{\partial}{\partial x}\left(\lambda \frac{\partial T}{\partial x}\right) + \sum_k \Phi_k(\eta, T),$$

$$\frac{\partial \eta}{\partial t} + U \frac{\partial \eta}{\partial x} = \phi(\eta, T). \tag{11}$$

Assuming that the temperature and concentration profiles do not change with time and further that there are no heat losses (i.e., constant-pattern propagation), we can set $\partial T/\partial t$ and $\partial \eta/\partial t$ equal to zero. Then Eq. (11) takes the following form:

$$\rho c_p U \frac{dT}{dx} = \frac{d}{dx}\left(\lambda \frac{dT}{dx}\right) + \sum_k \Phi_k(\eta, T), \tag{12a}$$

$$U \frac{d\eta}{dx} = \phi(\eta, T), \tag{12b}$$

along with the boundary conditions (BCs):

$$\begin{aligned} T &= T_0, \quad \frac{dT}{dx} = 0, \quad \eta = 0 \text{ at } x \to -\infty \\ T &= T_c, \quad \frac{dT}{dx} = 0, \quad \eta = 1 \text{ at } x \to +\infty \end{aligned} \tag{13}$$

The solution of Eqs. (12) and (13) was first obtained by Zeldovich and Frank-Kamenetskii (1938) in the context of gas flames. This solution was later adapted for solid mixtures by Novozilov (1961) and others (Khaikin and Merzhanov, 1966; Hardt and Phung, 1973; Margolis, 1983). In addition to those mentioned earlier, two other assumptions are made: (1) Heat evolution in the combustion

wave is a one-stage process, due only to one chemical reaction, and (2) the rate of heat evolution may be neglected everywhere, except in a narrow zone near the maximum combustion temperature, T_c, called the *combustion* (or *reaction*) *zone,* due to the strong dependence of the reaction rate on temperature. In this section, we describe a method for estimating the combustion velocity from Eqs. (12) and (13).

Using Eq. (7), we can rewrite Eq. (12a) as

$$\frac{d}{dx}\left(\lambda\frac{dT}{dx}\right) - \rho c_p U\frac{dT}{dx} + Q\rho U\frac{d\eta}{dx} = 0. \tag{14}$$

Integrating Eq. (14) from x to $+\infty$, using BC [Eq. (13)] leads to

$$\frac{\lambda}{\rho U}\frac{dT}{dx} = Q(1 - \eta) - c_p(T_c - T). \tag{15}$$

Dividing Eq. (12b) by Eq. (15) yields

$$\frac{\rho U^2}{\lambda}\frac{d\eta}{dT} = \frac{\phi(\eta,T)}{Q(1 - \eta) - c_p(T_c - T)} \tag{16a}$$

with the following BCs:

$$\begin{aligned} \eta &= 0 \text{ at } T = T_0, \\ \eta &= 1 \text{ at } T = T_c. \end{aligned} \tag{16b}$$

From the narrow-zone approximation, the heat release function, $\phi(\eta,T)$, is negligible everywhere except near T_c. Thus replacing the value of T in the denominator of the right side of Eq. (16a) with the combustion temperature T_c yields the equation

$$\frac{\rho U^2}{\lambda}\frac{d\eta}{dT} = \frac{\phi(\eta,T)}{Q(1 - \eta)}. \tag{17}$$

For most heterogeneous reactions, the kinetic function, $\phi(\eta,T)$ may be separated into two parts, each depending on one variable alone:

$$\phi(\eta,T) = \varphi(\eta)k_0 \exp(-E/RT).$$

In this case, Eq. (17) becomes

$$\frac{\rho U^2}{\lambda}\frac{d\eta}{dT} = \frac{\varphi(\eta)k_0 \exp(-E/RT)}{Q(1 - \eta)}, \tag{18}$$

which may be integrated through a separation of variables with BCs [Eq. (16b)]:

$$\frac{\rho U^2 Q}{\lambda}\int_0^1 \frac{1 - \eta}{\phi(\eta)}d\eta = k_0\int_{T_0}^{T_c} \exp(-E/RT)dT. \tag{19}$$

Unfortunately, the right side of Eq. (19) cannot be integrated analytically owing to the nature of the exponential function. However, using the *Frank-Kamenetskii approximation,*

$$\exp(-E/RT) \cong \exp(-E/RT_c)\exp\left[\frac{-E(T - T_c)}{RT_c^2}\right]$$

so that

$$\int_{T_0}^{T_c} \exp(-E/RT)dT = \frac{RT_c^2}{E}\exp(-E/RT_c). \tag{20}$$

From Eqs. (19) and (20), we obtain the following expression:

$$U^2 = \frac{\lambda}{\rho Q}\frac{RT_c^2}{E}\frac{k_0 \exp(-E/RT_c)}{\int_0^1 \frac{1-\eta}{\varphi(\eta)}d\eta}. \tag{21}$$

This expression can be solved for various types of kinetics, $\varphi(\eta)$. A simple approach is to ignore the influence of conversion, η, on the reaction rate [i.e., $\varphi(\eta)=1$], which is reasonable to an extent, since the temperature dependence of the reaction rate is generally much stronger than the concentration dependence. This, of course, corresponds to a zero-order reaction. Using this assumption, we can solve Eq. (4.17) to yield

$$U^2 = \frac{2\lambda}{\rho Q}\frac{RT_c^2}{E}k_0 \exp(-E/RT_c), \tag{22}$$

an expression first derived by Zeldovich and Frank-Kamenetskii (1938). This formula is widely used to determine effective kinetic constants from experimental data, since

$$\ln\left(\frac{U}{T_c}\right) = -\frac{E}{2RT_c} + \text{constant}. \tag{23}$$

Thus by varying T_c (by dilution or by changing T_0) and plotting $\ln(U/T_c)$ vs. $1/T_c$, the activation energy can be obtained readily. In this manner, the effective values of E have been measured for various SHS systems (cf Munir and Anselmi-Tamburini, 1989). However, it is not clear if these reported values correspond to actual elementary processes or whether they are the result of a complex interaction between transport and reaction phenomena. The simplifying assumptions made to derive Eq. (22) were stated earlier, and they all need to be satisfied under the experimental conditions in order to obtain *intrinsic* kinetic data.

In some systems, the effect of conversion on the heterogeneous reaction rate is significant. For example, substituting n'th order type kinetics [i.e., $\varphi(\eta)=(1-\eta)^n$] into Eq. (21) yields

$$U^2 = \frac{(2-n)\lambda}{\rho Q}\frac{RT_c^2}{E}k_0 \exp(-E/RT_c). \tag{24}$$

Note that Eq. (24) is not valid for $n\geq 2$, since it leads to zero ($n=2$) and imaginary ($n>2$) values of velocity. The origin of this discrepancy is that when the dependence of reaction rate on conversion is sufficiently strong (e.g., for higher-order reactions), the reaction rate away from the adiabatic combustion temperature may also be significant (Merzhanov and Khaikin, 1988). Utilizing this idea, while maintaining the thin-zone approximation, Khaikin and Merzhanov (1966) derived an expression for the case of n'th order kinetics:

$$U^2 = \left\{2\left[\Gamma\left(\frac{n}{2}+1\right)\right]^{1-n/2}\left(\frac{n}{2e}\right)^{n^2/4}\right\}\frac{\lambda}{\rho Q}\frac{RT_c^2}{E}k_0 \exp(-E/RT_c), \tag{25}$$

where $\Gamma(z) = \int_0^\infty e^{-t}t^{z-1}dt$ is the gamma function. For a zero-order reaction, the expression in brackets equals 2, and Eq. (25) simplifies to Eq. (22). For a first-order reaction, this expression equals 1.1, as compared to 1 in Eq. (24).

The theory discussed here applies mainly to kinetic-controlled reactions. However, combustion synthesis reactions involve many processes, including diffusion control, phase transitions, and multistage reactions, which result in a complex heat release function, $\Sigma\Phi_k(\eta,T)$. An analysis of the system of combustion equations for various types of heat sources was compared with experimental data, which led to the conclusion that in general, the combustion wave velocity can be represented as follows (Merzhanov, 1990a):

$$U^2 = A(\eta^*,T^*)\exp(-E/RT^*), \tag{26}$$

where T^* and η^* are the values of temperature and corresponding conversion, respectively, which control the combustion front propagation, and $A(T^*,\eta^*)$ is a function weaker than the exponential. Based on Eq. (26), four types of combustion reactions can be identified (Merzhanov, 1977):

1. *Combustion with a thin reaction zone* (discussed earlier), where $\eta^*=1$, $T^*=T_c\approx T_0+Q/c_p$, and for which the combustion velocity is determined by the adiabatic combustion temperature
2. *Combustion with wide zone,* which occurs when a product layer strongly inhibits the reaction, and $T^*=T_0+(Q/c_p)\eta^*$, where η^* is determined from

$$\frac{Q}{c_p}\frac{\partial\phi(\eta^*,T^*)}{\partial T} + \frac{\partial\phi(\eta^*,T^*)}{\partial\eta} = 0$$

3. *Combustion with phase transformations* (e.g., melting reactants), where $T^*=T_m$ (melting point) and $\eta^*=(T_m-T_0)/(Q/c_p)$
4. *Combustion with multistage spatially separated reactions,* where $\eta_1{}^*=1$ and $T^*\approx T_0+(Q_1/c_p)$, where the subscript 1 refers to the first low-temperature stage of the complex reaction.

2. *Temperature Profiles*

The temperature profile for the preheating zone of the combustion wave can be derived readily by introducing the variable $q=\lambda\, dT/dx$ for the heat flux, so that Eq. (14) rearranges as

$$q\frac{dq}{dT} - \rho c_p U q + \lambda Q \rho \phi(\eta,T) = 0, \tag{27}$$

and BCs [Eq. (13)] take the following form:

$$\begin{aligned} q &= 0, \quad \eta = 0 \text{ at } T = T_0, \\ q &= 0, \quad \eta = 1 \text{ at } T = T_c. \end{aligned} \tag{28}$$

Because there is no heat evolution in the preheating zone, we can neglect the third term of Eq. (27):

$$\frac{dq}{dT} - \rho c_p U = 0; \qquad x \le 0. \tag{29}$$

Direct integration of Eq. (29) with BCs [Eq. (28)] yields the Michelson (1930) solution for the temperature profile in the preheating zone:

$$T = T_0 + (T_c - T_0)\exp\left(\frac{U}{\alpha}x\right), \qquad x \le 0,$$

where $\alpha=\lambda/(\rho c_p)$, and $x_T=\alpha/U$ denotes the characteristic length scale of the combustion wave. Classic combustion theory does not describe the temperature profile in the reaction zone, since it is assumed to be close to T_c. For the four types of combustion synthesis reactions just discussed, the corresponding temperature profiles are shown schematically in Fig. 19a–d. The actual temperature profile may be a combination of several elemental ones (cf Zenin *et al.*, 1980, 1981). Some computer simulations of gasless combustion synthesis exhibit the temperature profile shown in Fig. 19e, where the temperature of the combustion front may exceed T_c^{ad} (Huque and Kanury, 1993). It is interesting to note that this profile resembles early works in combustion of gases, where an ignition temperature model was used (Mallard and Le Chatelier, 1883; Mason and Wheeler, 1917; Daniel, 1930).

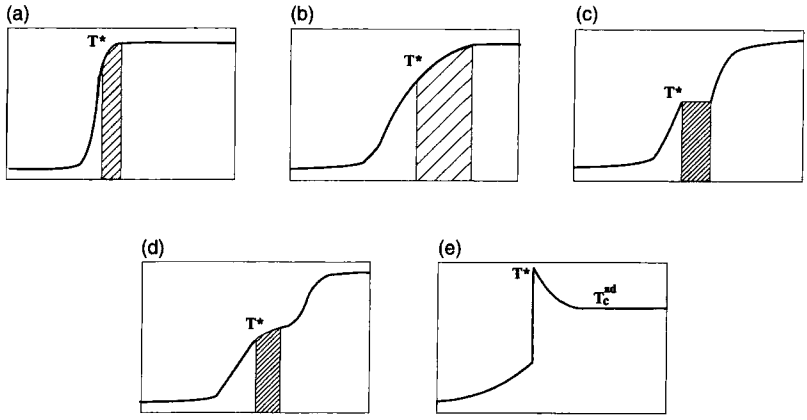

FIG. 19. Elementary temperature profiles of SHS propagation.

B. MICROSTRUCTURAL MODELS

While providing a simple method for analyzing the redistribution of energy in the combustion wave, the models discussed in the previous section do not account for the local structural features of the reaction medium. *Microstructural models* account for details such as reactant particle size and distribution, product layer thickness, etc., and correlate them with the characteristics of combustion (e.g., U, T_c).

The equations used to describe the combustion wave propagation for microstructural models are similar to those in Section IV,A [see Eq. (6)]. However, the kinetics of heat release, Φ_k, may be controlled by phenomena other than reaction kinetics, such as diffusion through a product layer or melting and spreading of reactants. Since these phenomena often have Arrhenius-type dependences [e.g., for diffusion, $\mathcal{D}=\mathcal{D}_0 \exp(-E_D/RT)$], microstructural models have similar temperature dependences as those obtained in Section IV,A. Let us consider, for example, the dependence of velocity, U, on the reactant particle size, d, a parameter of medium heterogeneity:

$$U=f(d)F(T). \tag{30}$$

The first microstructural models were developed independently and essentially simultaneously (Aldushin *et al.*, 1972a,b; Hardt and Phung, 1973; Aldushin and Khaikin, 1974). For these models, the elementary reaction cell, which accounts for the details of the microstructure, consists of alternating lamellae of the two reactants (A and B), which diffuse through a product layer (C), to react (see Fig. 20a). Assuming that the particles are flat allows one to neglect the change in reac-

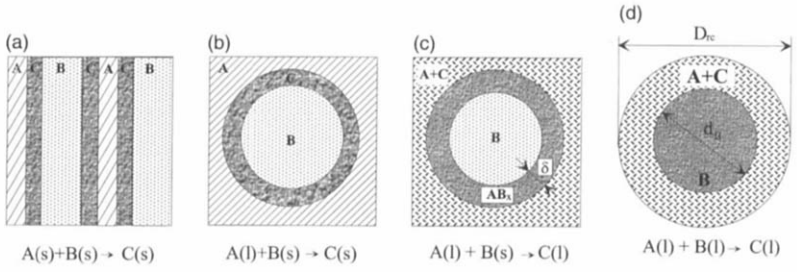

FIG. 20. Geometry of the reaction cells considered in the theoretical models.

tion surface area during synthesis. The characteristic particle size, d, is equivalent to the layer thickness, and the relative thicknesses of the initial reactant layers are determined by stoichiometry.

Hardt and Phung (1973) developed a simple analytical solution for the case of diffusion-controlled kinetics, and found that $f(d) \propto 1/d$. A more accurate expression, based on the same physical geometry, was developed by Aldushin *et al.* (1972b) using the following kinetic function:

$$\phi(\eta,T) = k_0 \exp(-E/RT) e^{-m\eta} \eta^{-n}, \tag{31}$$

which describes linear ($m=0$, $n=0$), parabolic ($m=0$, $n=1$), cubic ($m=0$, $n=2$), and exponential ($m>0$, $n=0$) kinetic dependences. The solution of Eqs. (6) and (7) for power-law kinetics (i.e., $m=0$, $n \geq 0$) yields

$$U = \frac{(n+1)(n+2)}{d^{n+1/2}} F(T), \tag{32}$$

and for exponential kinetics leads to:

$$U = \frac{m^2}{(e^m - 1 - m)d} F(T). \tag{33}$$

The velocity can also be calculated for polydispersed systems with a particle size distribution function, $\chi(d)$ (Aldushin *et al.*, 1976a). For a unimodal particle size distribution, an effective particle size, d_{eff}, defined as

$$d_{\text{eff}} = \left[\int_{d_{\min}}^{d_{\max}} d^2 \chi(d) dd \right]^{1/2},$$

where $d_{\max}$ and $d_{\min}$ are the upper and lower size limits, respectively, can be used in expressions such as Eqs. (32) and (33). For a bimodal distribution, the combustion wave has a two-stage structure similar to the multistage chemical reactions (Fig. 19d), where two combustion fronts propagate in sequence. Using ef-

fective particle sizes for fine (d_1) and coarse (d_2) particles, the velocity dependence for the *leading* combustion front is described by the following equation:

$$U = \frac{F(T)}{[d_1^2 m_1 + d_2^2(1 - m_1)]^{1/2}}, \tag{34}$$

where m_1 is the mass fraction of finer particles.

For the next two types of theoretical models, the elementary reaction cell consists of a spherical particle of one reactant surrounded by a melt of the other reactant. In the first case, the product layers (C) grow on the surface of the more refractory particles (B) due to diffusion of atoms from the melt phase (A) through the product layer (see Fig. 20b). At a given temperature, the concentrations at the interphase boundaries are determined from the phase diagram of the system. Numerical calculations by Nekrasov *et al.* (1981, 1993) have shown satisfactory agreement with experimental results for a variety of systems.

The second model (Fig. 20c) assumes that upon melting of reactant A, a layer of initial product forms on the solid reactant surface. The reaction proceeds by diffusion of reactant B through this layer, whose thickness is assumed to remain constant during the reaction (Aleksandrov *et al.*, 1987; Aleksandrov and Korchagin, 1988). The final product crystallizes (C) in the volume of the melt after saturation. Based on this model, Kanury (1992) has developed a kinetic expression for the diffusion-controlled rate. Using this rate equation, an analytical expression for the combustion wave velocity has been reported (Cao and Varma, 1994)

$$U = \left[\frac{1}{d}\left(\frac{2}{d} + \frac{1}{\delta}\right)\right]^{1/2} F(T), \tag{35}$$

where δ is the thickness of the initial product layer.

For the case where both reactants melt in the preheating zone and the liquid product forms in the reaction zone, a simple combustion model using the reaction cell geometry presented in Fig. 20d was developed by Okolovich *et al.* (1977). After both reactants melt, their interdiffusion and the formation of a liquid product occur simultaneously. Numerical and analytical solutions were obtained for both kinetic- and diffusion-controlled reactions. In the kinetic-limiting case, for a stoichiometric mixture of reactants (A and B), the propagation velocity does not depend on the initial reactant particle sizes. For diffusion-controlled reactions, the velocity can be written as

$$U = \frac{\bar{b}}{d} \cdot F(T), \tag{36}$$

where

$$\bar{b} = \begin{cases} 1 & , \quad \text{if } d < d_B^{st} \\ \dfrac{d^3}{D_{rc}^3 - d^3} \cdot \dfrac{\nu_B MW_B}{\nu_A MW_A}, & \text{if } d > d_B^{st}. \end{cases}$$

Here d_B^{st} is the diameter of the refractory reactant (B) in a corresponding stoichiometric mixture, and D_{rc} is diameter of the reaction cell.

The microstructural models described here represent theoretical milestones in gasless combustion. Using similar approaches, other models have also been developed. For example, Makino and Law (1994) used the solid–liquid model (Fig. 20c) to determine the combustion velocity as a function of stoichiometry, degree of dilution, and initial particle size. Calculations for a variety of systems compared favorably with experimental data. In addition, an analytical solution was developed for diffusion-controlled reactions, which accounted for changes in λ, ρ, and c_p within the combustion wave, and led to the conclusion that $U \propto 1/d$ (Lakshmikantha and Sekhar, 1993).

C. Cellular Models

As discussed in previous sections, the reaction medium for the study of combustion wave propagation in powder mixtures is typically assumed to be quasihomogeneous. The implicit assumption is that the width of the heat release zone is much larger than the heterogeneous scale of the medium. In other words, a reacting particle can be considered as a point heat source within the combustion zone. Thus, we replace the heterogeneous system with a homogeneous medium, characterized by some effective thermal properties. As a result, the relations for heat release and transport in a homogeneous medium can be used, as in the classical theory of flame propagation.

Cellular models (Kottke and Niiler, 1988; Astapchik *et al.*, 1993; Hwang *et al.*, 1997) represent another direction for modeling the combustion synthesis process. For these models, the reaction medium is tessellated into a discrete matrix of cells, where the temperature and effective properties are assumed to be uniform throughout the cell. The interactions between the cells are based on various rules, often a discretized form of the heat conduction equation.

At this point, a distinction should be made between cellular and finite difference/element models. The latter are finite approximations of continuous equations [e.g., Eq. (11)], with the implicit assumption that the width of the reaction zone is larger than other pertinent length scales (diffusion, heterogeneity of the medium, etc.). However, no such assumptions need to be made for cellular

models, and thus local transport processes in a heterogeneous medium can be accounted for (Hwang *et al.*, 1997).

As with continuous models, the basis of cellular models in CS is the simulation of heat conduction and reaction [see Eq. (11)]. The discrete form of this equation is often given as

$$[\rho c_p]^{(i,j)} \frac{\partial T^{(i,j)}}{\partial t} = \left(\lambda_x \frac{\partial T}{\partial x}\bigg|^{\left(i+\frac{1}{2},j\right)} - \lambda_x \frac{\partial T}{\partial x}\bigg|^{\left(i-\frac{1}{2},j\right)}\right) + \left(\lambda_y \frac{\partial T}{\partial y}\bigg|^{\left(i,j+\frac{1}{2}\right)} - \lambda_y \frac{\partial T}{\partial y}\bigg|^{\left(i,j-\frac{1}{2}\right)}\right) + \left[\rho Q \frac{\partial \eta}{\partial t}\right]^{(i,j)}, \tag{37}$$

where (i,j) refers to the (x,y) position in the grid coordinates. The thermal conductivity and temperature gradient between cells, respectively, are:

$$\lambda_x\bigg|^{\left(i+\frac{1}{2},j\right)} = \frac{2\lambda_x^{(i+1,j)}\lambda_x^{(i,j)}}{\lambda_x^{(i+1,j)} + \lambda_x^{(i,j)}}, \qquad \frac{\partial T}{\partial x}\bigg|^{\left(i+\frac{1}{2},j\right)} = \frac{T^{(i+1,j)} - T^{(i,j)}}{\Delta x}, \tag{38}$$

and similarly for λ_y and $\partial T/\partial y$.

In an early work by Kottke and Niiler (1988), a cellular model was used to simulate the combustion wave initiation and propagation for the Ti+C model system. The interactions between neighboring cells were described by the electrical circuit analogy to heat conduction. At the reaction initiation temperature (i.e., melting point of titanium), the cell is instantly converted to the product, TiC, at the adiabatic combustion temperature. The cell size was chosen to be twice as large as the Ti particles (44 μm). Experimentally determined values for the green mixture thermal conductivity as a function of density were used in the simulations. As a result, the effects of thermal conductivity of the reactant mixture on combustion wave velocity were determined (see Fig. 21). Advani *et al.* (1991) used the same model, and also computed the effects of adding TiC as a diluent on the combustion velocity.

In a similar manner, Bowen and Derby (1993) developed a cellular model for the reaction

$$3TiO_2 + 4Al + 3C \rightarrow 3TiC + 2Al_2O_3.$$

The one-dimensional form of Eq. (37) was used to describe the distribution of energy in the system. Also, the ignition temperature kinetics were used, where the cell instantly converts to TiC and Al_2O_3 when the ignition temperature (900°C) is reached (determined from DTA experiments). In addition, heat losses due to convection and radiation from the first cell were also taken into account.

The size of the cells was comparable to the largest powder size (i.e., Al). The thermal conductivity of each *phase* was determined using a model developed by Luikov *et al.* (1968), with the thermal conductivity of the *cell* determined using

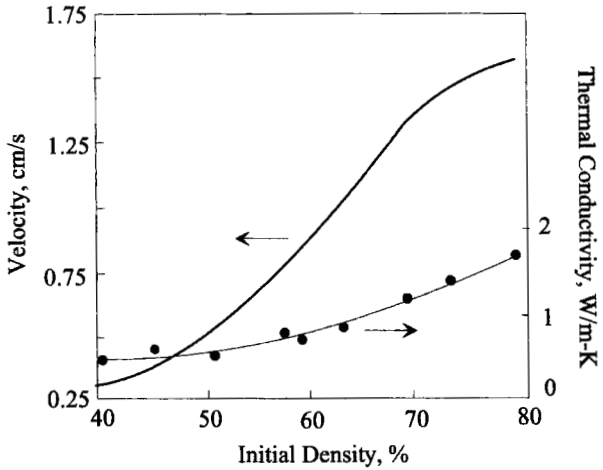

FIG. 21. Thermal conductivity of titanium and graphite compacts and predicted combustion velocity, as a function of sample density (Adapted from Kottke *et al.*, 1990).

the three-phase rule (Brailsford and Major, 1964). The temperature–time profiles were analyzed (see Fig. 22) and compared to the mechanism of structural transformation (i.e., melting of aluminum, solidification of alumina). The effect of varying cell size (i.e., the diameter of the Ti particle) was also considered for the Ti+2B system, where the reaction velocity decreased with increasing cell size.

Another application of cellular models was based on a stochastic, rather than deterministic, approach (Astapchik *et al.*, 1993). Based on the same equations for heat transfer as described earlier, the criterion for ignition was not when the tem-

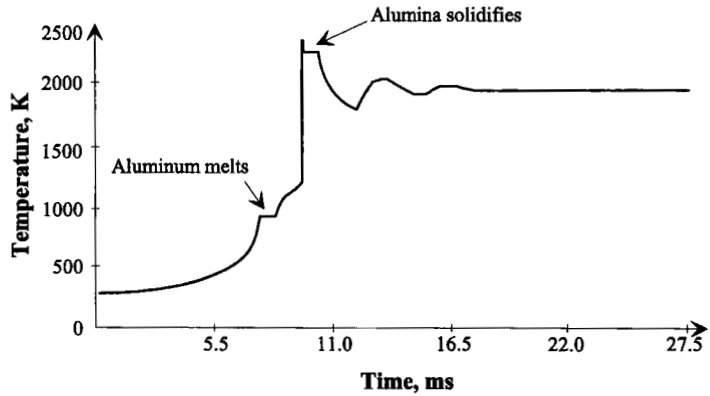

FIG. 22. Temperature–time profile of a single cell for the TiO_2-Al-C reaction (Adapted from Bowen and Derby, 1993).

perature of the cell reached an ignition temperature, but the *probability* that it would react (as a function of temperature of the cell):

$$p(T) = k_0 \tau \cdot \exp\left(-\frac{E}{RT}\right), \tag{39}$$

where τ is the time step and k_0 is the preexponential factor for the reaction rate. The stochastic approach accounts for any nonuniform surface structure, shape, size, etc. The results of the simulations were compared to deterministic velocities. The occurrence of oscillatory unstable behavior and its dependence on cell size was also studied using this approach.

In all the cellular models described, the cells throughout the medium were initially uniform. A *microheterogeneous cell model* has recently been developed, where the cells have varying initial properties (Hwang *et al.*, 1997). In such a model, the *structure* of the reaction medium is stochastic, and the heterogeneity of the reactant medium is considered explicitly. For example, the structure can be described as a regular two-dimensional matrix of circular cylinders (with nominally flat sides) in contact, with a number of cylinders randomly removed until the ratio of the voids to total volume equals the porosity (Fig. 23a). The cylinder diameter is assumed to be similar to the particle diameter.

The porous structure is divided into cells of dimension l (see Fig. 23b). An elastic contact model (Cooper *et al.*, 1969) is used to describe the contact region between two particles, which is related to the loading pressure and mechanical

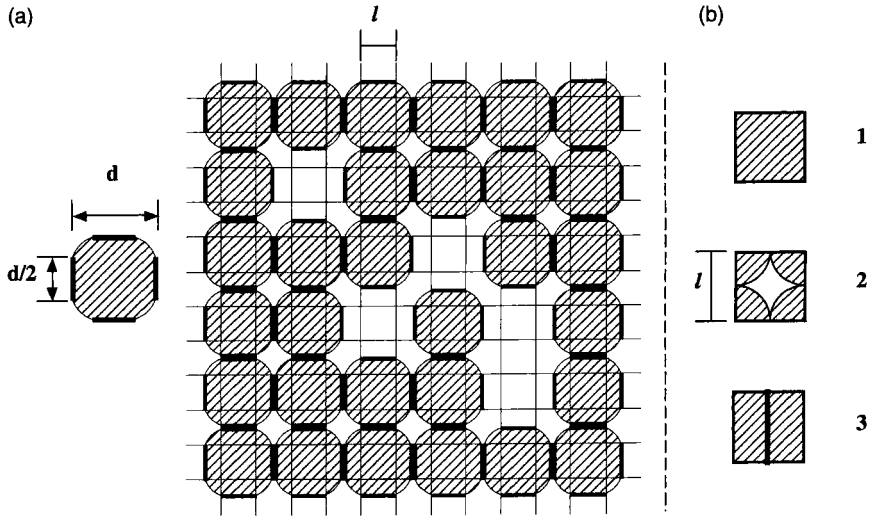

FIG. 23. Model structure of porous reaction medium: (a) Overall view, (b) schematic diagram of cell model structure.

properties of the particle. This gives rise to three basic cell types, which consist of "cores" (Fig. 23b, 1), "interstices" (Fig. 23b, 2), and "edges" (Fig. 23b, 3). The cylinder cores (Fig. 23b, 1) have the highest thermal conductivity corresponding to the bulk value for the solid, while the interstices (Fig23b, 2) have the lowest value owing to a large fraction of gas. The cylinder edges have an intermediate thermal conductivity, which corresponds to the thermal contact resistance between two particles. To determine the effective thermal conductivity of each cell, the work of Goel *et al.* (1992) was used, which accounts for the distribution of phases within the cell. The heat transfer between cells is described by Eq. (37). It is assumed that the reaction within the cell is initiated when the cell reaches a certain ignition temperature.

With this model, the microstructure of the combustion wave was studied, and compared with experimental results (Hwang *et al.*, 1997; Mukasyan *et al.*, 1996). For example, sequences of combustion front propagation at the microscopic level, obtained experimentally and by calculation, are shown in Fig. 24. In addition, it was demonstrated that fluctuations in combustion wave shape and propagation correlate with the heterogeneity of the reactant mixture (e.g., porosity and particle size).

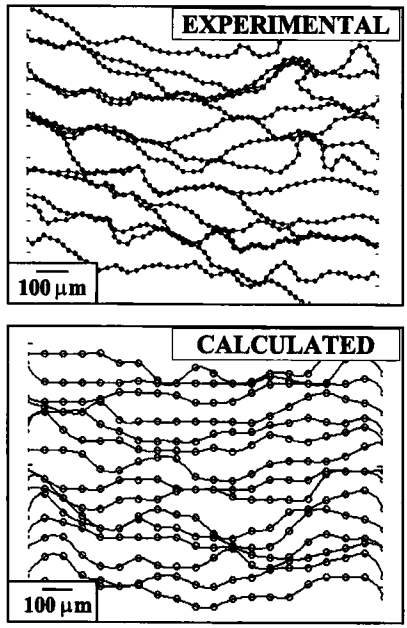

FIG. 24. Profiles of the experimental and calculated combustion wave microstructure.

D. Stability of Gasless Combustion

The stability of combustion wave propagation is an important factor in determining the quality of materials produced by CS. To produce uniform product, a stable combustion regime is desired. Furthermore, it is also important to know the boundaries where combustion, stable or unstable, can propagate.

From classic combustion theory (Zeldovich *et al.*, 1985), the following two conditions must be satisfied for a constant pattern combustion wave with thin reaction zone to be self-propagating:

$$\beta = \frac{RT_c}{E} \ll 1, \gamma = \frac{c_p}{Q}\frac{RT_c^2}{E} = \frac{c_pT_c}{Q}\beta = \frac{RT_c^2}{E(T_c - T_0)} \ll 1, \tag{40}$$

so that the wave velocity can be computed using Eq. (21).

Numerical results indicate, however, that a condition weaker than Eq. (40) is sufficient to ensure constant-pattern propagation (Aldushin *et al.*, 1978):

$$\Psi = \gamma - \beta = \frac{RT_0T_c}{E(T_c - T_0)} \ll 1. \tag{41}$$

In essence, the preceding conditions require the reaction rate at the combustion temperature, T_c, to be much greater than that at the initial temperature, T_0. The ratio of reaction rates at the two temperatures is proportional to

$$\frac{\exp(-E/RT_c)}{\exp(-E/RT_0)} = \exp\left(-\frac{1}{\Psi}\right). \tag{42}$$

Puszynski *et al.* (1987) have suggested the use of the homogeneous explosion criterion for the existence of constant-pattern propagation:

$$\frac{2RT_c}{E}\left(\frac{2T_c}{T_c - T_0} + 1\right) < 1, \tag{43}$$

which may be rearranged as

$$2\gamma + \beta < \frac{1}{2}. \tag{44}$$

According to the theory of Zeldovich (1941) developed for premixed gas flames, the velocity of the combustion front just before the wave ceases to propagate (e.g., by addition of inert dilent of mole fraction, b) is lower, compared to the maximum value (i.e., with no diluent added), by a factor of $\sqrt{e}$. It was shown experimentally that this conclusion can also be applied to gasless systems with a narrow reaction zone (Maksimov *et al.*, 1965). Based on this idea and using Eq.

(22), Munir and Sata (1992) have suggested a criterion to determine the SHS/non-SHS boundary:

$$\left(\frac{U^{\max}}{U^{\min}}\right)^2 = (1-b)\left(\frac{T^{\max}}{T^{\min}}\right)^2 \exp\left[-\frac{E}{R}\left(\frac{1}{T^{\max}}-\frac{1}{T^{\min}}\right)\right] = e, \qquad (45)$$

where the superscript "max" refers to the maximum combustion temperature (T_c) and "min" corresponds to the lowest combustion temperature where the reaction wave will still propagate. Based on Eq. (45), an interesting method to describe the regimes of combustion synthesis (called *SHS diagrams*) was proposed, and a good match with experimental data for a variety of systems was reported (Munir and Sata, 1992; Munir and Lai, 1992). An example of such a diagram for the TiB_2 synthesis is shown in Fig. 25.

A stability criterion for steady wave propagation was developed by numerical calculation, in the form of an approximate relation (Shkadinskii *et al.*, 1971):

$$\alpha_{st} = \left(9.1\frac{T_c}{T_c - T_0} - 2.5\right)\frac{RT_c}{E}. \qquad (46)$$

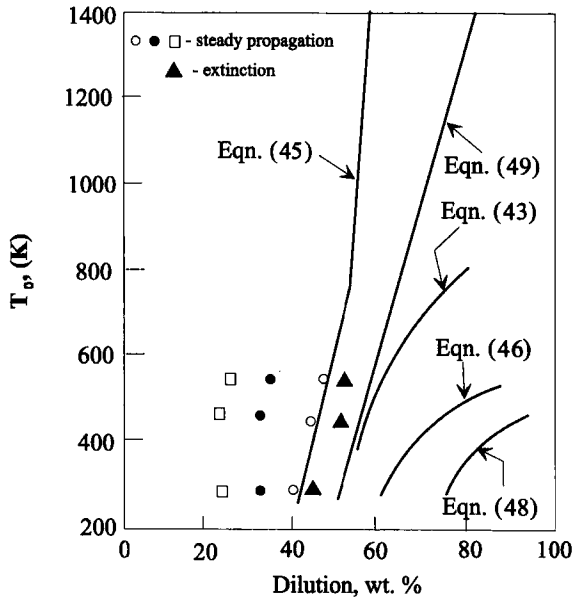

FIG. 25. The SHS diagram for TiB_2 synthesis (Adapted from Munir and Sata, 1992). The curves are computed values; the symbols represent experimental data.

The boundary separating the steady and oscillating combustion modes is given by the following conditions:

$$\begin{aligned} &\alpha_{st} > 1, \text{ stable steady-state combustion,} \\ &\alpha_{st} < 1, \text{ oscillatory combustion.} \end{aligned} \tag{47}$$

Formula (46) is in good agreement with an analytical criterion for stable propagation under the condition of a narrow reaction zone (Makhviladze and Novozilov, 1971; Matkowsky and Sivashinsky, 1978):

$$\frac{E(T_c - T_0)}{2RT_c^2} < (2 + \sqrt{5}). \tag{48}$$

For the case of melting reactants (Margolis, 1983, 1985), the stability criterion is modified as follows:

$$\frac{E(T_c - T_0)}{2RT_c^2\left\{1 - \exp\left[\dfrac{E(T_c - T_m}{RT_c^2}\right]\right\}} < (2 + \sqrt{5}). \tag{49}$$

Based on Eq. (49), it can be concluded that for gasless combustion processes, unstable combustion is more likely to occur for higher melting temperatures, T_m, in addition to higher activation energies and lower combustion temperatures (Margolis, 1992).

An interesting application of stability analysis was performed for the case of porous samples with melting and flow of reactants (Aldushin *et al.*, 1994a). It was determined how various parameters of the system affect stability, and the pulsing instabilities of uniformly propagating solutions were found. These instabilities can result in nonuniform composition of the product.

Analysis of the theoretical expressions proposed for the boundaries between stable propagation and oscillations, as well as between combustion and noncombustion regions, leads one to the conclusion that in spite of good agreement of theory with experimental data reported in some cases, a direct comparison is generally not available for most SHS systems. In this context, we agree with Novozilov (1992), who concluded that current theoretical results cannot be compared quantitatively with experimental data. According to his analysis, this is due, first, to the fact that in analytical and numerical investigations, the mechanism chosen to simulate combustion process was oversimplified. Thus, for example, most theoretical studies assume an infinitely narrow reaction zone, and the majority of the computations were performed for one-step reactions. In addition, accurate thermophysical and kinetic data are not available for the extreme conditions associated with the combustion wave. Hence, new experimental results describ-

ing the detailed mechanisms of combustion synthesis must be obtained in order to develop the theory further and to bridge the gap between the often abstract mathematical approach and the experimental reality of the process. Experimental techniques that provide details about the reaction mechanism are described in Section VI.

E. Filtration Combustion Theory

In contrast with the theory for gasless reactions (Sections IV,A and IV,B), which was adapted from classical combustion theory, filtration combustion (FC) theory was developed specifically to describe gas–solid reactions in CS (Merzhanov *et al.*, 1972; Aldushin *et al.*, 1974).

A general schematic of FC is shown in Fig. 26. The initial reaction medium consists of a porous matrix of solid reactants and inert diluents, where the pores are filled with gas-phase reactants. The combustion front propagates through the sample with a velocity, U, due to the chemical interaction between the gas- and condensed-phase reactants. Behind the front, the final product is formed, which in some cases may approach poreless structure, since the volume of the final product grains is typically greater than that of reactant particles. The amount of reactant gas present in the pores decreases rapidly in the combustion front owing to the intense gas–solid reaction. The resulting pressure gradient is the driving force for infiltration of gas from the surroundings, which transports the gas-phase reactant and thermal energy (by convection). With this type of combustion, the important consideration is the availability and permeability of reactant gas to the reaction zone.

Depending on reaction and permeation conditions, two modes of FC can be defined: *natural* and *forced* filtration. In the first case, infiltration flow is a consequence of the natural pressure gradient between the atmosphere (typically constant) and the reaction zone. In the second case, forced gas flow is induced by

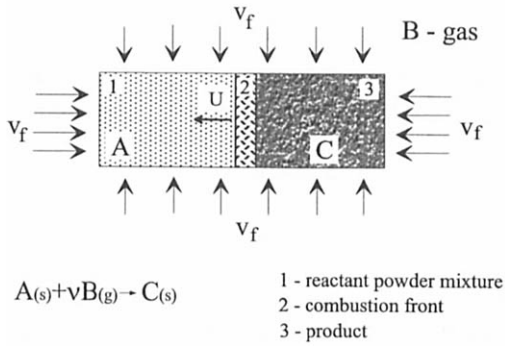

Fig. 26. Schematic of filtration combustion.

maintaining a pressure gradient along the sample. In general, current SHS technologies are based on the natural filtration combustion mode.

For natural permeation combustion, the reactant gas may flow in either the same (cocurrent flow, Fig. 27a) or opposite (countercurrent flow, Fig. 27b) direction as that of combustion wave propagation, and in some cases even in both directions Fig. 27c). One-dimensional flow regimes can be achieved by placing the sample in a quartz tube, which in turn can be closed at one end (Pityulin *et al.*, 1979). In the general case (see Fig. 26), the reactant gas also enters from the side surface, and the process can be described by two- or three-dimensional numerical simulations (cf Ivleva and Shkadinskii, 1981; Dandekar *et al.*, 1990, 1993). In this section, results for the simpler one-dimensional case are analyzed and features of the higher dimensional studies are briefly discussed.

1. One-Dimensional Models with Natural Permeation of Gas

Let us consider the reaction front propagation for a binary system:

$$A(s)+\nu B(g)\rightarrow C(s,l).$$

In addition to equations for heat conduction and chemical kinetics used for gasless systems [cf Eq. (6)], gas–solid reactions require equations describing the

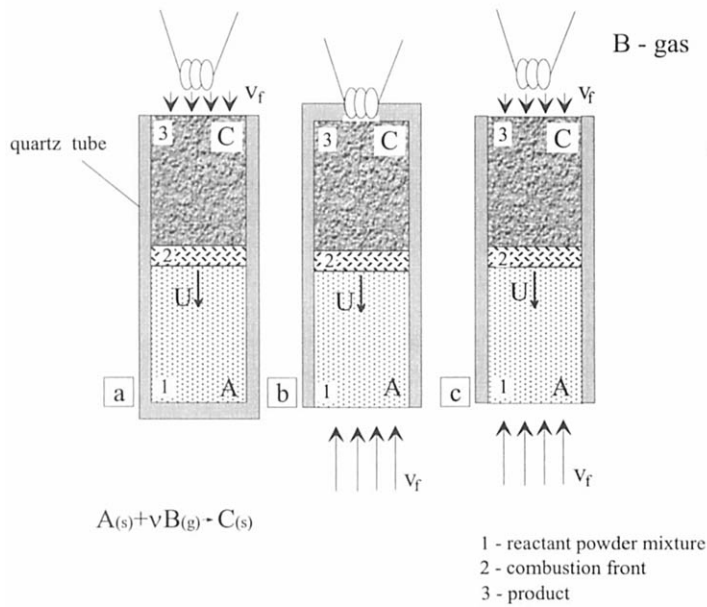

FIG. 27. Different types of filtration combustion (one-dimensional schemes).

mass balance for the gas-phase reactant, gas flow, and equation of state. In this case, stable combustion wave propagation with velocity U, where the coordinates are attached to the moving front, is described by the following set of equations (Aldushin *et al.*, 1976b):

$$U\frac{dT}{dx} = \alpha\frac{d^2T}{dx^2} + qU\frac{d\eta}{dx}, \tag{50}$$

$$\frac{d}{dx}(U\rho_g + v_f\rho_g) = -\nu\rho_s U\frac{d\eta}{dx}, \tag{51}$$

$$U\frac{d\eta}{dx} = W(\eta,T,p), \tag{52}$$

$$\rho_g = \frac{\epsilon p}{RT}, \qquad v_f = -k_f\frac{dp}{dx}, \tag{53}$$

where

$$q = \frac{Q}{c_{p,s}(1 + \Delta \cdot \eta_c)}, \quad \alpha = \frac{\lambda}{c_{p,s}\rho_s(1 + \Delta \cdot \eta_c)}, \quad \Delta = \nu\frac{c_{p,g}}{c_{p,s}}$$

and p is the gas pressure, ϵ is the sample porosity, ρ_i is the amount of reactant i per unit sample volume, $c_{p,i}$ is the specific heat of reactant i, λ is the effective thermal conductivity of the porous medium, v_f is velocity of gas filtration, k_f is the permeability coefficient (k/μ), $W(\eta,T,P)$ is the chemical reaction rate, ν is the stoichiometric coefficient of the gas reactant, and the subscripts "s" and "g" refer to the solid and gas reactants, respectively.

Because it is difficult to account for changes in the properties of the reaction medium (e.g., permeability, thermal conductivity, specific heat) due to structural transformations in the combustion wave, the models typically assume that these parameters are constant (Aldushin *et al.*, 1976b; Aldushin, 1988). In addition, the gas flow is generally described by Darcy's law. Convective heat transfer due to gas flow is accounted for by an effective thermal conductivity coefficient for the medium, that is, quasihomogeneous approximation. Finally, the reaction conditions typically associated with the SHS process ($T \geq 2000$ K and $p < 10^3$ MPa) allow the use of ideal gas law as the equation of state.

According to Aldushin *et al.* (1976b), there are two characteristic length scales that should be compared to examine the filtration of reactant gas from the atmosphere to the reaction front: the length of the sample, L, and the length of the filtration during combustion, l_f. If the characteristic filtration length is much shorter than that of the sample ($l_f << L$), then there is no filtration from the atmosphere to the combustion front, and the reaction propagation occurs only due to the gas present initially in the pores. On the other hand, when the characteristic length of fil-

tration is much longer than the sample length ($l_f >> L$), the reactant gas permeates from the atmosphere to the combustion front. In both cases, the reactant gas may infiltrate to the sample in the postcombustion zone *after* the combustion front has passed.

a. Combustion without Filtration to the Reaction Front from the Atmosphere. Because only the gas initially in the sample pores is available for propagation of the combustion wave, in practice, this FC regime can be realized at relatively high reactant gas pressures. For example, the minimum nitrogen pressures (p_0^{cr}) required to form nitrides from samples with initial porosities equal to 50% are presented in Table XVI. At such pressures, the amount of reactant gas in the sample pores is sufficient for full conversion to the final product. However, thermal expansion in the preheating zone and gas consumption in the reaction zone lead to pressure gradients in the medium. Thus, gas permeation within the sample may become an important factor for combustion front propagation.

Analysis of Eqs. (50)–(53), along with the BCs:

$$\begin{aligned} x &\to -\infty, \quad T = T_0, \quad \eta = 0, \quad p = p_0, \\ x &\to +\infty, \quad T = T_c, \quad \eta = \eta_c, \quad p = p_c, \end{aligned} \tag{54}$$

demonstrates that another dimensionless parameter, L_f, can be defined (Aldushin *et al.*, 1976b):

$$L_f = \frac{l_f}{x_T} = \frac{k_f p_0 / 2U}{\alpha / U} = \frac{k_f p_0}{2\alpha}, \tag{55}$$

which is the ratio of the filtration zone length, l_f, to the thermal length scale of combustion, x_T. Although analogous to the Lewis number, Le, the filtration parameter, L_f, is not assumed to be much smaller than unity [cf Eq. (5)], and can vary significantly for different conditions. Values for L_f are presented in Table XVII for

TABLE XVI
CRITICAL NITROGEN PRESSURES (p_0^{cr}) FOR COMPLETE CONVERSION (AT T = 300 K, ϵ = 0.5)

System	Product	Critical Pressure (atm)
Nb–N_2	NbN	885
Zr–N_2	ZrN	900
Ta–N_2	TaN	1000
Ti–N_2	TiN	1170
Al–N_2	AlN	1250
Si–N_2	Si_3N_4	1375
B–N_2	BN	2700

TABLE XVII
VALUES OF FILTRATION PARAMETERS FOR VARIOUS SOLID-NITROGEN SYSTEMS

System	p_0 (N/m^2)	α (m^2/s)	k_f [m^4/(N·s)]	L_f	L_f^{cr}	L_f/L_f^{cr}
Zr–N_2	10^5–10^7	10^{-4}	10^{-8}	10–10^2	~7	~1–10^2
Ta–N_2	2×10^6–3×10^8	2×10^{-5}	4×10^{-11}	10^2	10	10
Si–N_2	10^{-7}	10^{-7}	10^{-15}	~10^{-1}	~7	10^{-2}
B–N_2	3×10^8	10^{-7}	10^{-18}	~10^{-3}	~8	10^{-4}

various gas–solid systems at different initial pressures. The filtration parameter has been shown to determine the pressure distribution in the combustion wave (cf Aldushin, 1988). If L_f is above some critical value ($L_f^{cr}=T_c/T_0$), then the pressure decreases monotonically to the reaction front (Fig. 28a). Otherwise, a maximum in calculated pressure is observed (Fig. 28b), due to gas expansion in the preheating zone when the permeability of the medium is low. From a practical point of view, elevated pressures in the combustion front may adversely affect product quality, since cracks may form in the material. However, these reaction conditions may also yield unique phase compositions, such as cubic boron nitride (Borovinskaya, 1977).

Using Eqs. (50)–(53), along with the narrow-zone approximation, an expression for the combustion velocity in gas–solid systems can be obtained that is sim-

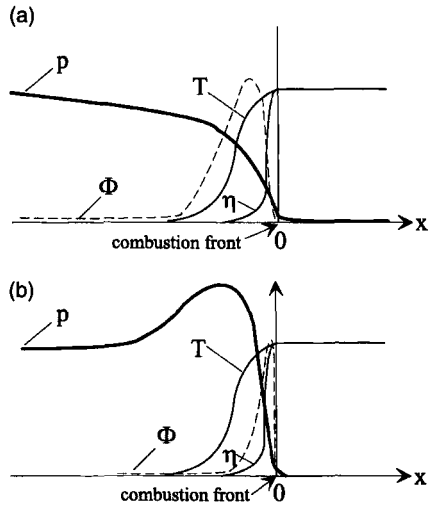

FIG. 28. Gas pressure (p), temperature (T), conversion (η), and heat release function (Φ) distributions in the combustion front: (a)$L_f/L_f^{cr} > 1$; (b) $L_f/L_f^{cr} < 1$ (Adapted from Aldushin *et al.*, 1976b).

ilar to that derived for gasless systems [Eq. (21)]. For this, let us consider a reaction rate function of the form

$$W(\eta,T,p) = \frac{d\eta}{dt} = k_0 \exp(-E/RT) \cdot f(\eta) \cdot p^m, \tag{56}$$

where $f(\eta)$ is the dependence of reaction rate on conversion of the solid reactant and m is the reaction order relative to the gaseous reactant. Using these kinetics and assuming an average gas pressure, $\bar{p}$, in the reaction zone, we obtain (Aldushin, 1988)

$$U^2 = \frac{\lambda \cdot F(\eta) \cdot k_0 \exp(-E/RT_c)}{Q(T_c)\rho_s} \cdot \frac{RT_c^2}{E} \cdot (\bar{p})^m, \tag{57}$$

where the function $F(\eta)$ depends on $f(\eta)$. For kinetics $f(\eta)=\eta^{-n}$, describing reaction retardation by the product layer, the function $F(\eta)$ becomes

$$F(\eta) = (n+1)\,(n+2). \tag{58}$$

As a result, the only convenient method for controlling the combustion velocity is by varying the average gas pressure, $\bar{p}$, in the reaction zone. For the case of excess gas reactant ($\nu_0=\rho_{g0}/\rho_{s0}>\nu$), $\bar{p}$ is approximately equal to the gas pressure of the combustion products:

$$\bar{p} = p_0 \frac{T_c}{T_0}\left(1 - \frac{\nu}{\nu_0}\right) \tag{59}$$

On the other hand, for the case where reactant gas is deficient (i.e., $\nu_0<\nu$), using the approximate relation $p^2=b(T_c-T)$, the following expression was obtained:

$$\bar{p} = \left(b \cdot \frac{RT_c^2}{E}\right)^{m/2} \Gamma(1 + m/2), \tag{60}$$

where $\Gamma(x)$ is the Gamma function, and

$$b = \frac{2\alpha\rho_{g0}RT_c}{\epsilon k_f} \frac{p_0}{(T_c - T_0)}. \tag{61}$$

It is interesting to note that the average gas pressure in the reaction zone (and consequently the combustion velocity) decreases with higher sample permeation coefficients, k_f, and porosity, ϵ, owing to higher reaction rates. In addition, the relationship between combustion temperature and initial pressure, for an excess of ($\nu_0>\nu$) and lack ($\nu_0>\nu$) of reactant gas, can be represented as

$$\begin{aligned} &\text{for } \nu_0 > \nu, \qquad T_c = T_0 + \frac{Q \cdot \rho_{s0}}{c_{p,g}\rho_{g0} + c_{p,s}\rho_{s0}}, \\ &\text{for } \nu_0 < \nu, \qquad T_c = T_0 + \frac{Q}{c_{p,g}\rho_{g0} + c_{p,s}\rho_{s0}} \cdot \frac{\rho_{g0}}{\nu}. \end{aligned} \tag{62}$$

In general, the maximum combustion temperature and velocity are achieved for a stoichiometric mixture of reactants.

b. Combustion with Filtration to the Reaction Front from the Atmosphere. Let us now consider the case when there is not enough reactant gas initially in the pores for propagation to occur. In this case, layer-by-layer combustion with complete conversion can only be achieved with infiltration of gas from the surroundings. Two directions of gas flow relative to that of propagation can be considered: countercurrent (Fig. 27b) and cocurrent (Fig. 27a). In both cases, for samples of finite length, the distance between the reaction front and the exposed surface, $L(t)$ changes with time. When wave propagation results from filtration to the combustion front rather than the gas initially present in the pores [i.e., $\eta_c >> (\rho_{g0}/\rho_s)\nu$], analysis has shown that a quasisteady approximation [i.e., $L(t)$ becomes a parameter] can be used to solve Eqs. (50)–(52). Furthermore, the reactant gas flow term, $U\rho_g$, attributed to front propagation is considered negligible when compared to filtration flow, and can be neglected in the gas balance equation (51).

(i) Countercurrent Infiltration. For gas flow in the direction opposite that of the combustion propagation, the boundary conditions may be written as (Aldushin *et al.*, 1974):

$$\text{at } x = L(t), \qquad T = T_0, \quad \eta = 0, \quad p = p_0, \tag{63}$$

$$\text{at } x = -L_1(t), \qquad \frac{dT}{dx} = \frac{dp}{dx} = 0, \quad W(\eta_c, T_c, p_c) = 0, \tag{64}$$

where $L_1(t)$ is the length of the reacted portion. For gas–solid systems, the reaction can terminate [i.e., $W(\eta,T,p) = 0$] when either the solid reactant is completely converted or when there is not enough reactant gas. The solution of Eqs. (50)–(53) determines which of the two cases is realized.

Theoretical analysis of the problem (Aldushin *et al.*, 1974, 1975) shows that combustion wave propagation can occur for incomplete conversion of the solid reactants. Whether full conversion is achieved can be estimated by the dimensionless parameter, $\omega = U_k/v_f$, the ratio of the kinetically controlled combustion velocity (U_k), and gas filtration (v_f) rates. The former can be calculated from Eq. (57), while the latter can be calculated as follows:

$$v_f = \frac{L_f \alpha}{L(t)} \cdot \frac{\rho_{g0}}{\rho_{s0}\nu} \cdot \frac{\Pi^{m/4}}{\sqrt{\Gamma(1 + m/2)}}, \tag{65}$$

where

$$\Pi = \frac{E(T_c - T_0)}{RT_c^2} \cdot \frac{T_0}{T_c} \cdot \frac{L_f(1 + \Delta)}{\nu}.$$

When $\omega<1$, there is no filtration limitation for the solid to react completely in the combustion front ($\eta_c=1$), and $T_c=T_c^{ad}$. In this case, the combustion velocity equals U_k. On the other hand, for $\omega>1$, full conversion is not achieved in the combustion front ($\eta_c<1$) and the combustion temperature is $T_c=T_0+Q/c_m(1+\eta_c\delta)$. For highly exothermic reactions (i.e., $\kappa=T_0c_{p,s}/Q\ll1$), the reaction conversion can be expressed as (Aldushin *et al.*, 1974)

$$\eta_c = \frac{1 - \kappa(1 + \Delta \cdot \dfrac{RT_c^{ad}}{E} \cdot \ln \omega}{1 + (1 + \Delta) \cdot \dfrac{RT_c^{ad}}{E} \cdot \ln \omega}. \tag{66}$$

Thus, the degree of conversion depends significantly on the heat of reaction, and not much on the other parameters. It is interesting that decreasing Q (e.g., by dilution) results in increasing η_c. This occurs because the decrease of T_c reduces the reaction rate, so that the effect of filtration limitation is not as severe. Finally, in this case, the combustion velocity is given by $U=v_f/\eta_c$.

Let us consider the tantalum–nitrogen system to illustrate different combustion regimes. Since the adiabatic combustion temperature for this system ($T_c^{ad}=3000$ K) is lower than the melting point of tantalum (3300 K), no melting occurs in the combustion front, and the permeability of the reaction medium changes only slightly in the preheating zone. As a result, the Ta-N_2 system can be described by the theory discussed earlier. In addition, the thermal conductivity of the sample remains essentially unchanged during reaction. The reaction kinetics for 10-μm Ta powders are given by

$$\frac{d\eta}{dt} = \frac{k(T)}{\eta}$$

where $k(T)=1.2\exp(-77600/RT)\ 10^6\ s^{-1}$ (Vadchenko *et al.*, 1980). Substituting the values for λ (59 W/m K), $m=0$, and Q (6.7×10^5 J/kg) (Samsonov, 1964) along with green mixture density, $\rho_0=20\%$, yields $U_k=3$ cm/s, which is comparable to the experimentally measured value, $U_{exp}\sim2$ cm/s (Pityulin *et al.*, 1979). From Eq. (65), the filtration velocity can be estimated from

$$v_f = \frac{k_f p_0}{2L} \cdot \frac{\nu_0}{\nu}. \tag{67}$$

Using the k_f data from Table XVII, the calculated value for U_k, and the criterion $\omega=1$, we can estimate the maximum sample length, L_{max}, in which complete conversion can be achieved for different nitrogen pressures, p_0 (Table XVIII). Thus, for example, the external nitrogen pressure must be greater than 100 atm in order to achieve complete conversion in a 1-cm-long sample.

TABLE XVIII
CRITICAL SAMPLE LENGTH (L_{max}) FOR COMPLETE SOLID CONVERSION IN TA-N_2 SYSTEM

p_0 (atm)	L_{max} (cm)
1	10^{-2}
10	10^{-1}
100	1
1000	10

(ii) Cocurrent Infiltration. In practice, cocurrent infiltration of reactant gas to the combustion front is rarely realized, because the permeability of the final product is generally lower than that of the initial mixture. Consequently, this type of combustion can be achieved experimentally only if the sample surface ahead of the combustion front is enclosed (Fig. 27a). However, the cocurrent regime is attractive from the applications viewpoint, because in contrast with the countercurrent mode, it can occur with *full* conversion over a wider range of reaction parameters.

The characteristics of this type of combustion were investigated first by Aldushin *et al.* (1980). It was shown that because the reactant gas flows over the product, the reaction is not limited by the concentration of reactant gas. However, since the filtration length increases progressively with time, the combustion velocity decreases ($U \sim t^{-1/2}$). On the other hand, the combustion wave maintains a constant temperature profile. Two possible cases can arise depending on the sample permeability. When it is low, the combustion temperature may be lower than the adiabatic value, due to heat carried away from the reaction front by the gas flow. For high sample permeabilities, the heat gained by the infiltration of reactant gas flowing through hot product may cause T_c to be greater than the adiabatic temperature.

A model of filtration combustion in a thin porous layer, immersed in a bath of gaseous reactant, has also been investigated (Shkadinskii *et al.*, 1992a). In this case, only filtration of gas from the surroundings to the sample, normal to the direction of combustion propagation (cross-flow filtration), should be considered. New pulsating instabilities associated with the gas–solid chemical reaction and mass transfer of gas to the porous medium were identified.

2. *Two-Dimensional Models with Natural Permeation of Gas*

Covering the side surfaces of the sample limits filtration to one dimension, which simplifies the experimental and theoretical study of gas–solid combustion

systems. However, two- and three-dimensional infiltration of the gaseous reactant is more commonly used in practice. Ivleva and Shkadinskii (1981) were the first to model and numerically analyze two-dimensional FC for cylindrical samples reacted under constant pressure.

More recently, the cross-flow filtration combustion configuration (Fig. 29), commonly used for powder production, was investigated (Dandekar *et al.*, 1990). Within the reactor, a rectangular container holds the solid reactant powder, and the gaseous reactant is transported from the surroundings to the front not only by longitudinal flow from above, but also by countercurrent flow from ahead of the front. The assumptions used in the model were as follows:

- The gas pressure of the surroundings remains constant (i.e. an open reactor).
- The reaction rate is diffusion controlled at the single particle level.
- The reactant mixture is pseudohomogeneous.
- The physical properties of all reactants are constant.
- The permeability of the reaction medium is a function of porosity, given by the Kozeny–Carman equation.
- The thermal conductivity and heat capacity of the reaction medium are linear functions of porosity.
- No dissociation of the formed product occurs.

Also, changes in reaction mixture porosity, ϵ, during the process were accounted for by the volumetric expansion of solids due to chemical reaction.

It was shown that the reactant gas pressure strongly influences front propagation (Dandekar *et al.*, 1990). At high pressures ($\nu_0 \geq \nu$), the combustion front is essentially planar, although a hot-spot may appear under certain conditions. This effect may lead to melting or sintering of the solid, creating an undesired nonuniform structure. At low pressures ($\nu_0 < \nu$), the filtration resistance controls reaction front propagation and for this reason, the front is skewed forward at the top of the sample. Also, the conversion is complete at the surface, and decreases deeper into the sample. Thus, the depth of the container is also an important pa-

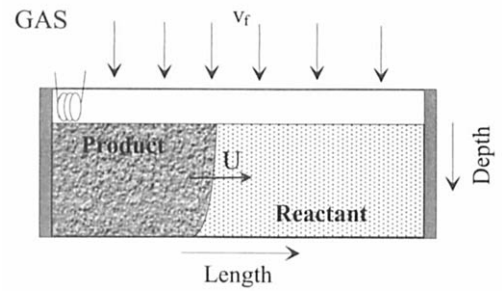

FIG. 29. Cross-flow combustion configuration, two-dimensional scheme.

TABLE XIX
TYPICAL VALUES OF EXPANSION COEFFICIENT, Z

Solid Reactant	Nitride	Z
Hf	HfN	1.02
Zr	ZrN	1.06
Ti	Ti	1.11
Nb	NbN	1.19
Ta	TaN	1.23
Si	Si_3N_4	1.20
Al	AlN	1.25
B	BN	2.40

rameter. For a given pressure, it was shown that there exists a critical container depth above which the combustion front extinguishes in the bulk. In addition, the ratio of solid product and solid reactant volumes, Z, was used to analyze the process. For example, if $Z>1$, then the solid expands on reaction, decreasing the medium permeability. Typical values of Z for several nitrogen–solid systems are given in Table XIX.

Numerical simulations analyzed the effect of sample porosity on reaction. For $\epsilon_0=0.4$, $L_f=17.5$, and $Z=1.2$, the porosity decreased rapidly along with sample permeability, due to high conversion near the point of ignition (see Fig. 30a). The

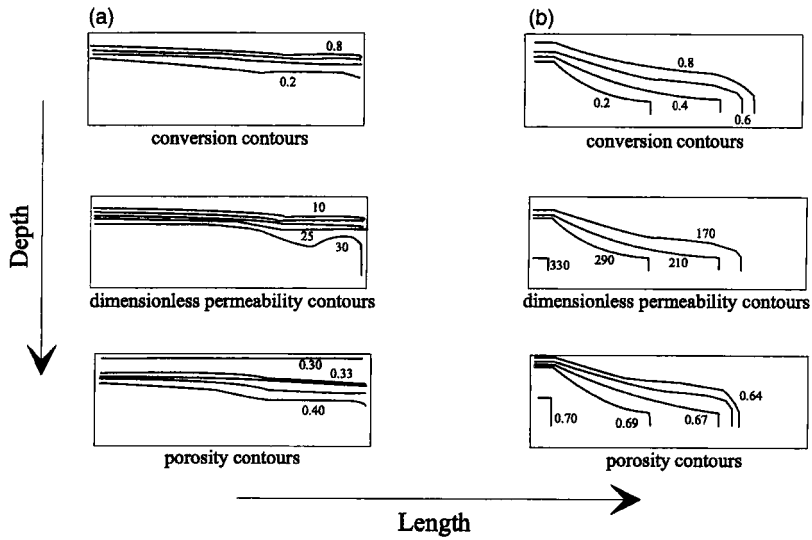

FIG. 30. Effect of initial porosity on reaction: (a) lower initial porosity, $\epsilon_0 = 0.4$, $\tau = 40$; (b) higher initial porosity, $\epsilon_0 = 0.7$, $\tau = 11$ (Adapted from Dandekar *et al.*, 1990).

reaction front eventually stops when gas filtration becomes severely limited. For higher porosity (ϵ_0=0.7), the filtration parameter L_f equals 165, and permeation of gas to the deeper layers is not restricted, so complete conversion can be achieved (see Fig. 30b).

Recently, the cross-flow configuration was also investigated for a closed reactor, that is, constant volume (Grachev *et al.*, 1995). In this case, the amount of gas-phase reactant decreases due to chemical reaction, which would decrease the gas pressure. However, the gas is heated during reaction, which would increase the gas pressure. Depending on the reactor volume, for typical reaction conditions, the gas pressure was shown to have a maximum either at full or intermediate conversion. This conclusion is important, since in practice a decrease in gas pressure is usually associated with reaction completion.

The role of changing porosity and medium permeability due to volumetric expansion of the solids during chemical reaction was also studied for the titanium–nitrogen system (Borovinskaya *et al.*, 1993). In this work, it was assumed that the reaction of titanium and nitrogen followed the equilibrium phase diagram. Thus, the feasibility of combustion due to formation of solid solution was demonstrated, and changes in the melting point of intermediate phases with addition of nitrogen could be described.

F. Other Aspects

A variety of results in FC for heterogeneous systems have recently been reported. Some of these are briefly discussed next.

1. Forced Gas Permeation

As mentioned previously, the gas–solid CS process can be conducted with forced infiltration of the reactant gas through the porous medium. In this case, two combustion modes can be realized, depending on the parameter (Aldushin and Sepliarskii, 1987a,b):

$$\pi = \frac{v_T}{U},$$

which is the ratio of the velocity of the convective heat exchange front, $v_T = c_{p,g} G/c_{p,v}$ (where G is the forced gas velocity, and $c_{p,v}$ is the effective specific heat capacity of the reaction medium) and the combustion velocity, U.

In the case of a relatively low forced gas flux ($\pi < 1$), a *normal wave* structure is observed; that is, the cold reactants are ahead of the combustion front, while the hot products are behind. However, a so-called *superadiabatic* condition is achieved, where the temperature in the front exceeds the adiabatic combustion

temperature, due to additional energy carried by filtration flow from the high-temperature products (Fig. 31a). This type of FC is promising, since weakly exothermic reactions (e.g., Cr-N_2, Si-C) can be conducted in the SHS mode.

In the case of strong forced gas flux ($\pi > 1$), the so-called *inverse wave* structure of FC occurs (Fig. 31b). The unreacted solids in zone *I** are heated by a gas flux to a high combustion temperature $T_c < T_c^{ad}$, but reaction does not occur since there is no reactant gas present. In some cases (e.g., Si-N_2, B-N systems), dissociation of the product occurs in the combustion front, limiting final conversion. Decreasing combustion temperature by strong gas flow alleviates this problem (Aldushin, 1993).

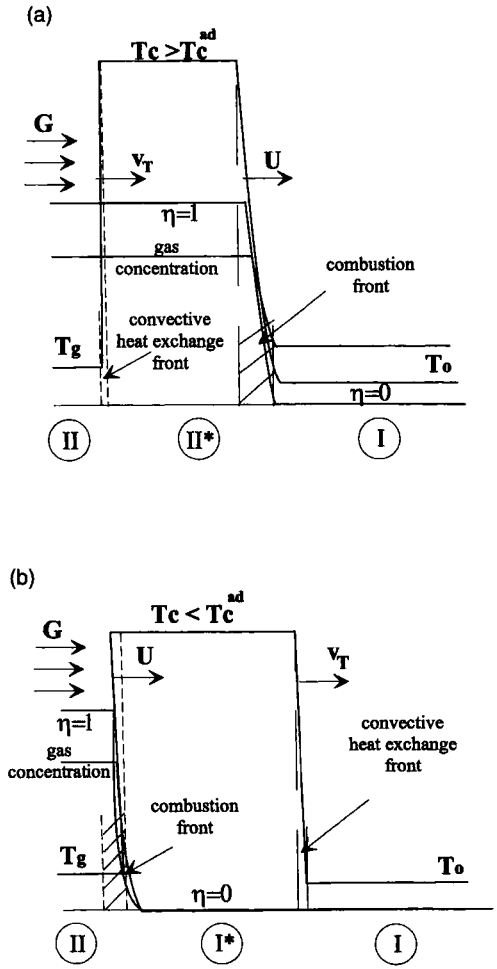

FIG. 31. Combustion wave structure in the case of forced gas filtration: (a) low gas flux ($\pi < 1$); (b) high gas flux ($\pi > 1$) (Adapted from Aldushin, 1993).

2. Effects of Other Forces

Different external (gravitational, centrifugal, etc.) or internal (e.g., the gas pressure gradient between the reaction zone and surroundings) forces may lead to densification or expansion of the reaction medium during FC (cf Shkadinskii *et al.,* 1992b). Product expansion and cracking due to gravity and impurity gasification have been investigated. In addition, the possibility of self-compaction during reaction has also been demonstrated. These works have relevance for the production of compact and foamed materials by the SHS method in gas–solid systems.

3. Interaction of Gasless and Filtration Combustion

The interaction of gasless and filtration combustion has also been examined (Aldushin *et al.,* 1994b). The competition between simultaneous gasless and gas–solid reactions

$$A(s)+B(g)\rightarrow D,$$

$$A(s)+C(s)\rightarrow E,$$

was considered. Assuming that both reactions have large activation energies, the combustion wave may propagate uniformly, with both reactions localized near the maximum temperature. The simultaneous occurrence of parallel reactions may also be used to intensify weakly exothermic reactions that otherwise would not occur. Also, in this case, the combustion temperature may be higher than the adiabatic value, due to heating by gas filtration from the high-temperature product region.

V. Phenomenology of Combustion Synthesis

As described in Section IV, the characteristic feature of combustion synthesis, as compared to conventional powder metallurgy, is that the process variables, such as combustion wave velocity, U, and temperature–time history, $T(t)$, are strongly related. For example, a small change in the combustion temperature may result in a large change in the combustion front velocity [see, for example, Eq. (23)] and hence the characteristic time of synthesis. The process parameters (e.g., green mixture composition, dilution, initial density, gas pressure, reactant particle characteristics) influence the combustion velocity and the temperature–time profile, and in turn can be used to control the synthesis process. In this chapter, the effects of reaction conditions on the characteristics of combustion are analyzed, leading to some general conclusions about controlling the CS process.

A. Thermodynamic Considerations

For any reaction system, the chemical and phase composition of the final product depends on the *green mixture composition,* gas pressure, reactive volume, and initial temperature. As shown in Section I, CS reactions can be represented in the following general form:

$$\sum_{i=1}^{N_X} \nu_i X_i^{(s)} + \sum_{i=1}^{N_Y} \nu_i Y_i^{(g)} + \sum_{i=1}^{N_{MO_X}} \nu_i (MO_X)_i^{(s)} + \sum_{i=1}^{N_Z} \nu_i Z_i^{(s)} = \sum_{j=1}^{N_P} \nu_j P_j^{(s)} + \sum_{j=1}^{N_M} \nu_j M_j^{(s)}, \quad (68)$$

where $X_i^{(s)}$ are the metal or nonmetal solid reactants, $Y_i^{(g)}$ the gas-phase reactants, $(MO_X)_i^{(s)}$ the oxide reactants, $Z_i^{(s)}$ the reducing metal reactants, $P_i^{(s)}$ the solid products (e.g., carbides, borides, nitrides), and $M_i^{(s)}$ the reduced metal products. In limiting cases, Eq. (68) leads to the three main classes of CS reactions discussed in Section I. Thus we have

$N_Y=0$, $N_{MO_X}=0$, and $N_M=0$,	gasless combustion [cf Eq. (1)]
$N_{MO_X}=0$, $N_Z=0$, and $N_M=0$,	gas-solid combustion [cf. Eq. (2)]
$N_{MO_X}\neq 0$ and $N_Z\neq 0$,	reduction-type combustion [cf. Eq. (3)]

Thermodynamic calculations can identify the adiabatic combustion temperature, as well as the equilibrium phases and compounds present at that temperature. The composition of the equilibrium final products is determined by minimizing the thermodynamic potential. For a system with $N^{(g)}$ gas and $N^{(s)}$ solid number of components, at constant pressure, this may be expressed as

$$F(\{n_k\},\{n_l\}) = \sum_{k=1}^{N^{(g)}} n_k \left(\ln \frac{p_k}{p} + G_k \right) + \sum_{l=1}^{N^{(s)}} n_l G_l, \quad (69)$$

where p_k is the partial pressure of the k'th gas-phase component, while n_i and G_i are the number of moles and molar Gibbs free energy of component i (cf Prausnitz *et al.,* 1986). The adiabatic combustion temperature, T_c^{ad}, is determined by total energy balance:

$$\sum_{i=1}^{N_0} H_i(T_0) = \sum_{k=1}^{N(g)} n_k H_k(T_c^{ad}) + \sum_{l=1}^{N(s)} n_l H_l(T_c^{ad}), \quad (70)$$

where the enthalpy of each component is

$$H_i(T) = \Delta H_{f,i}^{\circ} + \int_{T_0}^{T} c_{p,i} dT + \sum \Delta H_{s,i} \quad (71)$$

and $\Delta H^{\circ}_{f,i}$ is the heat of formation at 1 atm and reference temperature T_0, $c_{p,i}$ is the heat capacity, and $\Delta H_{s,i}$ is the heat of s'th phase transition for component i.

Thermodynamic calculations of adiabatic combustion temperatures and their comparison with experimentally measured values have been made for a variety of systems (cf Holt and Munir, 1986; Calcote *et al.*, 1990; Glassman *et al.*, 1992). Under conditions that lead to full conversion, a good agreement between theoretical and experimental values has generally been obtained (Table XX).

TABLE XX
ADIABATIC AND MEASURED COMBUSTION TEMPERATURES FOR VARIOUS REACTION SYSTEMS

System	Adiabatic Combustion Temperature, T_c^{ad} (K)	Measured Combustion Temperature, T_c (K)	Lowest Melting Point On the Phase Diagram (K)
Carbides			
Ta + C	3290	2550	3295 (Ta)
Ti + C	1690	3070	1921 (eut)
Si + C	1690	2000[a]	1690 (Si)
Borides			
Ta + B	2728	2700	2365 (B)
Ti + 2B	3193	3190	1810 (eut)
Ti + B	2460	2500	1810 (eut)
Silicides			
Mo + 2Si	1925	1920	1673 (eut)
Ti + 2Si	1773	1770	1600 (eut)
5Ti + 3Si	2403	2350	1600 (eut)
Intermetallics			
Ni + Al	1912	1900	921 (eut)
3Ni + Al	1586	1600	921 (eut)
Ti + Al	1517	n/a	933 (Al)
Ti + Ni	1418	n/a	1215 (eut)
Ti + Fe	1042	n/a	1358 (eut)
Nitrides[b]			
$2Ta + N_2$	3165	2500	3000 (Ta)
$2Nb + N_2$	3322	2800	2673 (NbN)
$2Ti + N_2$	3446	2700	1943 (Ti)
$2Al + N_2$	3639	2300	933 (Al)
$3Si + 2N_2$	2430	2250	1690 (Si)
$2B + N_2$	3437	2600	2350 (B)
Reduction type			
$B_2O_3 + Mg$	2530	2420	1415 (eut)
$B_2O_3 + Mg + C$	2400	2270	n/a
$B_2O_3 + Mg + N_2$	2830	2700	n/a
$SiO_2 + Mg$	2250	2200	1816 (eut)
$SiO_2 + Mg + C$	2400	2330	n/a
$La_2O_3 + Mg + B_2O_3$	n/a	2400	n/a

[a]With preheating.
[b]T_c^{ad} calculated for 1 atm.

Thermodynamic calculations have also been used to determine the equilibrium products (Mamyan and Vershinnikov, 1992; Shiryaev *et al.*, 1993), and to illustrate new possibilities for controlling the synthesis process, even for complex multicomponent systems. Correlating these calculations with the equilibrium phase diagram for each system provides a basis for predicting possible chemical interactions and even limits of combustion during CS of materials. Some examples are discussed in the following subsections.

1. Gasless Systems

For the Ti-Si system, a comparison of the calculated T_c^{ad} and the phase diagram (Fig. 32) shows (Rogachev *et al.*, 1995) that the combustion temperature of all silicide compounds exceeds the following:

- The melting point of both eutectic compositions (1330°C)
- The silicon melting point (but lower than the titanium melting point), for combustion of Ti+Si, 5Ti+4Si and 3Ti+Si mixtures
- The titanium melting point in the case of the 5Ti+3Si mixture (with up to 15 wt % of the final product molten).

Consequently, the two temperature regions of interest in the experimental study of the combustion mechanism are

Region I: $1330°C < T < 1670°C$
(interaction of solid Ti particles with melt of Si or eutectics)

Region II: $1670°C < T < 2130°C$
(melting of both Si and Ti)

These regions correspond to zones I and II, respectively, in the temperature profile, also shown schematically in Fig. 32. It was confirmed experimentally that the interaction in zone I occurs through a solid–liquid reaction, $Ti(s)+Si(s,l)+L_1(eut.) \rightarrow TiSi_2(s)+L_2$, for $1330°C < T < 1670°C$. However, in zone II, a liquid–liquid interaction, $Ti(l) + Si(l) \rightarrow Ti_5Si_3$ (l,s), takes place with the formation of Ti_5Si_3 for the temperature range 1670–2130°C:

$$Ti(l)+Si(l) \rightarrow Ti_5Si_3(s,l).$$

2. Reduction-Type Systems

The thermodynamic calculations for the equilibrium combustion temperature and product compositions for a three-component (Ni-Al-NiO) reduction-type system are shown in Figs. 33a and b, respectively (Filatov *et al.*, 1988). In Fig. 33a, the curves correspond to constant adiabatic combustion temperature at $P=1$ atm. The maximum T_c^{ad} was calculated to be 3140 K for the 2Al+3NiO green mixture

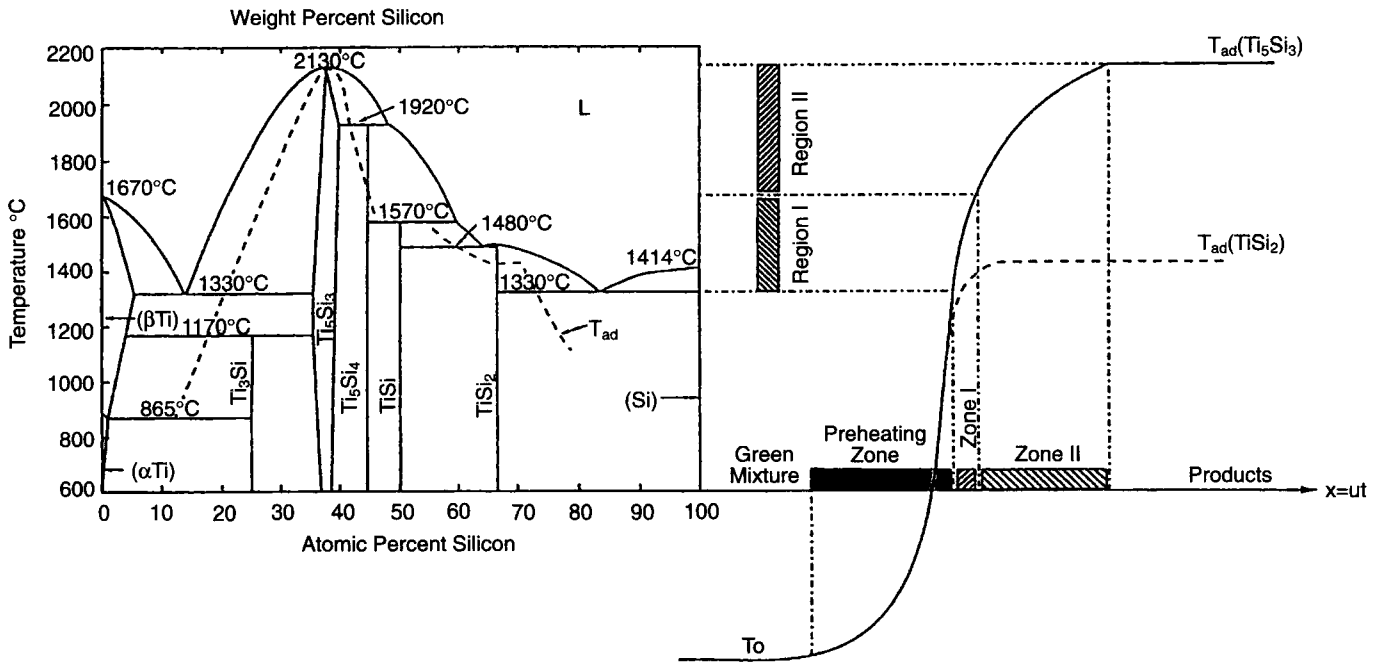

FIG. 32. Equilibrium combustion temperature and phase diagram of Ti-Si system (Adapted from Rogachev *et al.*, 1995).

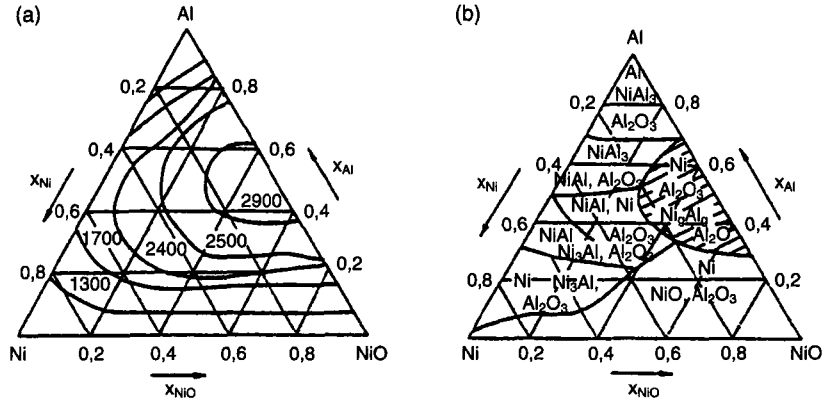

FIG. 33. For the Ni-Al-NiO system: (a) equilibrium combustion temperatures; (b) product composition (Adapted from Filatov *et al.*, 1988).

(Q=810 kcal/g), and is constrained by the nickel boiling point. Also, it was shown that the adiabatic combustion temperature for the 5Al+3NiO composition, with a higher heat of reaction (Q=860 kcal/g) was only 3000 K. The lower T_c^{ad} in the latter case can be attributed to the dissociation of formed nickel aluminides and the consequent reduction in overall heat generation. Note that the thermodynamic calculations reveal the presence of a gas-phase product for initial mole fractions of Al from 0.3 to 0.7 (hatched region of Fig. 33b). Increasing the amount of nickel in the green mixture reduces T_c^{ad}, and promotes the formation of nickel aluminides. With relatively low melting points, these compounds add another liquid phase to the system, allowing better contact for reaction and expanding the limits of combustion. These calculations have also been confirmed by experimental investigations (Filatov and Naiborodenko, 1992).

3. *Gas–Solid Systems*

The thermodynamic results discussed previously were calculated for constant gas pressure. However, it is also necessary to treat the case of constant reaction volume, especially for gas–solid systems where the initial reactant ratio may be varied by changing the reactant gas pressure.

Consider the combustion reaction between a solid reactant and a gas oxidizer present initially in the constant volume of a porous medium (see Section IV,D,1). In this case, thermodynamic calculations for the silicon–nitrogen system have been made for constant volumes (Skibska *et al.*, 1993b). The calculations yield the adiabatic combustion temperature, as well as pressures and concentration, as functions of the silicon conversion. As shown in Fig. 34a, the reactant gas pressure (curve 3) increases even though conversion increases. This occurs because

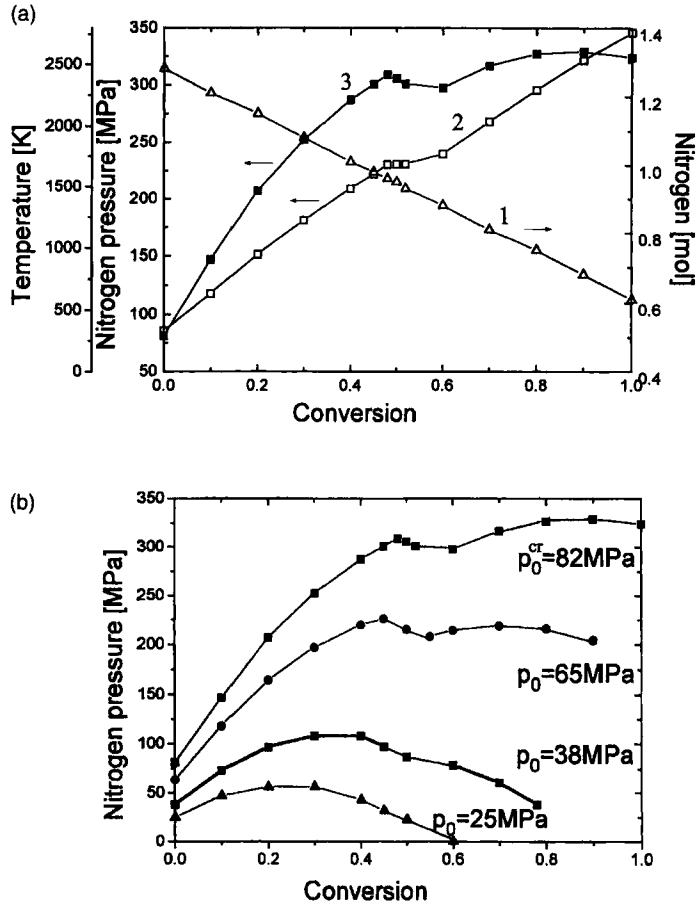

FIG. 34. Thermodynamic calculations of combustion characteristics as a function of degree of conversion in Si-N_2 system; T_0 = 300 K, ϵ = 0.6 (Adapted from Skibska *et al.*, 1993b).

the temperature (curve 2) also increases with conversion, while the amount of nitrogen gas (curve 1) in the system decreases. The discontinuity in slopes of the various curves occurs at the melting point of silicon (1414°C). In addition, the change in nitrogen pressure during reaction depends on its initial value, p_0 (see Fig. 34b). Above a critical initial value (p_0^{cr}), the nitrogen pressure increases with increasing conversion to full reaction. However, for lower initial nitrogen pressures, a maximum is observed. These results provide an explanation for the unusual dependence of U vs. p_{N_2}, and suggest methods for optimizing the synthesis process (Skibska *et al.*, 1993a,b).

As shown by the preceding examples, changes in the initial composition of the green mixture can result in a wide variation of synthesis conditions and products.

Equilibrium thermodynamic calculations can help to elucidate these conditions and products, and provide useful information for controlling the process.

B. Dilution

One of the most effective and commonly used procedures to modify the synthesis conditions is to dilute the initial mixture with a chemically inert compound, often the final product. The typical dependencies of combustion temperature and velocity on the amount of dilution, b, are shown in Fig. 3e. In general, an increase in dilution decreases the overall heat evolution of the system, and therefore decreases the combustion temperature and velocity. Some examples of this type are presented in the review by Rice (1991), where experimental data for group IV metals with boron and carbon, as well as Mo-Si systems are summarized. A similar result was obtained for the Hf-B system shown in Fig. 35 (Andreev *et al.*, 1980).

However, some exceptions to these trends have also been observed. In Fig. 36, the dependencies of combustion temperature and velocity on dilution for the Ni-Al system are shown (Maslov *et al.*, 1976). As expected, the combustion velocity decreases with increasing dilution. Similarly, for lower ($b < 11.5\%$) and higher ($b > 35.5\%$) dilutions, T_c decreases with increasing dilution. However, for intermediate dilutions ($11.5\% < b < 35.5\%$), the combustion temperature is constant,

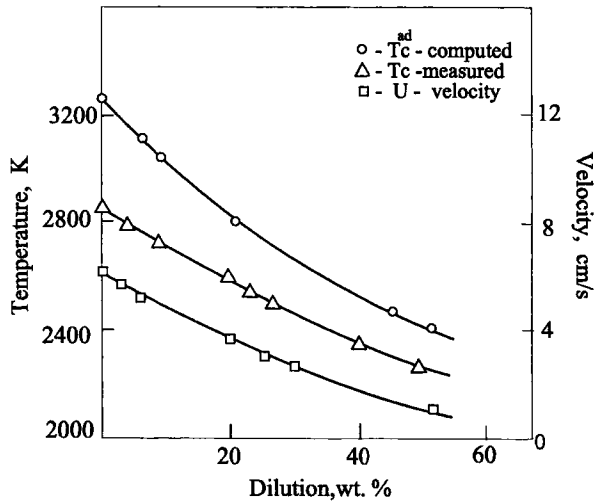

FIG. 35. Combustion temperature and velocity of hafnium–boron mixture as a function of dilution by final product (Adapted from Andreev *et al.*, 1980).

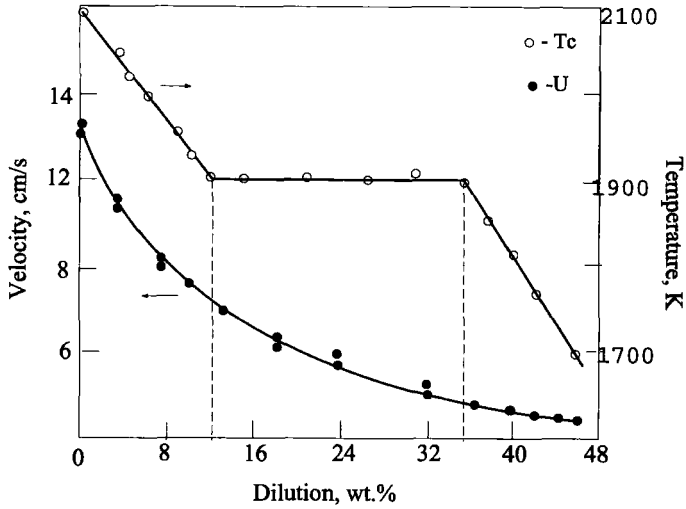

FIG. 36. Dependence of combustion velocity and temperature on dilution by final product in Ni-Al system; T_0 = 740 K (Adapted from Maslov *et al.*, 1976).

and corresponds to the melting point of NiAl. This type of behavior has also been observed for other systems, when the T_c^{ad} may correspond to the melting point of the product (Shcherbakov and Pityulin, 1983; Subrahmanyam *et al.*, 1989; Kottke *et al.*, 1990).

The particle size of the inert diluent may also influence combustion characteristics. For example, the combustion velocity in the Ti-C system as a function of dilution for different TiC particle sizes is shown in Fig. 37 (Maslov *et al.*, 1990). For the smaller particles (d_{TiC}<100 μm), the combustion velocity decreased with increasing b (curve 1). However, for larger TiC particles (d_{TiC}>1000 μm), owing

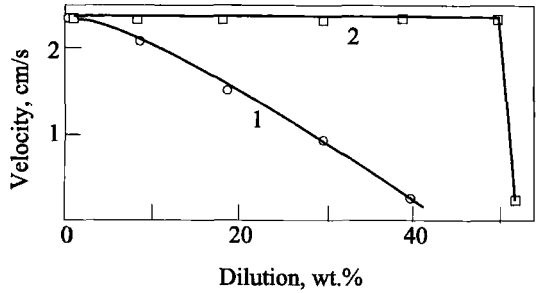

FIG. 37. Combustion velocity as a function of inert dilution: curve 1, d_{TiC} = 50–90 mm; curve 2, d_{TiC} = 1000–1500 mm (Adapted from Maslov *et al.*, 1990).

to their incomplete heating in the combustion wave, U remained practically constant up to about 50 wt % dilution before eventually decreasing (curve 2).

The dependence of combustion temperature and velocity for the Si-N_2 system as a function of dilution with β-Si_3N_4 powder is shown in Fig. 38. In this case, at constant gas pressure, T_c remains constant and is equal to the dissociation temperature of silicon nitride, for dilutions up to 60 wt %. However, with increasing dilution, the combustion front velocity increases. Also, increasing the overall heat evolution, smaller dilution by nonmelted nitride powder promotes coalescence of liquid Si particles, leading to an increase in the average reactant particle size, as well as to formation of thin liquid Si films, which blocks nitrogen infiltration to the reaction zone (Mukasyan *et al.*, 1986). The same effects were also observed for the Al-N_2 and B-N_2 systems (Mukasyan, 1994), which are characterized by dissociation of the final product in the combustion wave.

Moreover, dilution is an effective method of increasing the final extent of conversion for some gas–solid systems, especially when melting of the reactants or products occurs, and the sample permeability is reduced. Figure 39 shows the dependence of final conversion, η, on the extent of dilution for the Ti-N_2 system. In this case, the adiabatic and measured combustion temperatures (see Table XX) are higher than the melting point of titanium (1670°C) and the conversion in the combustion front, η^*, is less than unity. With an increase in solid-phase dilution, the combustion temperature decreases, which diminishes the effect of titanium melting and coalescence on sample permeability. However, excessive dilution leads to a decrease in conversion and eventual process extinction.

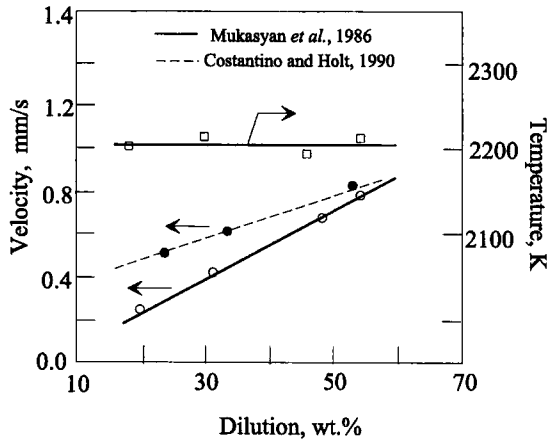

FIG. 38. Combustion velocity and temperature as a function of dilution by final product in Si-N_2 system.

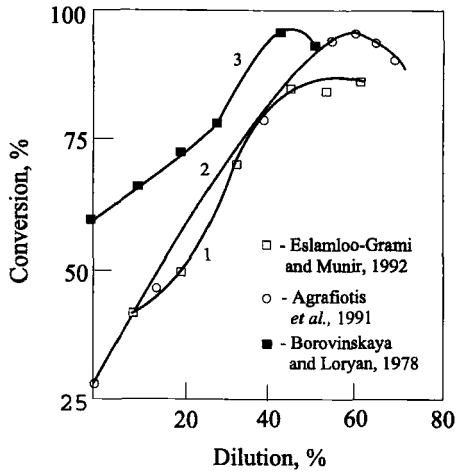

FIG. 39. Effect of solid phase dilution on conversion for Ti-N_2 system: curve 1, P = 1 atm; curve 2, P = 10 atm; 3, P = 2000 atm.

In the Ta-N_2 system, the measured combustion temperature is lower than the melting points of both the metal and final products. In this case, there is no significant influence of dilution on final conversion. However, an interesting effect of dilution on the product phase composition was found by Borovinskaya *et al.* (1975a). Increasing dilution results in a change, from δ-TaN (cubic) to the ϵ-TaN (hexagonal) phase (see Table XXI).

Finally, the following conclusions may be made about the effects of dilution:

- For a wide range of systems, the combustion front velocity and temperature decrease with increasing dilution.
- The atypical dependencies of T_c and U as a function of dilution are usually associated with phase transition processes occurring in the combustion wave (e.g., melting, dissociation, evaporation).

TABLE XXI
PHASE AND CHEMICAL COMPOSITIONS OF SHS TANTALUM NITRIDE POWDERS

Dilution (wt %)	Product Chemical Composition	Product Phase Composition
0	$TaN_{1.05}$	δ–TaN(cub)
6.25	$TaN_{1.03}$	δ–TaN(cub)
18.75	$TaN_{1.01}$	δ–TaN(cub)
31.25	$TaN_{0.97}$	TaN2+δ–TaN(cub)
43.75	$TaN_{0.94}$	TaN2+δ–TaN(cub)
56.25	$TaN_{0.91}$	ϵ–TaN(hex)

- For gas–solid systems with combustion temperatures higher than the melting points of the reactants or products, dilution is an effective method for increasing final conversion, by inhibiting the effects of melting, particle coalescence, and the subsequent reduction of sample permeability.

C. Green Mixture Density for Gasless Systems

As shown earlier in Fig. 2b, the dependence of combustion velocity on green mixture density for gasless systems is frequently characterized by a maximum at some intermediate value (Merzhanov, 1983; Rice, 1991). However, combustion theory [Eq. (20)] suggests that the velocity under adiabatic conditions should increase with increasing density, since higher densities correspond to higher thermal conductivities (Aleksandrov *et al.*, 1985; Kottke *et al.*, 1990). Different explanations have been suggested to explain this discrepancy.

It has been proposed that the effect can be attributed to two competing phenomena (Varma and Lebrat, 1992). As the density increases, intimate contact between the reactant particles is augmented, which enhances both reaction and front propagation. On the other hand, due to an increase in thermal conductivity at higher densities, greater heat is lost due to conduction from the reaction zone to the unreacted portion, inhibiting front propagation. However, this idea, which considers the thermal conductivity as a function of reactant particle contact and thermal losses, has not been investigated experimentally. Furthermore, most theoretical models do not take into account the contact resistance. Kottke *et al.* (1990) calculated the velocity dependence on initial density, based on experimental measurements of $\lambda = f(\rho_0)$, and showed that U increases monotonically with increasing ρ_0 (Fig. 21).

Another hypothesis was suggested by Kirdiyashkin *et al.* (1981) for the combustion synthesis systems characterized by melting of a reactant metal (e.g., Ti-C, Ti-B), where capillary spreading may control the combustion process (Shkiro and Borovinskaya, 1976). In these cases, it was suggested that an optimal density occurs where the volume of pores equals the volume of the molten metal. However, an analysis of the experimental data for the Ti-B system showed that this hypothesis may not be valid over the entire range of particle sizes investigated (Munir and Anselmi-Tamburini, 1989).

It is well known that powders with high surface areas usually have a large amount of adsorbed gas impurities. In Fig. 40, the dependence of combustion velocity on green density in the Ni-Al system is shown for combustion of mixtures with (curve 2) and without (curve 1) heat treatment of powders to remove adsorbed contaminants. While the untreated samples exhibit a maximum, for the pretreated samples, the velocity increases monotonically with increasing density (Kasat'skiy *et al.*, 1991). The monotonic increase of combustion velocity and

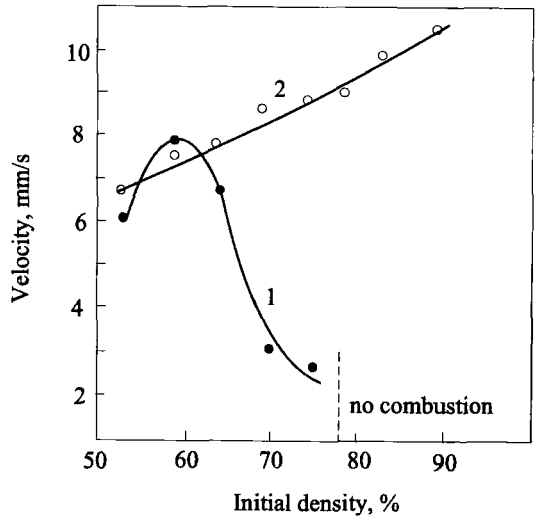

FIG. 40. The combustion velocity as a function of initial sample density for the Ni-Al system: curve 1, with no pretreatment; curve 2, with pretreatment at T = 570 K and P = 13.3 Pa (Adapted from Kasat'skiy *et al.*, 1991).

temperature with increasing green density (see Fig. 41) was also observed for 3Ni+Al samples pressed from high-purity powders (Lebrat and Varma, 1992a). In addition, for Ti+C and 5Ti+3Si systems, without preliminary outgassing of adsorbed hydrogen from the surface of powders (mainly Ti), a maximum in the U dependence with density was observed at ρ_0~0.56. However, heat treatment (400°C) of the green mixture under vacuum (~10^{-5} atm) resulted in a monotonically increasing combustion velocity for densities up to ρ_0=0.75 (Vadchenko 1994, 1996).

In an early work on combustion in the Ti-C system (Shkiro and Borovinskaya, 1975), stable combustion propagation was observed with increasing velocity for ρ_0=0.38–0.56, while for higher densities, the oscillatory mode occurred and the average velocity decreased (Fig. 42). The oscillatory mode also occurred for the Nb-B and Ti-B systems (Filonenko, 1975) and was shown to be related to the formation of thin flaky layers due to stratification of the reactant medium during combustion. In constrained samples, stratification did not occur and the combustion wave propagated without oscillations. The formation of the flaky layers was associated with adsorbed gas escaping from the sample.

Based on these results, an explanation for the combustion velocity dependence on green mixture density has recently been suggested (Vadchenko *et al.*, 1996). For relatively low sample densities (ρ_0<0.6), escape of desorbed gases in the combustion wave is not limited by permeation and occurs without destruction of the reactant medium structure. In this case, increasing the green density

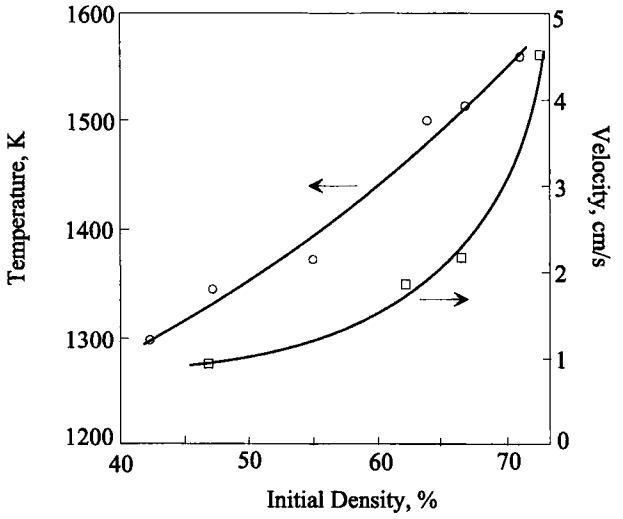

FIG. 41. Effect of initial density on combustion temperature and velocity in 3Ni-Al system (Adapted from Lebrat and Varma, 1992a).

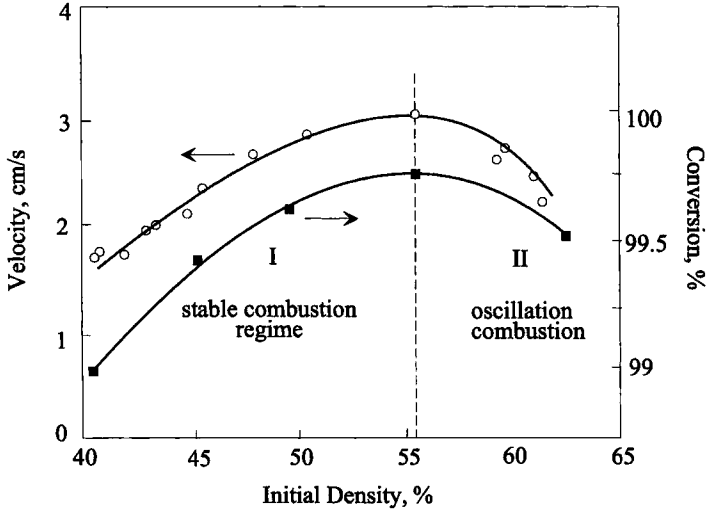

FIG. 42. The dependences of combustion velocity and conversion on initial sample density in Ti-C system (Adapted from Shkiro and Borovinskaya, 1975).

(ρ_0=0.45–0.6) results in increasing thermal diffusivity of the medium, and hence increasing velocity. At higher densities (ρ_0>0.6), adsorbed gases are unable to escape due to low sample permeability. As the temperature increases, the gas pressure inside the pores also increases, forming cracks in the sample, which lower the effective thermal conductivity of medium in the combustion zone. With higher green densities, ρ_0, the extent of crack formation is greater, which leads to lower combustion velocities.

The effect of the expansion of adsorbed gases on the sample final density was also found in the investigation of the Nb-3Al system, using volume combustion synthesis technique (Kachelmyer *et al.,* 1995). In pellets with higher initial densities, the passage of expanding contaminant gases during sample preheating was restricted due to lower permeability. This leads to a lower density of the final product. However, at lower ρ_0, the expanding gases are expelled with greater ease, resulting in higher final density.

D. Green Mixture Density and Initial Gas Pressure for Gas–Solid Systems

For gas–solid systems, the green density affects not only the thermal conductivity, but also the availability and permeability of the reactant gas within the compact. For this reason, in gas–solid systems, it is necessary to analyze the effects of green density along with initial reactant gas pressure on the combustion synthesis process. As discussed in Section IV, different combustion regimes can occur in these systems, depending on the initial sample porosity and reactant gas pressure. Two types of reaction propagation may be distinguished: with and without reactant gas infiltration to the combustion front. In both cases, reactant gas permeation may take place after passage of the front (i.e., postcombustion reaction).

1. Without Gas Infiltration to the Combustion Front

This type of propagation may follow three different combustion modes, including *surface combustion* and *layer-by-layer combustion* with either incomplete or complete conversion. The specific mode followed depends on the initial amount of reactant gas present in the sample pores.

a. Surface Combustion. In this case, the initial amount of gas present in the pores is not enough to sustain chemical reaction within the bulk of the sample. Thus the combustion wave propagates *only* on the outer surface of the sample in a relatively thin layer (usually 0.5–2 mm). However, reaction in the postcombus-

tion zone may play a significant role in the final product formation process. Surface combustion mode typically occurs with reactant gas pressures, $P_g<10$ MPa and initial sample density $\rho_0>0.5$, and has been investigated primarily for various nitrogen-metal systems: Ti-N_2 (Eslamloo-Grami and Munir, 1990a,b; Agrafiotis *et al.,* 1991; Borovinskaya *et al.,* 1992a), Zr-N_2 (Merzhanov *et al.,* 1972), Ta-N_2 (Agrafiotis *et al.,* 1991), Hf-N_2 (Borovinskaya and Pityulin, 1978), V-N_2 (Maksimov *et al.,* 1979), and Nb-N_2 (Mukasyan, 1994).

b. Layer-by-Layer Combustion (with Incomplete Conversion). Above a critical initial gas reactant pressure, the combustion wave can propagate in a layer-by-layer regime through the sample without additional gas infiltration. However, the amount of gaseous reactant in the pores may not be sufficient for complete conversion of the solid reactant. This mode is possible owing to the fact that in many gas–solid systems, the combustion wave can be sustained by *only* a relatively small degree of conversion (e.g., η^*~0.1). For example, in the Ti-N_2 system, this type of combustion occurs when nitrogen pressure is in the range of 10–15 MPa and green density $0.6>\rho_0>0.5$, where η^* achieved does not exceed 0.2 (Borovinskaya *et al.,* 1992a). Of course, complete conversion may be achieved during postcombustion reaction. This mode of combustion has been observed in several systems, including Ti-N_2 (Hirao *et al.,* 1987; Borovinskaya *et al.,* 1992a) and Ta-N_2 (Borovinskaya *et al.,* 1975a; Agrafiotis *et al.,* 1991).

c. Layer-by-Layer Combustion (with Complete Conversion). This mode occurs when the amount of reactant gas within the pores of the sample is enough for complete conversion of the solid reactant. In this case, the reaction is complete *immediately* after the combustion wave propagates through the sample. Calculations for the critical reactant gas pressure as a function of initial density to realize this mode of combustion have been reported (Munir and Holt, 1987; Merzhanov, 1993a). For example, in solid–nitrogen systems, for an initial green density of $\rho_0 \sim 0.5$, the critical nitrogen pressure ranges from about 100 MPa for Ta, up to 300 MPa for B (see Table XVI). These critical conditions have been studied experimentally for several systems: Zr-N_2 and Ti-N_2 (Borovinskaya and Loryan, 1978), Ta-N_2 (Borovinskaya and Pityulin, 1978), and B-N_2 (Mukasyan, 1986).

2. *With Gas Infiltration to the Combustion Front*

In this case, the combustion front propagates due to the interaction between the solid reactant and the gas infiltrated to the reaction zone from the surrounding atmosphere (see Section IV,D). For metal–nitrogen reactions, this type of combustion was observed for low initial sample density (~0.2) in the Ta–N_2 system, where the metal does not melt in the combustion wave (Pityulin *et al.,* 1979; Ku-

mar, 1988). Additional examples were identified during the synthesis of nonmetallic nitrides, including Si_3N_4 (Mukasyan *et al.*, 1986; Hirao *et al.*, 1987; Costantino and Holt, 1990), AlN (Dunmead *et al.*, 1990a), and BN (Mukasyan and Borovinskaya, 1992). In these systems, the rates of chemical reactions are relatively small, hence low gas permeation rates, achievable with gas pressures up to ~100 atm, are sufficient to sustain the infiltration mode of combustion.

The dependencies of combustion velocity on the sample green density for several gas–solid systems are presented in Fig. 43. In general, the velocity decreases with increasing density. Even more important from the practical point of view is the extent of final conversion as a function of initial density. For the Hf-N_2 (Borovinskaya and Pityulin, 1978) and B-N_2 (Mukasyan, 1986) systems, the conversion decreases with increasing density, owing to the lower availability and permeability of nitrogen in the sample (curves 1 and 2, Fig. 44). However, for the Ti-N_2 system at 1-atm nitrogen pressure, a maximum final conversion was observed at ρ_0=0.58 (curve 3, Fig. 44). At low densities, the high temperature in the reaction zone (~1800°C) partially melts the titanium, which reduces the permeability

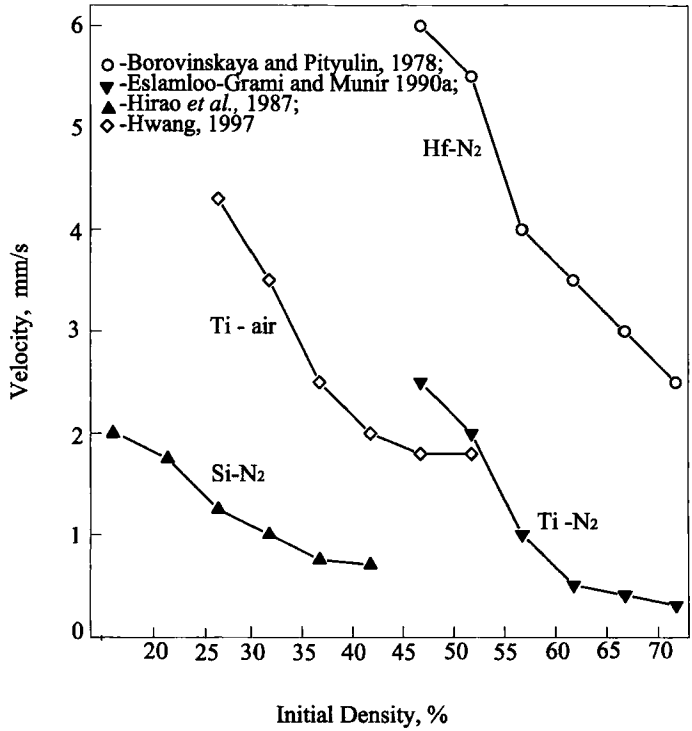

FIG. 43. Effects of initial density on combustion velocity in gas–solid systems.

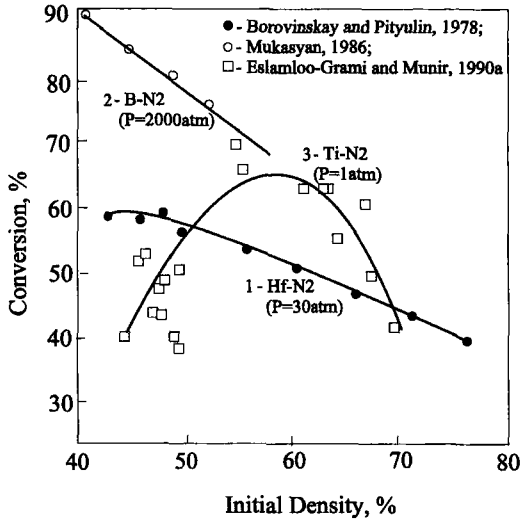

FIG. 44. Effect of initial density on conversion to the nitride.

of the sample surface. As a result, the amount of reactant gas available in the post-combustion zone is reduced, lowering the final conversion. Increasing the green density decreases the combustion temperature, until it becomes lower than the melting point of titanium (1760°C). Since Ti does not melt, the surface permeability does not change dramatically, and consequently a relatively wide post-combustion zone was observed, with higher conversions. For higher green densities (>60%), the initial sample permeability is lower, and it further decreases due to chemical reaction leading to less final conversion.

Nonmonotonic behavior of final conversion was also observed for the Zr-N_2 system as a function of initial nitrogen pressure (Merzhanov *et al.*, 1972). Again, it was shown that this effect is related to the melting of zirconium in the combustion zone. The gravimetric curves of zirconium nitridation at different initial pressures (Fig. 45) demonstrate that for relatively low pressure (P=5 atm), there exists a wide postcombustion zone where conversion in the reaction front, η^* is about 0.20, and nearly 0.60 in the final product (curve 1). At higher pressure (P=30 atm), η^* is higher (~0.25), but no reaction occurs in the postcombustion zone. Increasing the initial nitrogen pressure even further (>30 atm) increases final conversion, which is due only to an increase in the amount of nitrogen reacted in combustion front (curve 4, P=100 atm). For the Nb-N_2 system, in which no melting of metal occurs at P=30 atm, a wide postreaction zone is obtained (curve 5). The reactant pressure can also influence the phase composition of the product, as was demonstrated for Ti-N_2 (Borovinskaya and Loryan, 1978) and Ta-N_2 (Borovinskaya *et al.*, 1975a; Agrafiotis *et al.*, 1991) systems.

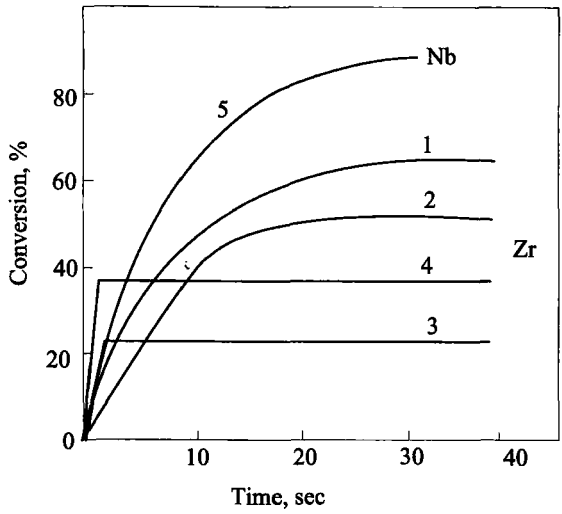

FIG. 45. Continuous gravimetric measurements for Zr (curves 1–4) and Nb (curve 5) samples reacted with nitrogen at different gas pressures: curve 1, $P = 5$ atm; curve 2, $P = 10$ atm; curves 3 and 5, $P = 30$ atm; curve 4, $P = 100$ atm. (Adapted from Merzhanov *et al.*, 1972).

Finally, note that a relationship between the product density, ρ_f, with that of the initial mixture, ρ_0, can be obtained readily as follows:

$$\rho_f = \rho_0(1 + A\eta_f)\chi, \tag{72}$$

where A is constant for the investigated system, and $\chi = V_0/V_f$ is the ratio of the initial and final sample volumes. For net-shape production of articles, $\chi = 1$, although if a densifying load is applied during synthesis, then $\chi > 1$. Examples of relationship (72) for the B-N_2 (Mukasyan, 1986) and Al-N_2 (Dunmead *et al.*, 1990a) systems are presented in Fig. 46. To obtain materials with high final density (i.e., low porosity), we need to increase both initial density and conversion η_f. However, as discussed earlier (Fig. 44), η_f generally decreases with increasing ρ_0. Thus optimization of these two parameters is the main problem when attempting to produce materials with a tailored composition and mechanical properties.

E. PARTICLE SIZE

To date, the dependencies of combustion velocity, temperature, and conversion as functions of reactant particle size have not been studied as extensively as the other parameters described earlier. This is somewhat surprising in light of the fact that particle diameter is an important parameter that can be conveniently

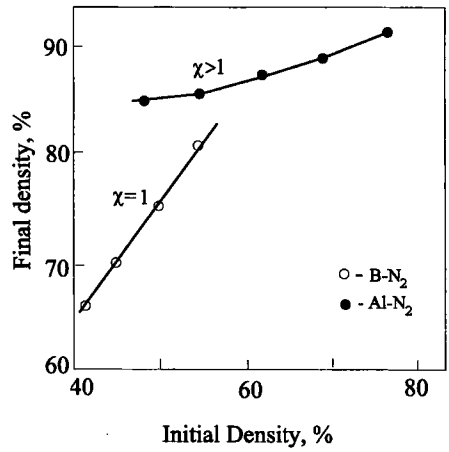

FIG. 46. Final sample density as a function of initial density for B-N_2 (Mukasyan, 1986) and Al-N_2 (Dunmead *et al.*, 1990a) systems.

studied experimentally. Some investigations have shown that the particle size, d, influences the process, and typical relationships are shown in Fig. 3b. While the combustion velocity generally decreases with increasing particle size, the actual function may vary: $U \sim 1/d$, $U \sim 1/d^2$, $U \sim 1/d^{1/2}$ (Merzhanov, 1981). These relationships were developed theoretically (see Section IV), taking into account the mechanisms of chemical interaction in the combustion wave. Often, the differences can be explained by comparing the adiabatic combustion temperature to the melting points of the reactants (see Table XX).

1. "Solid" Flame Systems

Tantalum–carbon, tantalum–boron, and niobium–boron mixtures may be classified as so-called "solid flame" systems, where T_c^{ad} is lower than the melting points of both reactants and products. Consequently, the sizes of reactant particles are not expected to change in the combustion wave. The dependence of U on the average metal particle size for these systems is presented in Fig. 47.

The tantalum–nitrogen system is also characterized by a relatively low measured combustion temperature (see Table XX) compared to the melting points of Ta and TaN. However, it was shown that the propagation velocity and temperature in this system are essentially independent of the Ta particle size (Agrafiotis *et al.*, 1991). This phenomenon was explained by accounting for the morphology of the fine and coarse powders. The coarser particles used were highly porous and had a large surface area, while the finer particles were nonporous. Thus, each coarse particle acted as a large number of discrete nonporous grains, and resulted in the same U as the fine powders.

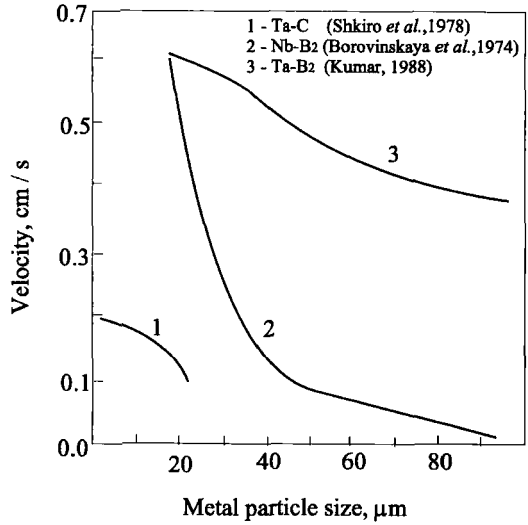

FIG. 47. Effect of metal particle size on combustion velocity in "solid flame" systems.

2. Systems with One Reactant Melting

In this case, the adiabatic combustion temperature is higher than the melting point of one reactant. The titanium–carbon system is the most widely investigated in this category. Data from different investigators for the $U=f(d)$ dependence for the TiC system are presented in Fig. 48. Only one study (Kumar *et al.*, 1988a) demonstrated a constant velocity for the range of Ti particle sizes investigated (up to 100 μm), which one may expect if the metal were to melt in the preheating zone. The others show a general trend where U decreases with increasing Ti particle size in the range of 40–250 μm. A similar trend was observed when the Ti particle size was constant, while the carbon particle size (d_C) was varied from 2 to 70 μm (Deevi, 1991). For relatively small Ti particle sizes (<20 μm), Shkiro and Borovinskaya (1976) have shown that the combustion velocity is independent of titanium particle size.

Nekrasov *et al.* (1978) considered three possible situations, which can be used to explain these results. When rather small metal particles are used, that is,

$$d_{\mathrm{Ti}}^2 < \sigma\lambda r_C \mu U^2 \ln\left(\frac{T_c - T_0}{T_m - T_0}\right), \tag{73}$$

where μ and σ are the viscosity and surface tension of the liquid, the interaction is controlled by the rate of chemical reaction between molten Ti and solid C, and the

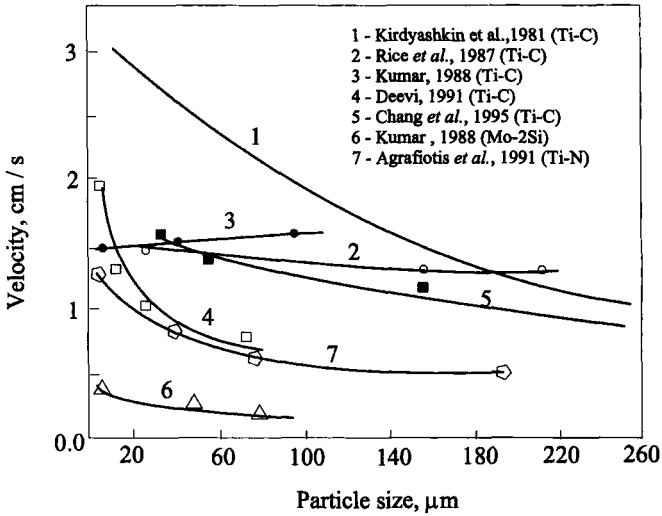

FIG. 48. Effect of metal particle size on combustion velocity in systems with one melting reactant.

combustion velocity is essentially independent of d_{Ti}. When relatively large Ti particles are used,

$$d_{Ti}^2 > \frac{\sigma \cdot r_c^3}{\mu D}, \tag{74}$$

where D is the diffusion coefficient of the molten reactant in the product, capillary flow becomes significant, and spreading of molten titanium through the solid carbon matrix dominates. Accordingly, the velocity decreases with increasing Ti particle size. For intermediate sizes, diffusion of titanium through the solid TiC product layer controls the interaction.

The molybdenum–silicon and titanium–nitrogen systems also belong to this group. For both, it was shown that U decreases when metal (Mo, Ti) particle size increases (curves 6 and 7, Fig. 48).

It has been shown that the ratio of reactant particle sizes influences the microstructure of the final product. In the 3Ni-Al system, the use of Ni (32–44 μm) and Al (<10 μm) led to the optimum microstructure (i.e., full conversion and dense final product) as d_{Ni}/d_{Al} approached 3.0. For example, using smaller Ni (<10 μm) and the same Al (<10 μm) particles, a more porous final product was obtained (Lebrat and Varma, 1992a).

3. Systems with Both Melting Reactants

Results for titanium–boron and several intermetallic systems (Ni-Al, Ti-Al, Ni-Ti, Co-Ti) are presented in Fig. 49. In all cases, the measured combustion tem-

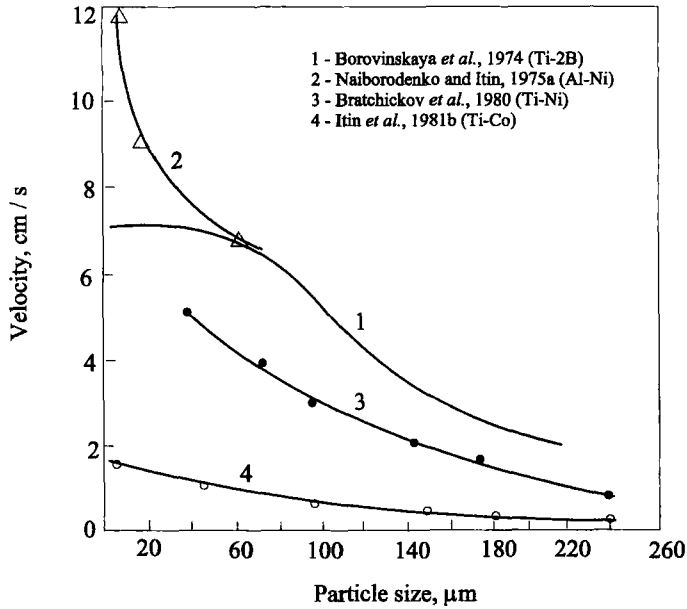

FIG. 49. Effect of metal (Ti, Al) particle size on combustion velocity in systems with both melting reactants.

peratures were higher than melting points of both reactants (see Table XX), and no exceptions to general trends (Fig. 3b) were obtained.

F. OTHER EFFECTS OF COMBUSTION CONDITIONS

In addition to the main variables already considered, other parameters also influence the combustion synthesis process. These include the ignition conditions, initial temperature of the green mixture, sample dimensions, and their effects and they are discussed next.

1. Initiation of SHS Process

A recent review by Barzykin (1992) summarizes experimental and theoretical studies on the initiation of CS systems. In this section, we focus only on the effects of initiation conditions on the reaction pathway during CS.

It has been shown theoretically that for the case of two competing parallel reactions, two stable combustion modes can exist (Khaikin and Khudiaev, 1979), where the reaction route depends on the ignition conditions. This effect was first observed experimentally by Martirosyan *et al.* (1983) for the Zr-C-H_2 system (Fig. 50). Using relatively low ignition temperatures (1300 K), the combustion

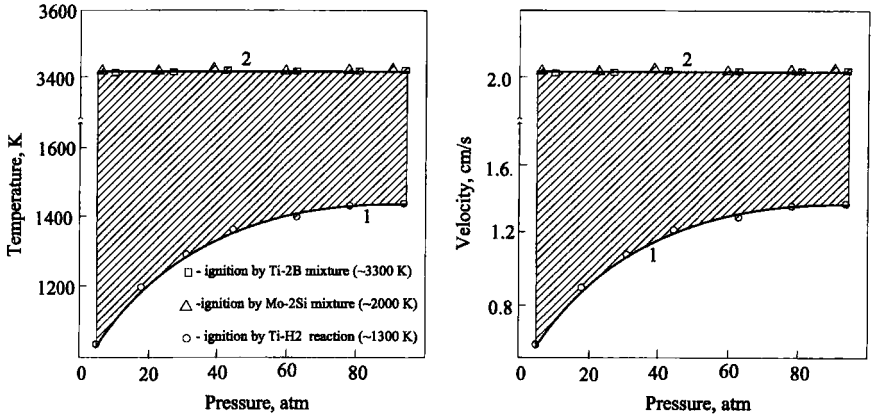

FIG. 50. Nonuniqueness of combustion modes in the Zr-C-H_2 system (Adapted from Martirosyan *et al.*, 1983).

proceeded via the low-temperature mode (curves 1) forming zirconium hydrides as the final product. For higher ignition temperatures (2100–3300 K), the high-temperature mode was realized (curves 2), and zirconium carbides were formed.

Recently the nonuniqueness of combustion modes due to different ignition conditions was observed both for the Ti-N_2-O_2 (Merzhanov *et al.*, 1995; see also Section VI,D,2) and Nb-B-O_2 (Mukasyan *et al.*, 1997a) systems. In the latter case, for ignition temperatures lower than 2050 K, a stable low-temperature (~1000 K) combustion regime resulted in the formation of niobium oxide (Nb_2O_5), while for ignition temperatures higher than 2350 K, NbB_2 was formed in a high-temperature (~2700 K) combustion wave (Fig. 51). It is worth noting the main difference between phenomena observed in the Nb-B-O_2 and Zr-C-H_2 systems. While both Nb_2O_5 and NbB_2 products are stable in the range of ignition temperatures used, zirconium hydride dissociates at temperatures higher than 1300 K and ZrC is the only stable phase existing under these conditions.

2. *Initial Temperature*

Experimental data for the combustion velocity dependence on initial temperature for different systems are presented in Fig. 52. Examples of intermetallic systems (Al-Ni and Co-Ti) with melting of both reactants show a general trend in which U increases with increasing T_0. The same behavior was obtained for the Mo-Si (Kumar *et al.*, 1988b), Ti-C (Kirdyashkin *et al.*, 1981) and 3Ni-Al (Lebrat and Varma, 1992a) systems, which are characterized by melting of only one reactant.

For gas–solid systems, this effect has not been studied well. In the only example available, which involves combustion of silicon in nitrogen, it was observed

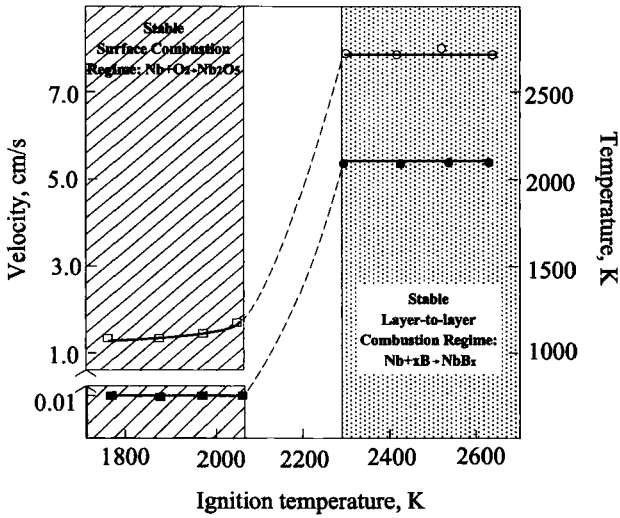

FIG. 51. Competition of chemical reactions in the Nb-B-O_2 system (Adapted from Mukasyan *et al.*, 1997a).

that the combustion velocity does not always increase monotonically with increasing T_0 (Fig. 53). For low dilutions ($\leq$30%), the combustion velocity has a maximum (curve 3). This effect can be attributed to greater melting and coalescence of silicon particles in the combustion zone for increasing T_0, which decreases the sample permeability.

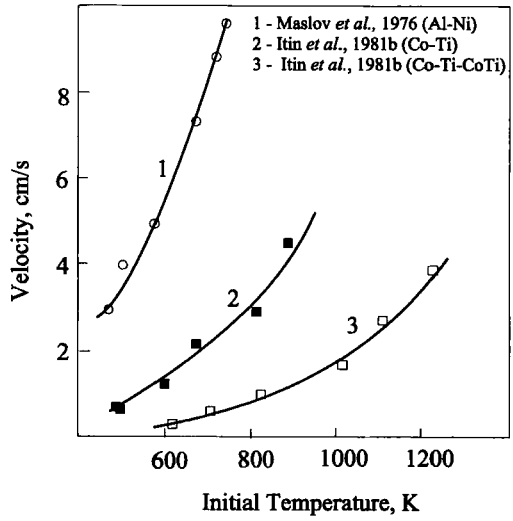

FIG. 52. Combustion velocity for intermetallic systems as a function of initial temperature.

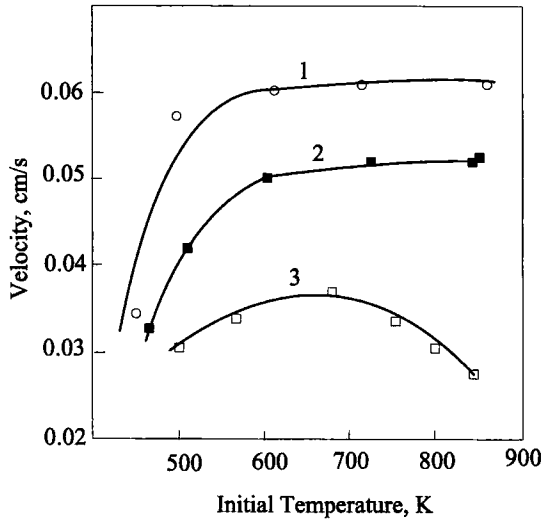

FIG. 53. Combustion velocity for Si-N_2 system as a function of initial temperature; P = 120 atm and different dilution levels: curve 1, 60 wt %; curve 2, 40 wt %; curve 3, 30 wt % (Adapted from Mukasyan, 1986).

3. Sample Dimensions

Increasing the sample diameter (D) increases the ratio of volumetric heat generation ($\propto D^3$) to surface heat loss ($\propto D^2$). The dependence of U on D, for different systems, is shown in Fig. 54. By increasing the diameter above a critical value, the combustion temperature approaches the adiabatic value, and U becomes constant. This behavior has been observed for the "solid flame" Ta-C system (curve 1), the Ti-C system (curve 2) where one reactant melts, and in Ni-Al (curve 3) where both reactants melt. The maximum measured temperature as a function of radial position in a cylindrical pellet with a diameter of 2 cm for the Mo+2Si system is presented in Fig. 55. The data show significant heat losses from the specimen. For this reason, incomplete combustion often occurs for samples with small diameter and may lead to an undesirable product phase composition (Martynenko and Borovinskaya, 1975; Bratchikov *et al.*, 1980).

For gas–solid systems, adjusting the sample diameter may alter the combustion regime due to changes in the characteristic filtration length (Section IV,D,2). For small diameters, a layer-by-layer infiltration mode with a high degree of conversion is observed in the Ti-N_2 system (Borovinskaya *et al.*, 1992a). However, to achieve high conversion for systems with a wide post-combustion zone, a slow rate of cooling is desired. In Fig. 56, the dependence of final conversion on sample diameter for the B-N_2 system is presented. A complete reaction was achieved only for samples with a relatively large diameter ($\geq$8 cm).

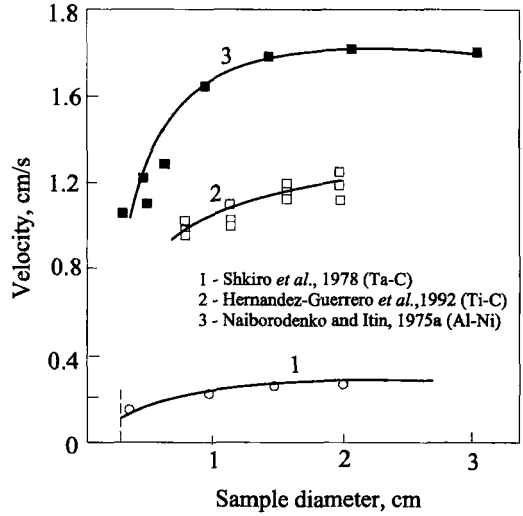

FIG. 54. Combustion velocity as a function of sample diameter.

4. *Effects of Gravity*

To control the product properties during the synthesis of advanced materials, the mechanism of product synthesis must be understood (see also Section VI). In other words, it is essential to develop a fundamental understanding of the physi-

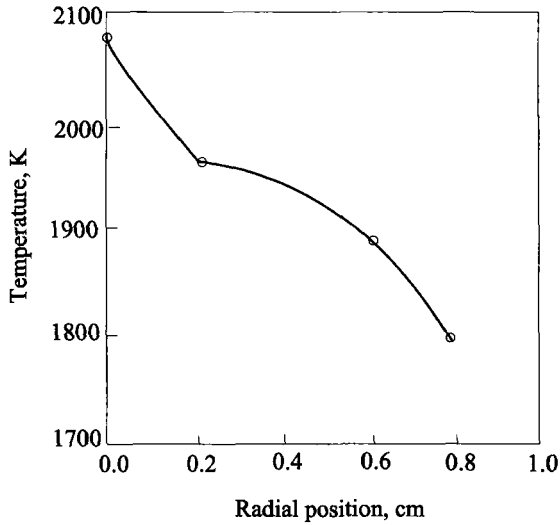

FIG. 55. The maximum combustion temperature as a function of radial position in the cylinder pellet; Mo-2Si system (Adapted from Kumar *et al.*, 1988b).

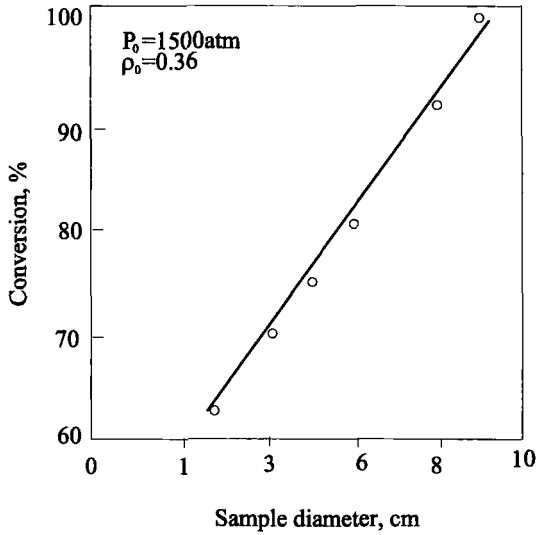

FIG. 56. Final conversion as a function of initial sample diameter for the B-N_2 system (Adapted from Mukasyan, 1986).

cochemical processes that occur during the extreme conditions of the combustion wave. A variety of reaction systems have been studied previously under normal gravity conditions, and results have shown that the mechanisms of combustion and structure formation involve several stages. These include melting of reactants and products, spreading of the melt, droplet coalescence, diffusion and convection in the molten phase, nucleation of solid products, crystal growth, buoyancy of solid particles and bubbles in the melt, and natural convection in the gas phase. Most of these processes are affected by gravity.

Relatively little research has been done to date on combustion synthesis of materials under microgravity. Aircraft experiments carried out in Russia (Shteinberg *et al.*, 1991) resulted in production of highly porous (up to 95%) TiC-based materials. The materials were produced using combustion synthesis from elements, with the addition of special gasifying compounds to the reaction mixture to increase pore formation. It was shown that the materials synthesized in microgravity (10^{-2} *g*) had higher degrees of expansion, with larger final porosities (see Fig. 57), than those produced in normal gravity conditions. Moreover, the distribution of porosity along the sample was more uniform under microgravity conditions. In the United States, foamed ceramic B_4C-Al_2O_3 composites were synthesized during parabolic flights on-board a Lear jet, using a thermite-type reaction (Moore *et al.*, 1992). Note, however, that the mechanical and physical properties of these foamed materials have not been well characterized. Nevertheless, they may provide interesting combinations of materials properties, especially if the

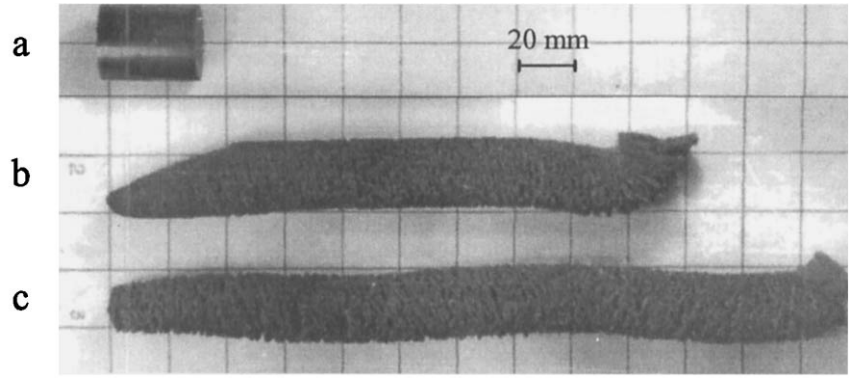

FIG. 57. Photographs of (a) initial sample and products (TiC) synthesized in (b) terrestrial and (c) microgravity conditions (Adapted from Shteinberg *et al.*, 1991).

distribution and morphology of the porosity, as well as micro- and macrostructures, can be controlled.

Another promising direction is production of poreless materials in microgravity. Reducing the effects of gravity during synthesis can inhibit segregation of phases with different densities (Yi *et al.*, 1996). Some experiments have been conducted in Lear jet planes (Hunter and Moore, 1994) to obtain dense ceramic–metal composites (e.g., TiC-Al_2O_3-Al, TiB_2-Al_2O_3-Al, ZrB_2-Al_2O_3-Al, $B_4CAl_2O_3$-Al) in thermite-type systems. These studies have shown that gravity significantly influences the CS of composite materials (Moore, 1995). For example, a more uniform product microstructure was obtained in μG as compared with normal gravity conditions. Also, experiments in microgravity for thermite systems (Zr-Al-Fe_2O_3) have been conducted in Japan (Odawara *et al.*, 1993).

In a recent work by Mukasyan *et al.* (1997b), experiments were conducted in a 2.2-s drop tower (NASA Lewis Center, Cleveland, OH) providing microgravity conditions ($\sim 10^{-4}$ m/s^2) during 2.2 s of drop time. The role of gravity on the combustion process and product microstructure during synthesis of various materials was examined. For example, in the Ni_3Al-TiB_2 composite system, the Ni_3Al ($-\Delta H_f^\circ$ = 153.1 kJ/mol) phase melts during reaction, allowing the buoyancy of the ceramic solid phase to be examined. The amount of liquid phase was controlled by varying the TiB_2 ($-\Delta H_f^\circ$ = 323.8 kJ/mol) content, which generates the additional heat. It was observed that gravity influences not only propagation of the combustion wave, but the microstructure of the final product as well. Statistical analysis revealed that the average particle size of TiB_2 grains in the material produced in normal gravity was 1.2 μm, while in microgravity it was 0.9 μm. These results were confirmed with quenching experiments, where the rate of grain growth during combustion synthesis can be obtained (Fig. 58). These experiments indicate that the difference is related to the process of grain growth dur-

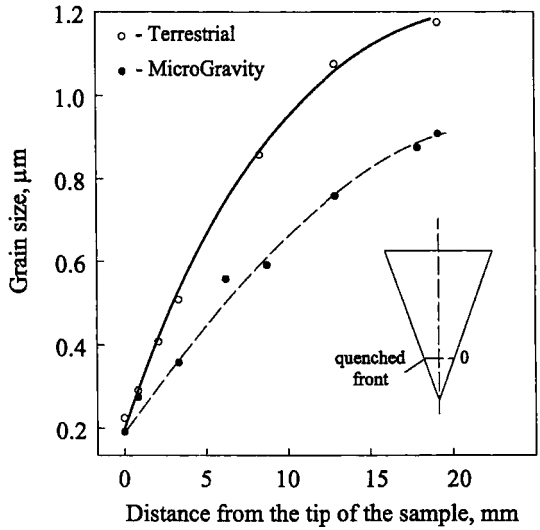

FIG. 58. Evolution of TiB_2 (dark phase) grain size in Ni_3Al (bright phase) matrix during combustion synthesis in the (Ti-2B)-(3Ni-Al) system (Adapted from Mukasyan *et al.*, 1997b).

ing CS. Although this effect should be investigated in more detail, it appears that enhanced mass transfer, owing to melt convection and buoyancy in normal gravity, promotes grain growth. Thus, gravity appears to be a promising way for controlling the microstructure of composite materials produced by combustion synthesis, and opens the possibility of nanophase materials production in the combustion wave.

VI. Methods and Mechanisms for Structure Formation

The characteristics of the combustion wave, including velocity and combustion temperature, are determined by the processes occurring in the heating and reaction zones and in some cases, the postcombustion zone. These different synthesis zones were determined experimentally for many systems by an analysis of the temperature profiles measured using microthermocouples (cf. Zenin *et al.*, 1980, 1981; Dunmead *et al.*, 1992a,b,c), and are shown schematically in Fig. 59. The length of the preheating zone varies from 0.05 to 0.3 mm, while the heating time and rate are equal to 10^{-4}–1 s and 10^2–10^6 K/s, respectively. The total wavelength (including zones of preheating, combustion and post-combustion) is generally 1–2 mm and may be as wide as 20–30 mm for multistage reactions. The reaction time within the combustion zone does not exceed 10 s even in the case of

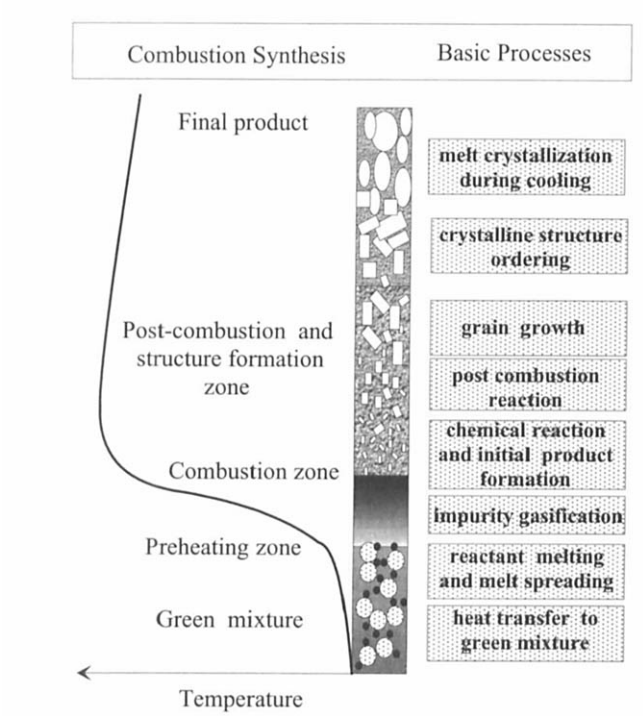

FIG. 59. Characteristic structure of combustion wave.

broad-zone waves and the temperature of most systems in this zone varies within the range of 2000–3000 K. Hence, the characteristic features of combustion synthesis are high temperatures, fast heating rates, and relatively short reaction times.

In addition to the specific features of the zones (i.e., temperature, length, heating rate, and time), the divisions between them can also be distinguished by the differences in physicochemical nature of the initial and final product structures. The initial stage of structure formation is concurrent with the chemical reaction, where the driving force of the process is the reduction of Gibbs free energy resulting from the formation of new chemical bonds, under nonequilibrium conditions (see Fig. 59). In the final structure formation process, physical effects are predominant where the free energy reduces further due to interfacial surface reduction, ordering of the crystal structure, and other related processes that occur without changes in the chemical composition under quasi-equilibrium conditions. In general, the initial product structure may be defined as that formed during a chemical reaction in the combustion zone, which becomes the starting point of the final structure formation step that yields the desired product in the postcombustion zone.

The boundary between the initial and final structure formation often coincides with the zone between combustion and postcombustion. However, in the case of considerable changes in the chemical composition taking place behind the combustion zone (e.g., during a multistage reaction), the boundary between the initial and final structure formation may coincide with the zones between postcombustion and cooling. If many intermediate products are formed in a multistage reaction, the initial structure of each should be considered.

As discussed earlier, analysis of temperature profiles obtained by microthermocouple measurements have elucidated the unique conditions associated with the combustion synthesis process. However, this approach does not directly identify the composition or microstructure of the phases formed. It is important to recognize that most published investigations in the field of combustion synthesis only address the *final* product structure. Considerably less has been reported about the structure formation processes leading to the final product. Most results that describe the evolution from the initial reactants to the final product are inferred by the effects of processing variables (e.g., density, dilution, particle size) on the final microstructure (see Section V). To date, only a few investigations have directly identified *initial* product structure. As discussed earlier, identification of this structure is important since the initial structure represents the starting point for all subsequent material structure formation processes. Thus, the focus of this section is on the initial stages of the structure formation mechanisms in combustion synthesis and novel methods developed especially for this purpose.

A. Major Physicochemical Processes Occurring during Combustion Synthesis

The following physicochemical processes affecting structure formation during combustion synthesis can be identified:

1. Heat transfer from the reaction zone to unreacted particles in the green mixture ahead of the reaction front
2. Phase transitions of solid reactants (e.g., αTi$\rightarrow$ βTi)
3. Formation of eutectic melts and contact melting
4. Melting of reactants
5. Spreading of a molten phase under the action of capillary forces and due to the reduction of surface tension
6. Coalescence of fused particles
7. Gasification of volatile impurities and reactants
8. Chemical reaction with initial product formation
9. Melting of intermediate products
10. Melt crystallization upon cooling

11. Crystal growth
12. Phase transitions in solid products during cooling
13. Ordering of the crystal structure

The first nine processes proceed during the rapid increase in temperature to a maximum at the combustion front and the last four take place behind the combustion front with a constant or gradual lowering of temperature. Therefore, dynamic methods of investigation providing *in situ* monitoring of fast processes with a short duration are necessary to describe adequately the first group of synthesis steps during rapid heating. On the other hand, methods that analyze quenched reaction waves or final products can be applied to the study of the processes occurring during cooling (processes 10–13).

B. Quenching of the Combustion Wave

Before the development of dynamic techniques discussed in later sections, the quenching technique, where there is rapid cooling of the combustion front, was the only method available to study mechanisms of structure formation during combustion synthesis. Following quenching, the phase composition and microstructure of the different zones in the combustion wave can be identified using a layer-by-layer analysis of the quenched regions by scanning electron microscopy (SEM) and X-ray diffraction (XRD). Several methods have been developed to quench the combustion wave during synthesis and are described next.

1. Quenching in Liquid

The first attempt to terminate the combustion wave and obtain quenched products was by immersing the sample in liquid argon (Merzhanov *et al.*, 1972). A schematic of this method is shown in Fig. 60a along with the measured cooling rate. However, the cooling rates were not high due to a gaseous layer that formed on the surface of the sample, which acted as a thermal insulator and decreased the quenching rate. The Zr-N_2 solid–gas system quenched in liquid argon revealed that the driving force for combustion wave propagation is heat evolution from a highly exothermic solid solution formed in the reaction zone (Borovinskaya and Loryan, 1976). The mechanism of nickel and cobalt aluminide formation in the reaction zone was also investigated by dropping the reacting mixtures in water (Naiborodenko and Itin, 1975a). In this work, the conclusion was made that the direct dissolution of Ni into molten Al is the controlling step at higher temperatures, while the interaction through a solid product layer limits the process at lower temperatures.

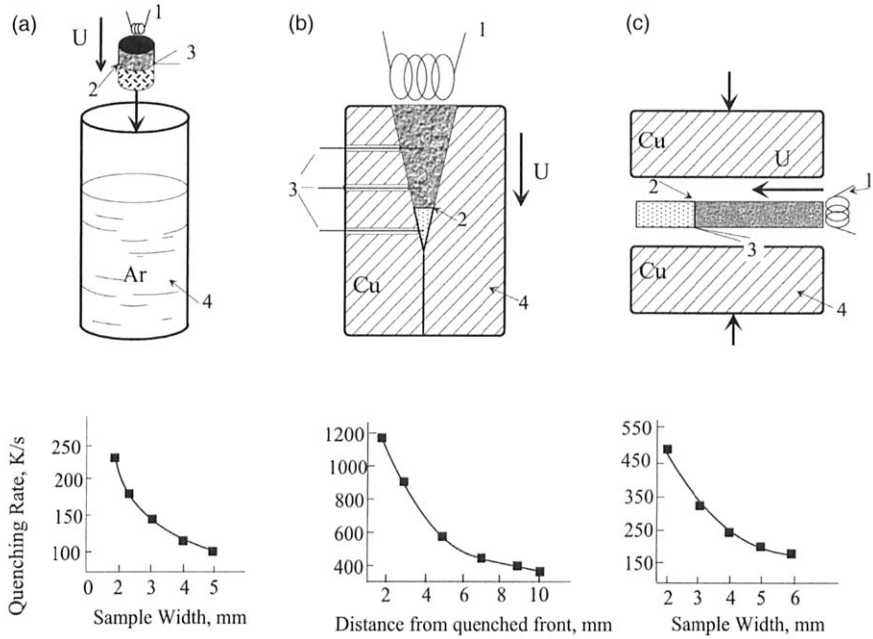

FIG. 60. Schematic drawings of quenching methods and cooling rates in (a) liquid argon; (b) a wedge-shaped cut in a copper block; (c) between two copper plates. 1, ignitor; 2, quenched front; 3, thermocouples; 4, quenching medium (Adapted from Mukasyan and Borovinskaya, 1992).

The highest rate of cooling (10^4–10^5 K/s) was reported for a relatively thin sample quenched with a high-speed water jet (Khusid *et al.*, 1992). However, the high water velocity (up to 150 m/s) necessary to achieve high rates of quenching often destroyed the sample and interaction occurred between the water and reacting sample.

2. *Quenching with Copper Block*

The use of a massive copper block to remove heat rapidly was originally demonstrated during the combustion of heterogeneous solid fuels (Andreev, 1966). This technique was later applied to quench reacting pellets during combustion synthesis (Rogachev *et al.*, 1987). In this method, a reactant mixture is pressed into a wedge-shaped cut in a copper block (Fig. 60b). The sample is ignited and the reacting mixture progressively quenched due to a decrease of the reactant mixture volume, which increases conductive heat losses to the walls of the copper block as the combustion wave travels to the apex of the wedge. A series of

photodiodes and/or thermocouples can be used to measure the temperature at several locations of the reacting pellet. The continuous acquisition of temperature during the experiment where quenching rates and times can be determined directly from temperature measurements is clearly an advantage of this method over quenching in a liquid.

Another quenching method utilized in gas–solid reacting systems involves a thin rectangular sample and two copper plates (Mukasyan and Borovinskaya, 1992). At an appropriate instant during the progress of the combustion wave, the reacting sample is squeezed between the copper plates. Thus, the copper plates serve not only as heat sinks but also isolate the reacting solid compact from the gaseous reactant (Fig. 60c). However, it can be seen from Fig. 60 that the quenching rate with copper plates is not as high as with the wedge-shaped cut of a copper block.

3. Quenching with Shock Waves

The use of shock waves has also been investigated to quench the combustion synthesis reaction in some systems, including titanium and air (Molokov and Mukasyan, 1992). In this method, the titanium compact was placed in a steel tube, which permitted access of air to the combustion zone. The steel tube was surrounded by an explosive charge. The titanium sample was ignited by a tungsten coil at one end. When the combustion wave reached a specific location in the sample, it was detected by an embedded thermocouple, and the explosive charge was detonated at the other end. This explosive shock wave rapidly altered the heat release conditions in the reacting sample by forcing the sample to contact the steel liner, which was at a lower temperature. In addition, the detonation force increased the sample density, which in turn increased the thermal conductivity, and quenched the reacting mixture. A quenching rate of $\sim 10^4$ K/s for this method was estimated indirectly from microstructural features. Using this technique, it was observed for the first time that titanium reacted with air in a two-stage process. The first stage was the interaction between titanium and nitrogen, while oxygen was involved in the postcombustion zone. A similar result was obtained by time-resolved X-ray diffraction, a technique discussed later in this section.

4. Quenching Results

Most quenching results reported in the literature to identify structure formation mechanisms during combustion synthesis were obtained by a wedge-shaped sample pressed into a copper block. As discussed earlier, this method is relatively simple and provides high cooling rates. The stages of structure formation were identified using this technique in several systems, including Ti-C and Ti-B (Rogachev *et al.*, 1987), Ti-C-Ni (Rogachev *et al.*, 1988), Ti-Al-C (Volpe and

Evstigneev, 1992), Ni-Al (Lebrat *et al.*, 1994), and Ti-Si (Rogachev *et al.*, 1995). Some of these results are discussed here.

Figure 61 shows the velocity measurements and temperature profiles for a TiC sample pressed in a wedge-shaped cut of a copper block and quenched (Merzhanov *et al.*, 1990a). With the exception of regions near the point of ignition and the quenched combustion front, the velocity of the combustion front remained approximately constant (Fig. 61a), which implies that within the region of constant velocity, conditions of product formation in the combustion zone are not significantly influenced by heat losses. A relatively high velocity near the ignition of the sample was attributed to an excess of enthalpy provided by the ignition heat pulse and a lower velocity near the point of extinction due to significant heat loss to the copper. However, there is a gradual decrease in quenching time in the sample as the front propagates from the top (wide portion) to the bottom (apex), as shown in the temperature profiles at different locations (Fig. 61b). Thus, different regions in the sample have progressively less reaction completeness and represent

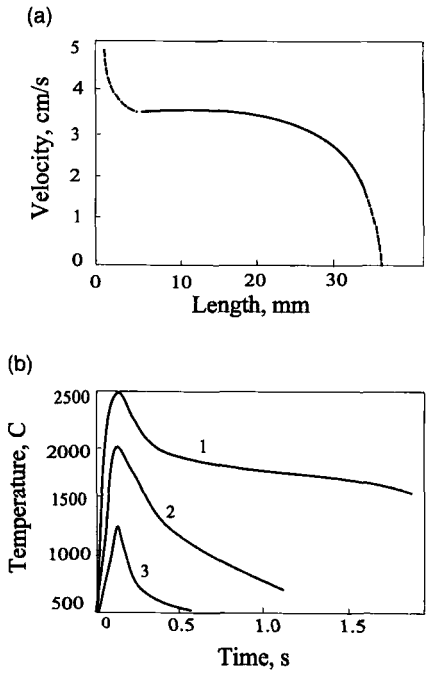

FIG. 61. Combustion front quenching in a wedge-shaped cut of a copper block for Ti-C system: (a) velocity as a function of distance from ignition surface; (b) temperature profiles at different locations relative to ignition surface: curve 1, 3 mm; curve 2, 26 mm; curve 3, 36 mm (Adapted from Rogachev *et al.*, 1987).

the sequence of steps in the structure formation process of the postcombustion zone. By combining the resulting phase formation with the measured quenching time, it is possible to evaluate the kinetic characteristics of the final structure grain growth. The initial structure formation processes can be identified by studying the extinguished area.

The microstructure of the initial titanium-graphite mixture is shown in Figure 62a. When the temperature in the combustion wave reaches 1660°C, titanium melts. It was determined from quenching results that a thin film (~0.1 μm) of the Ti melt spreads over the solid carbon surface with *simultaneous* formation of titanium carbide grains (Fig. 62b). Small rounded TiC particles were observed to appear *within* the liquid rather than in the form of a continuous product layer (Rogachev *et al.*, 1987). To illustrate this fact further, the typical microstructure formed during combustion reaction of titanium melts with graphite whiskers (10 μm in diameter) is shown in Fig. 62c.

A similar mechanism of initial product formation within a molten film was also observed for TiB_2, with the difference that at a distance ~1 mm from the combustion front, the rounded boride particles acquired morphological anisotropy followed by crystallographic faceting. Also, in a study of various quenched Ti+C+Ni mixtures (Rogachev *et al.*, 1988), it was determined that titanium carbide grains (~1 μm) were surrounded by a metallic melt composed of Ti and Ni. The product grains continued to grow in the postcombustion zone. The fraction of C in the product TiC_x grains was greater than the initial C/Ti ratio, owing to the reaction of titanium with nickel.

The product grain growth rate was determined from measurements of the grain size in the different quenched regions obtained by SEM observations. For example, a sequence of microstructures taken from different zones of Ti-C-Ni quenched samples is shown in Fig. 63. The results of statistical analysis of such microstructures for Ti-C, TiB_2, and Ti-C-Ni systems are presented in Fig. 64, and illustrate an initial rapid increase in grain size that approaches a constant value in

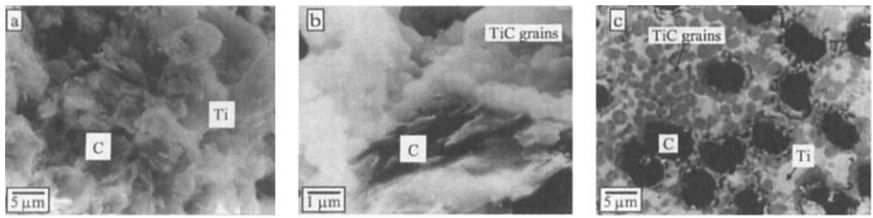

FIG. 62. Characteristic microstructures during synthesis of Ti-C system: (a) initial reactant mixture, Ti+graphite; (b) initial product formation; (c) formation of TiC grains in Ti melt around graphite whiskers.

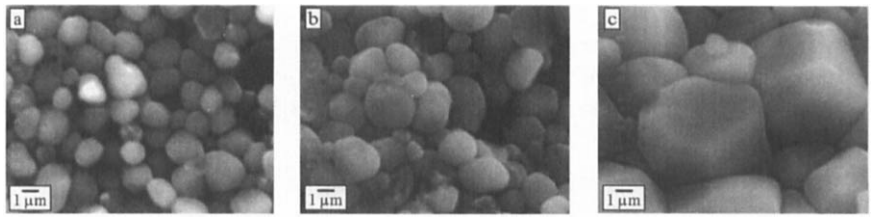

FIG. 63. Sequence of microstructures taken from different zones of Ti-C-Ni (Rogachev *et al.*, 1988): (a) 1 mm; (b) 10 mm; (c) 35 mm behind quenched front.

the postcombustion zone. The growth rate of the mean product grains ranges between 1 and 30 μm/s and demonstrates that the initial product grains increase by an order of magnitude in a few seconds after passage of the combustion front. A layer-by-layer X-ray diffraction (XRD) phase composition analysis of quenched Ti+C and Ti+2B mixtures confirms that the refractory carbide and boride crystal

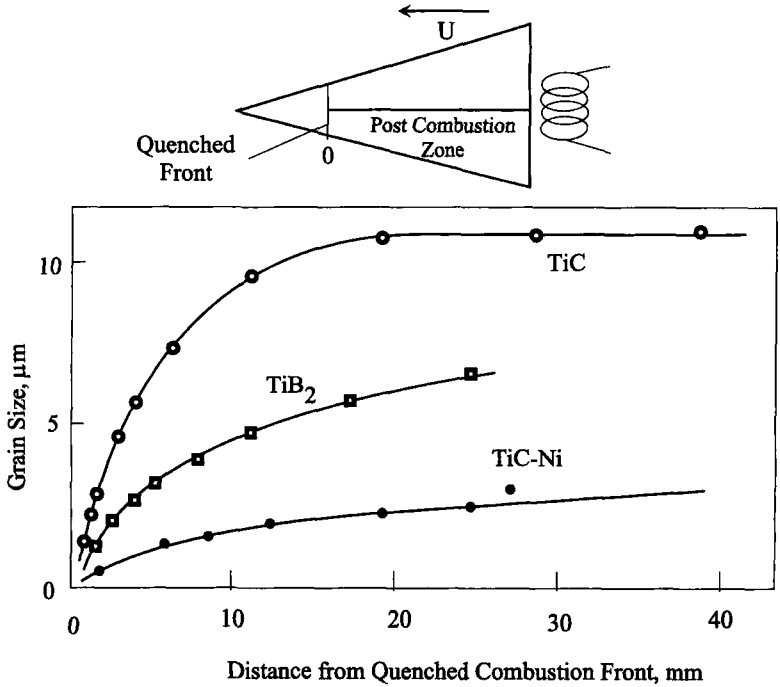

FIG. 64. Product grain growth in quenched samples of different systems (Adapted from Merzhanov and Rogachev, 1992).

structures form in the reaction zone, and the phase composition does not change behind the combustion front (Fig. 65).

The evolution of the microstructure in combustion synthesis of Ni_3Al, showed that the Ni_2Al_3 and NiAl layers initially appear on the surface of Ni, followed by formation of the final Ni_3Al product (Lebrat *et al.*, 1994). It was shown that the *dissolution* of Ni into the Al melt controls the process. On the other hand, an investigation of quenching Ni+Al mixtures (Rogachev *et al.*, 1993) led to the conclusion that Ni and Al particles melt simultaneously and coalesce in the reaction zone, resulting in the appearance of NiAl crystals in the volume of melt. Homogenization of the chemical composition occurred in the postcombustion zone. This mechanism of structure formation was observed for the first time and is referred to as the *reaction coalescence* mechanism (Rogachev *et al.*, 1993). The results from the two studies demonstrate that in the case of the 3Ni+Al system, the final product is preceded by the NiAl and Ni_2Al_3 intermediate phases, whereas in the Ni+Al reaction, the initial product has the same overall phase composition as the final product.

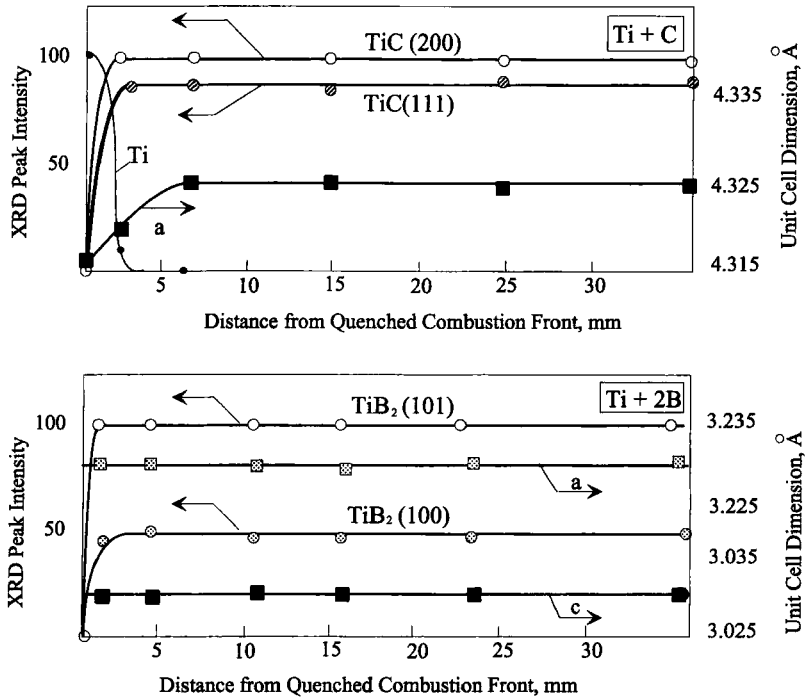

FIG. 65. Results of layer-by-layer X-ray diffraction phase composition analyses of quenched Ti-C and Ti-2B mixtures (Adapted from Rogachev, 1995).

C. Model Systems for Simulation of Reactant Interaction

The spatial structure of a heterogeneous reactant powder mixture with its random distribution of reactant particles is too complex for a study of the elemental stages of structure formation mechanisms. This problem has been overcome by the development of experimental techniques that utilize reactants with simpler geometries, such as wires and foils. These methods isolate the reactant interaction, thus yielding additional information.

1. Metal Wires

The *electrothermography* method, in which metal wires are heated by electric current in an oxygen gas atmosphere, was originally developed to study oxidation processes (Grigor'ev, 1975). This technique was also used to study the mechanism of ignition for Ti+C and Zr+C systems, by coating Ti and Zr wires with carbon black (Vadchenko *et al.*, 1976). The interaction between reactants was quenched by simply shutting off the current to the wire. In this work, after the metal filament (Ti or Zr) was heated to the melting point, the liquid metal penetrated the pores of carbon under the action of capillary forces. This led to self-propagating reaction conditions in which chemical heat evolution was due to the dissolution of carbon in the liquid metal, forming carbide phases. The interaction mechanism was also investigated with titanium and aluminum wires electrodeposited with nickel (Vadchenko *et al.*, 1987). In this study, cross-sections of the reacted wires were polished and the influence of initial temperature on intermetallic layer growth was investigated. The critical temperatures of the two systems were also determined. In titanium wires coated with nickel, the critical temperature of 1220 ± 20 K corresponded to the eutectic reaction $\beta Ti+Ti_2Ni$ (1128 K) below the melting points of Ti and Ni. For nickel-coated aluminum wires, the temperature of 910 ± 20 K was close to the eutectic reaction $Al+NiAl_3$ (913 K) and the aluminum melting point (933 K). The dependence of interaction on the Ti wire diameter and the nickel coating thickness was also identified.

2. Laminated Metallic Foils

To provide a well-defined boundary between reactants, experiments have been conducted using ensembles of laminated Ni and Al metallic foils (Anselmi-Tamburini and Munir, 1989). These experiments were motivated by modeling efforts that used a foil geometry to understand interactions between powder reactants (Hardt and Phung, 1973; see Section IV,B). In the experimental technique, nickel (12.5 and 125 μm) and aluminum (12.5 μm) foils were laminated in specific stoichiometric amounts corresponding to the NiAl and $NiAl_3$ compounds. These ensembles were then ignited in a chemical oven consisting of Ni+Al pow-

ders. An inert layer (Al_2O_3), placed at the bottom of the laminated foils, quenched the wave propagation through the foils. In both the NiAl and $NiAl_3$ foil compositions, melting of aluminum occurred ahead of the wave and ignition was triggered at the nickel melting point.

The appearance of molten aluminum *ahead* of the combustion front was not observed in quenching studies for nickel aluminides (Lebrat *et al.*, 1994). However, the quenched foil result using a Ni+Al composition is in partial agreement with quenching experiments for NiAl (Rogachev *et al.*, 1993) where the presence of molten nickel and aluminum was observed *at* the combustion front. It is possible that the presence of an oxide film on the aluminum foils could have delayed ignition until the nickel melting point. In any case, it appears that the foil assembly does not adequately model the interaction between particulate reactants during combustion synthesis.

3. *Particle-Foil Experiments*

In both the electrothermographic and foil assembly methods, the rapid heating rates associated with combustion synthesis are reproduced. However, the powder reactant contact found in a compacted green mixture of particulate reactants is not adequately simulated. One way to overcome this is to investigate interactions of particles of one reactant placed on the surface of the coreactant in the form of a thin foil. The physical simulation corresponds to the reaction of a powder mixture where the particle size of one reactant is small while that of the coreactant is relatively large. Two methods have been used to initiate the interaction.

a. Reaction Initiated by Electron Beam. This method was proposed by Korchagin and Podergin (1979), where the electron beam not only initiates the reaction but also allows *in situ* observation of morphological and microstructural changes in a transmission electron microscope (TEM). The beam creates temperature conditions (i.e., rapid heating rates) similar to those found in a combustion wave propagating through a pressed compact of reactants. It was switched off at various stages in order to quench the interaction and the product formed was examined with the microscope.

The interactions of Fe_2O_3 particles over Al (Korchagin and Podergin, 1979) and Ti particles over C (Korchagin and Aleksandrov, 1981) were investigated using this technique. It was determined that the reaction between components is initiated after the appearance of a liquid phase that diffuses into the solid phase. This is followed by the formation of a primary product layer, which permits the solid to pass to the liquid phase by dissolution. It is interesting to note that the diffusion coefficients of the liquid component, estimated from the growth rate and width of

the primary product layer, exceeded known values for bulk bimetallic samples by several orders of magnitude.

In similar TEM work by Sharipova and coworkers (1992), the interaction of Cr_2O_3 particles with a sputter coated Al film was observed. From this work, it was determined that Cr_2O_3 was reduced in stages: $Cr_2O_3 \rightarrow CrO \rightarrow Cr$. The chromium aluminides that formed ($CrAl_2$, Cr_3Al_2, Cr_9Al_{17}) were found to depend on the aluminum content of the sample and on the initial temperature, maintained using a tungsten coil prior to initiation of combustion with the electron beam.

b. Reaction Initiated by Electric Current. Based on microscopy and electrothermographic methods, another experimental technique (Shugaev *et al.*, 1992a,b) involving particle and foil reactants has been developed that allows a direct continuous observation of the process (see Fig. 66). In this approach, the foil substrate and particles are heated at rates up to 10^3–10^4 K/s by passing an electrical current through the foil, which allows better control in heating the two reactants and simulates heating rates found in the combustion wavefront. It is apparent that the upper

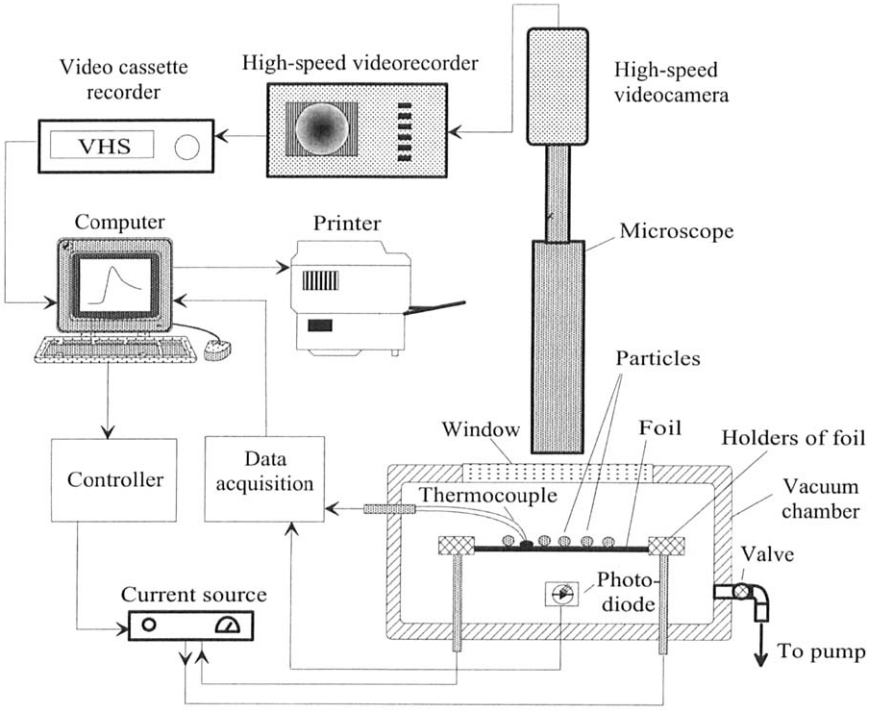

FIG. 66. Schematic drawing of a particle-foil experimental setup (Adapted from Rogachev *et al.*, 1994b).

temperature limit of this method is the melting point of the foil reactant. In the works cited earlier, the temperature of the heated foil was calculated from the emissivity registered with a photodiode, and the error in the temperature measurement was $\pm 1\%$. The extent of interaction between the reactants was controlled by varying the current and quenching that resulted from switching off the current, making it possible to examine the initial stages of structure formation. A direct continuous observation of the interaction was obtained with a high-temperature microscope attached to a high-speed motion picture camera. The quenched intermediate structures were analyzed by means of SEM and electron probe microanalysis (EPMA).

Two groups of systems have been identified: (1) with rapid and broad spreading of the reaction area and (2) without considerable spreading (Rogachev *et al.*, 1994a). In the first case, the spreading rate is on the order of 1 mm/s where a thin, fine-grained product layer appears on the surface of a nonmelting foil substrate. In the second case, the spreading rate is less than 0.1 mm/s, where the molten particles penetrate into the substrate rather than spread over the surface. The first group includes most carbide, boride, and silicide systems (Ti-C, B-Nb, B-Ta, B-Mo, Si-Nb, Si-Ta, Si-Mo, etc.) while the second group consists mainly of intermetallic systems (Al-Ni, Al-Ti, Al-Nb, etc.). Some systems (e.g., Si-Ti) exhibit intermediate behavior.

It is important to note that the initial product microstructures observed in the model particle-foil experiments are similar to those detected in the quenched reaction zone of the combustion wave in bulk samples. For example, grain size distributions for both experiments in the TiC system are shown in Fig. 67. Rather fine grains form at the early stages of both experiments (curves 1 and 2), followed by significant coarsening of grains which takes place in a few seconds up to tens of seconds (curves 3 and 4). Their agreement suggests that the particle-foil experiment simulates particulate reactant interaction within a pressed compact.

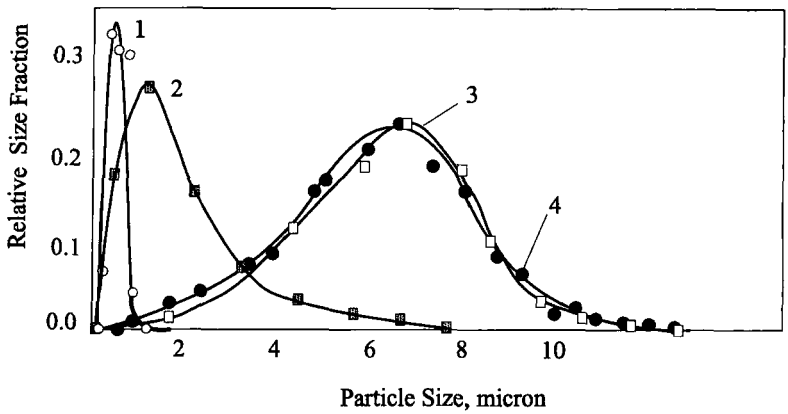

FIG. 67. A comparison of the TiC product grain size distributions in the initial (curves 1, 2) and final (curves 3, 4) stages of product formation obtained by quenching (curves 2, 4) and particle-foil techniques (curves 1, 3) (Adapted from Rogachev, 1995).

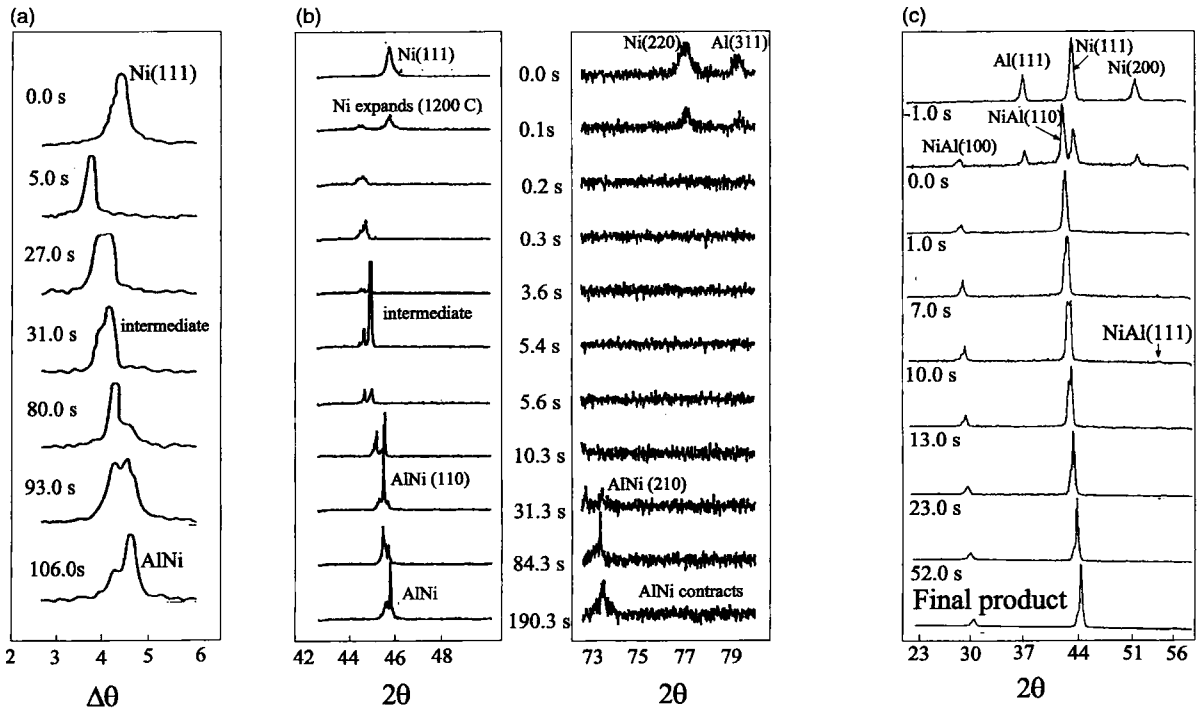

FIG. 68. Comparison of TRXRD results on the dynamic of phase formation in Ni-Al system: (a) Adapted from Boldyrev et al., 1981; (b) Adapted from Wong *et al.* 1990; (c) Adapted from Rogachev *et al.*, 1994a.

D. Time-Resolved X-ray Diffraction (TRXRD)

1. TRXRD Using Synchrotron Radiation

Continuous monitoring of crystal structure formation during combustion of a heterogeneous mixture of reactants is a powerful tool for understanding the structure-forming mechanisms. This idea was first realized using synchrotron radiation (Boldyrev *et al.*, 1981) and provided interesting results. A sequence of XRD patterns in the vicinity of 100% Ni and NiAl peaks, recorded during the combustion synthesis of a Ni+Al mixture, demonstrated that the diffraction line of nickel monoaluminide appeared 70–75 s after the combustion wave passage. The formation of the NiAl product was preceded by two lines shifted into a region of larger interplanar spacing (i.e., lower angles) than that of NiAl (Fig. 68a), which were assigned to unidentified intermediate phases.

The TRXRD synchrotron radiation method was developed further by Holt *et al.* (1990) where the scanning time of each XRD pattern was reduced to 0.01 s and two position-sensitive detectors allowed simultaneous monitoring of two regions of the X-ray diffraction spectrum. The combustion syntheses of NiAl, TiC, TiC-NiTi (Holt *et al.*, 1990; Wong *et al.*, 1990), TaC, and Ta_2C (Larson *et al.*, 1993) were investigated by this improved method. In an investigation of the Ni+Al reaction, the most intensive XRD peak of NiAl (110) appeared about 10 s after the passage of the combustion front and was preceded by several shifted and split peaks that were attributed to an unidentified intermediate product. The appearance of the NiAl (210) peak, 20 s after the NiAl (110) line, was attributed to the process of crystal lattice ordering after passage of the combustion front (Fig. 68b).

2. TRXRD Using an X-Ray Tube

A significant advance in this field was achieved by Merzhanov and coworkers (1993) with a new method of TRXRD using an ordinary X-ray tube (~2 kW). A schematic diagram of the apparatus is shown in Fig. 69. Using a one-dimensional position-sensitive detector, a wide range of XRD spectra (up to 30–40 degrees) can be monitored, which allows simultaneous observation of several nonoverlapping lines of each phase in complex systems. To calculate the XRD peak shift due to thermal expansion of the crystal lattice during combustion, the temperature of the sample area under investigation was measured by a thermocouple.

Several SHS systems have been investigated using this equipment, including Ti-air, Ti-N_2 and Ti-O_2 (Khomenko *et al.*, 1993), Ni-Al (Rogachev *et al.*, 1994b), Ti-Si (Rogachev *et al.*, 1995), Nb-B, Ti-C, Ta-C, and Ti-Cr-C (Merzhanov *et al.*, 1995). The results from these investigations demonstrate one or multistage mechanisms of product structure formation, where the sequence of stages was generally found to be different in the combustion wave relative to synthesis by conventional methods involving lower heating rate conditions.

The TRXRD patterns obtained during combustion of a Ni+Al mixture are shown in Fig. 68c (Rogachev *et al.*, 1994b). Corrections made taking into account thermal expansion led to the conclusion that partially disordered NiAl is the first phase to appear in the combustion synthesis wave rather than an unidentified phase as previously concluded by Boldyrev *et al.* (1981) and Wong *et al.* (1990). The splitting of peaks was determined to be due to the ordering process in NiAl that takes place in the postcombustion zone. In 2Ni+3Al mixtures, the disordered Ni_2Al_3 phase was found as a primary product during combustion. An ordering process of the crystal lattice was observed during the cooling of samples. These results suggest the possibility of obtaining disordered intermetallic phases by combustion synthesis.

Another example of the application of the TRXRD method involved combustion of Ti in air (Khomenko *et al.*, 1993). A complicated mechanism was observed involving five intermediate phases that preceded the formation of the final TiO_2 product. In general, the TRXRD results were similar to those found in quenching the reaction with shock waves (Molokov and Mukasyan, 1992) where the first stage involves the titanium–nitrogen reaction, followed by the interaction with oxygen in the postcombustion zone. The TRXRD experiment identified the formation of additional oxide phases that may have remained undetected during microprobe analysis of the quenched sample. The kinetics of the appearance and disappearance of each phase are shown qualitatively in Fig. 70.

An interesting TRXRD result during the combustion of titanium with air is the dependence of the reaction mechanism on temperature. At low heating rates (10°C/s), where the maximum combustion temperature was determined to be ~650°C, the Ti reacts directly with oxygen to form TiO_2 (Merzhanov *et al.*, 1995). At a considerably higher heating rate of ~10^3°C/s, the maximum combustion tem-

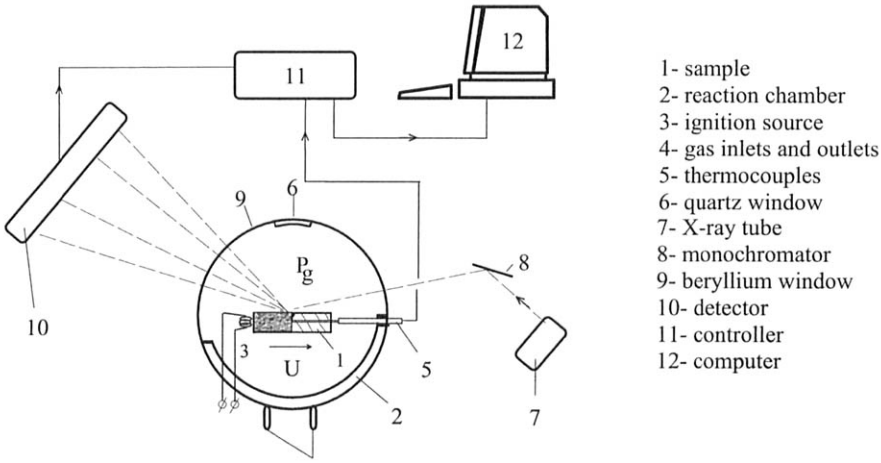

FIG. 69. Schematic diagram of the laboratory TRXRD apparatus (Adapted from Khomenko *et al.*, 1993).

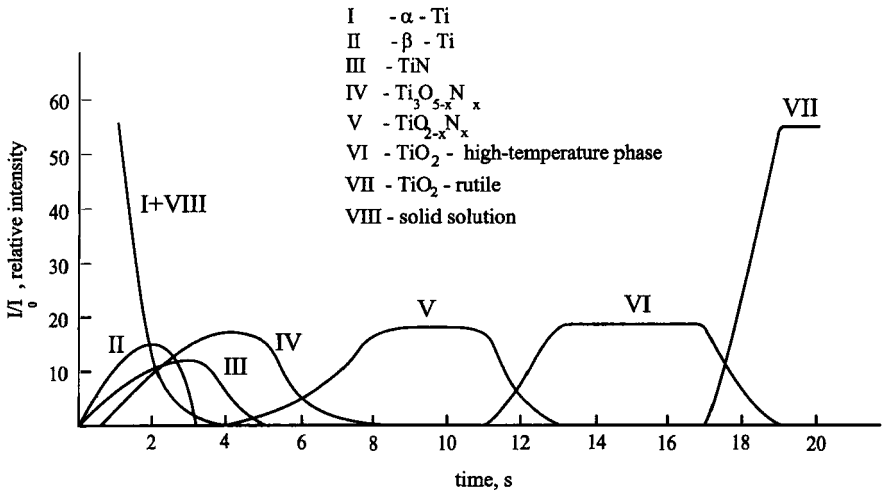

FIG. 70. Dynamics of phase formation during combustion reaction between titanium and air in high-temperature mode (Adapted from Khomenko *et al.*, 1993).

perature was ~1700°C and a more complex mechanism occurs: $\alpha Ti \rightarrow \beta Ti \rightarrow TiN_x \rightarrow Ti_3O_{5-x}N_x \rightarrow Ti_6O_{11-x}N_x \rightarrow TiO_{2-x}N_x \rightarrow TiO_{2-x}N_x$ (rutile structure). These results demonstrate that the sequence of intermediate phases formed may depend strongly on the heating rate.

E. MICROSTRUCTURE OF COMBUSTION WAVE

While the microscopic processes occurring in the combustion wave need to be understood, the microstructure of the combustion wave itself is also a significant consideration. In other words, it is important not only to understand the local structural transformations occurring during CS, but to link them with variations in local conditions of the combustion wave. The two approaches for investigating the combustion wave microstructure examine the temperature–time profiles and heterogeneity of the combustion wave shape and propagation, at the local level.

In the first approach, the temperature–time profiles of the combustion wave are measured using thin thermocouples (Zenin *et al.*, 1980; Dunmead *et al.*, 1992a,b,c). In the work of Zenin *et al.* (1980), 7-μm-diameter microthermocouples protected by a layer of boron nitride were used. The temperature–time profiles were analyzed using the one-dimensional heat conduction equation with heat generation (see Section IV,A,1) taking numerical derivatives of the spatial temperature distribution. An implicit assumption in the analysis is that the combustion wave is stable and planar at both the macro- and microscopic scales.

Several reaction systems (e.g., Nb-B, Zr-B, Ti-Si, Ti-C) have been studied using this approach. For example, the results for a Nb+2B mixture are shown in

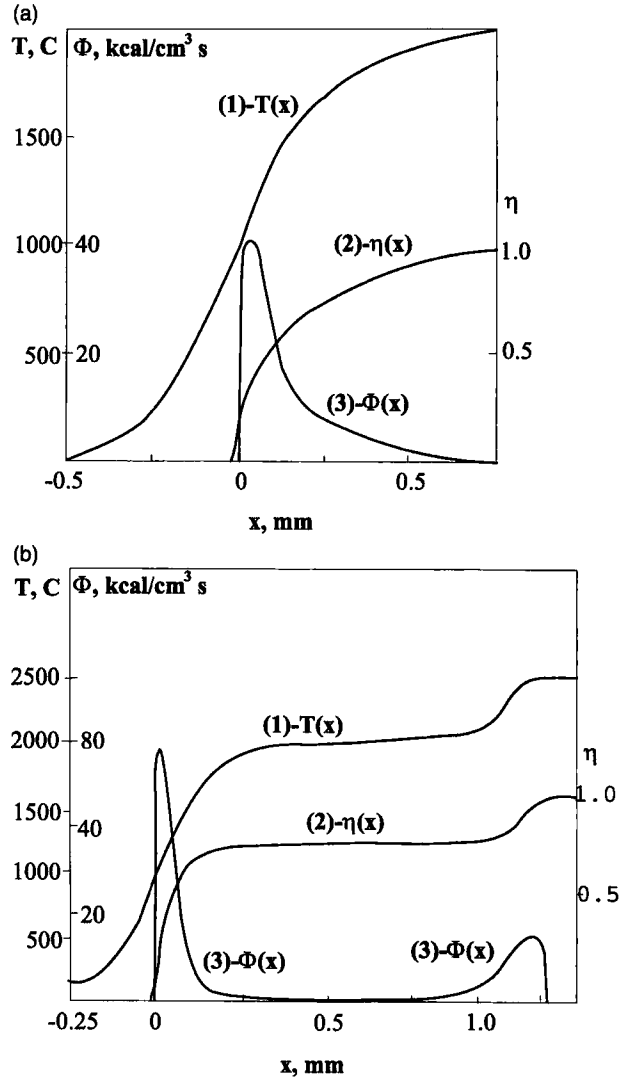

FIG. 71. Average temperature distribution over the combustion zones of the mixture Nb+xB, rate of heat release Φ, and degree of conversion, η: (a) the mixture Nb+2B; (b) Nb+B (Adapted from Zenin *et al.*, 1980).

Fig. 71. Based on the measured temperature profile data (curve 1), the distribution of conversion along the combustion wave, $\eta(x)$ (curve 2), and the heat release function, $\phi(x)$ (curve 3), have been determined using Eq. (15). The characteristic length of the zones, L_r is given by the size of the domain where $\phi(x)$ is nonzero. The preheating zone, x_T, is defined as the sample length ahead of the front where

the heat flux (i.e., $q=\lambda \cdot dT/dx$) varies linearly with temperature, T (see Section IV,A,2).

The second approach considers the heterogeneous structure of the compact particulate reaction mixture. Since the combustion wave propagates through a mixture of powder reactants with varying particle sizes (0.1–100 μm), nonuniformity of the combustion front and variations in propagation velocity can be expected at the microscopic scale.

Using a high-speed movie camera, the heterogeneity of the combustion front for Ti-C-Ni-based systems (reacted in air) was observed (Levashov *et al.,* 1991). Recently, a new method using microscopic high-speed video imaging was developed (Rogachev *et al.,* 1994b) to study the microstructure of the combustion wave for various systems including Ti-C, Ti-Si, Ti-N_2, and Ni-Al. A schematic of the experimental apparatus is shown in Fig. 72. The setup is equipped with a long-focus microscope (K-2, Infinity Photo-Optical Company) and a high-speed video camera (EktaPro 1000 Imager and Processor, Kodak). With this method, the combustion wave can be observed at high spatial (800×) and temporal (1-ms) resolutions.

Figure 73 shows the propagation of the combustion front (bright field) through the green mixture (dark field) for the gasless Ti-Si system. At conventional mag-

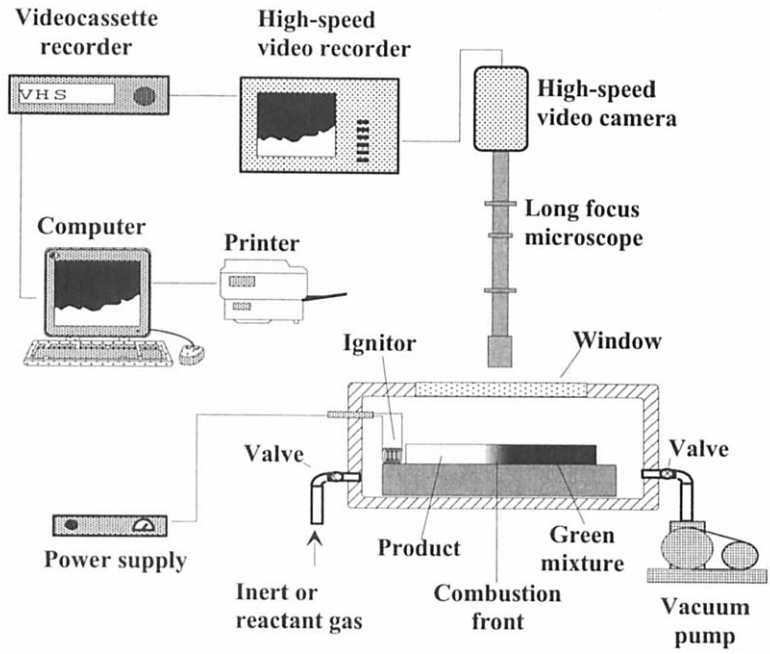

FIG. 72. Scheme of experimental technique for microstructure of combustion wave study (Adapted from Rogachev *et al.,* 1994b).

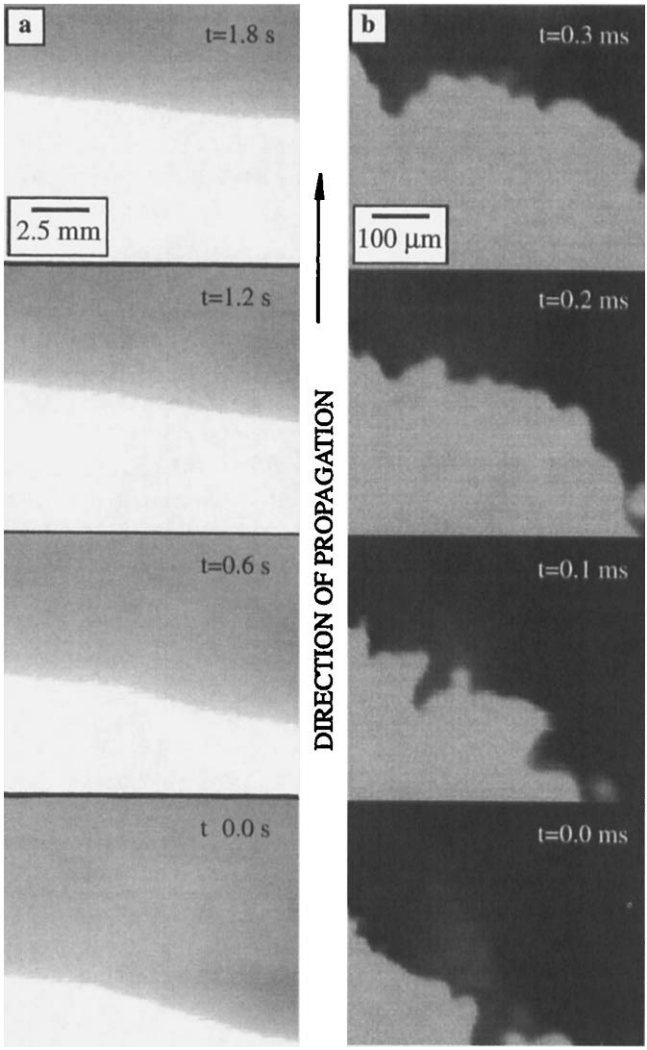

FIG. 73. Frames of combustion front propagation through the 5Ti-3Si system obtained with different magnifications and image rates: (a) 4× and 30 frames/s; (b) 100× and 1000 frames/s (Adapted from Mukasyan *et al.*, 1996).

nification (4×) and imaging rate (30 frames/s), the combustion front profile appears flat, and moves steadily through the pellet (Fig. 73a). However, at high magnification (100×) and imaging rate (1000 frames/s), the shape of the combustion front is seen to be irregular with pronounced arc-shaped convexities and concavities (see Fig. 73b). Also, the combustion wave moves in an unsteady manner, often hesitating or moving rapidly. The results show that the microstructure of the combustion front is comparable to the titanium particle size and shape.

TABLE XXII
CHARACTERISTICS OF COMBUSTION FRONT PROPAGATION[a]

Characteristic	Parameter
Average position of combustion front at time t	$\bar{F}(t) = \dfrac{\int_0^{y_0} F(y,t)dy}{y_0}$
Dispersion of combustion front	$\sigma_F = \sqrt{\dfrac{\int_{t_i}^{t_f}\int_0^{y_0}[\bar{F}(t) - F(y,t)]^2 dy\,dt}{y_0(t_f - t_i)}}$
Instantaneous combustion front velocity	$U(y,t) = \dfrac{\partial F(y,t)}{\partial t} \approx \dfrac{F(y,t_i) - F(y,t_{i-1})}{t_i - t_{i-1}}$
Average combustion front velocity for duration of experiment	$\bar{\bar{U}} = \dfrac{\int_{t_i}^{t_f}\int_0^{y_0} U(y,t)dy\,dt}{y_0(t_f - t_i)}$
Dispersion of combustion velocities for duration of experiment	$\sigma_U = \sqrt{\dfrac{\int_{t_i}^{t_0}\int_0^{y_0}[\bar{U}(t) - U(y,t)]^2 dy\,dt}{y_0(t_f - t_i)}}$

[a]Data from Mukasyan *et al.* (1996).

The microscopic high-speed video recording method has recently been developed further and used to investigate the combustion wave microstructure in the Ti-Si and Ti-N_2 systems (Mukasyan *et al.*, 1996; Hwang *et al.*, 1997). The location of the combustion front was estimated using image analysis techniques, and its shape and propagation were characterized quantitatively.

Table XXII shows some of the parameters used to characterize the microstructure of the combustion wave. In general, the parameters can be divided into two groups. The first group characterizes the *shape* of the combustion front, and includes the local $[F(y,t)]$ and average $[\bar{F}(t)]$ front profiles, as well as the front dispersion, σ_F, which is a measure of "roughness" of the combustion front. The second group describes the combustion front *propagation* at the microscopic level. For this, the instantaneous, $U(y,t)$ and average, $\bar{\bar{U}}$, velocities of the combustion wave, as well as the dispersion of the instantaneous velocities, σ_U, are calculated.

The microstructure of the combustion wave was investigated as a function of two parameters characteristic of the heterogeneity of the reactant medium: the average particle size, d, of the more refractory titanium (note that the Ti-Si system initiates with the melting of silicon; Rogachev *et al.*, 1995) and the initial sample porosity, ϵ. Similar results were observed for both the gasless Ti-Si and gas–solid Ti-N_2 systems. Either with increasing particle size or increasing porosity, the fluctuations of the combustion wave, both in terms of shape and propagation, increase monotonically (e.g., see Fig. 74).

Further, we can normalize three measures of the combustion wave microstructure: d, σ_F, and σ_U, with the appropriate length (x_T) or velocity (U_{macro}) scales (see

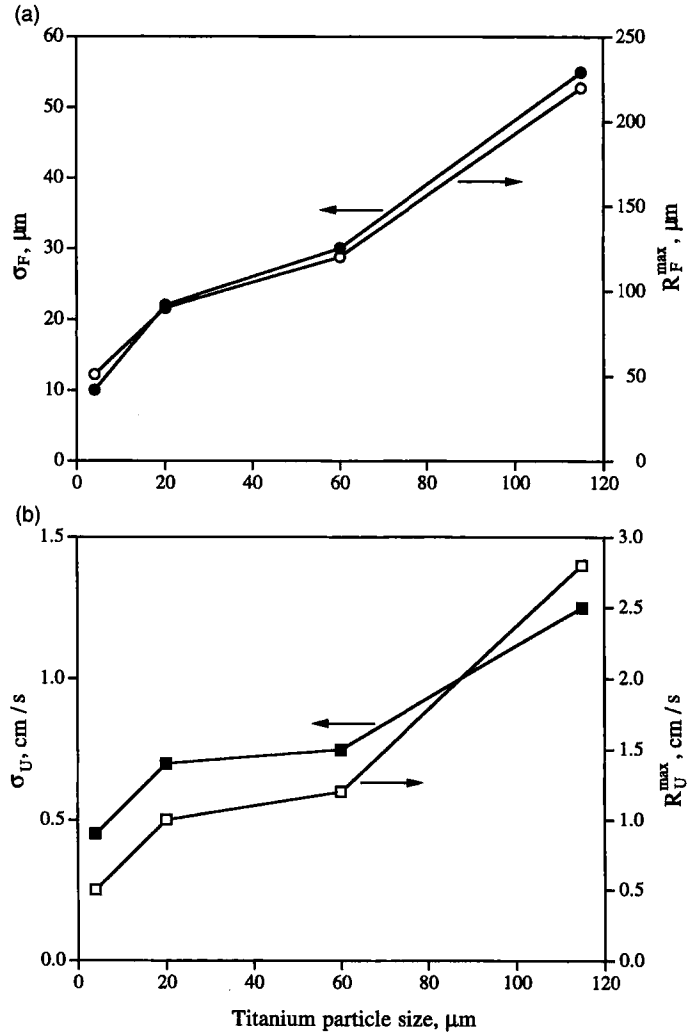

FIG. 74. Dependence of combustion front heterogeneity on Ti particle size in the 5Ti-3Si system: (a) shape; (b) propagation (Adapted from Mukasyan *et al.*, 1996).

Table XXIII). The length scale of combustion, x_T, can be evaluated using the relation:

$$x_T = \alpha/U, \tag{75}$$

where α is the medium thermal diffusivity. In addition, an estimate of the length scale during combustion conditions can also be obtained from the temperature profiles (Zenin *et al.*, 1980). Table XXIII shows that thermal length scales obtained from the two approaches are comparable in magnitude.

TABLE XXIII
COMPARISON OF EXPERIMENTAL AND CALCULATED THERMAL LENGTH SCALES, X_T, μm FOR THE 5Ti+3Si SYSTEM[a]

d (μm)	ϵ	$X_T = \alpha/U$	From Zenin *et al.* (1980)
4	0.5	20	—
20	0.5	35	60 ± 20
60	0.5	40	—
110	0.5	50	60 ± 20
115	0.5	50	70 ± 20

[a]Data from Mukasyan *et al.* (1996).

Several characteristic ratios of heterogeneity as functions of titanium particle size and sample porosity are shown in Figs. 75a and b, respectively. For the quasi-homogeneous approximation to be valid, the heterogeneity of the reactant medium should be small in comparison to the thermal length scale. As a result, the heterogeneity of the combustion front (shape and propagation) should also be small relative to the macroscopic behavior:

$$d/X_T \ll 1, \quad \sigma_F/X_T \ll 1, \quad \sigma_U/U_{macro} \ll 1. \tag{76}$$

The data in Fig. 75 indicate that the characteristic measures of heterogeneity increase with increasing reactant particle size (at fixed porosity) and sample porosity (at fixed particle sizes). Also, these ratios are small *only* for relatively small particle sizes and porosity values, limiting the regions where the quasi-homogeneous approximation may be expected to hold (region I). For larger particle sizes and sample porosities, the microscopic scales of heterogeneity are large (region II), and consequently the nature of combustion wave propagation is more complex.

Based on the results described earlier, the following mechanism of heterogeneous combustion was suggested (Mukasyan *et al.*, 1996). This process consists of two sequential steps: rapid reaction of a single reactant particle, typically the most refractory, followed by ignition delay during which preheating of the neighboring particle occurs. Since in this case the particles react sequentially, one after another, this mechanism may be called a *relay-race* mechanism of heterogeneous combustion. The thermal resistance between particles is significant in heterogeneous systems such as powder mixtures, which leads to the delay between reactions of neighboring particles.

F. CONCLUDING REMARKS

To study the variety of structural transformation processes that occur simultaneously in the combustion wave, it is necessary to utilize a wide range of methods. The evolution and morphological features of the microstructure during com-

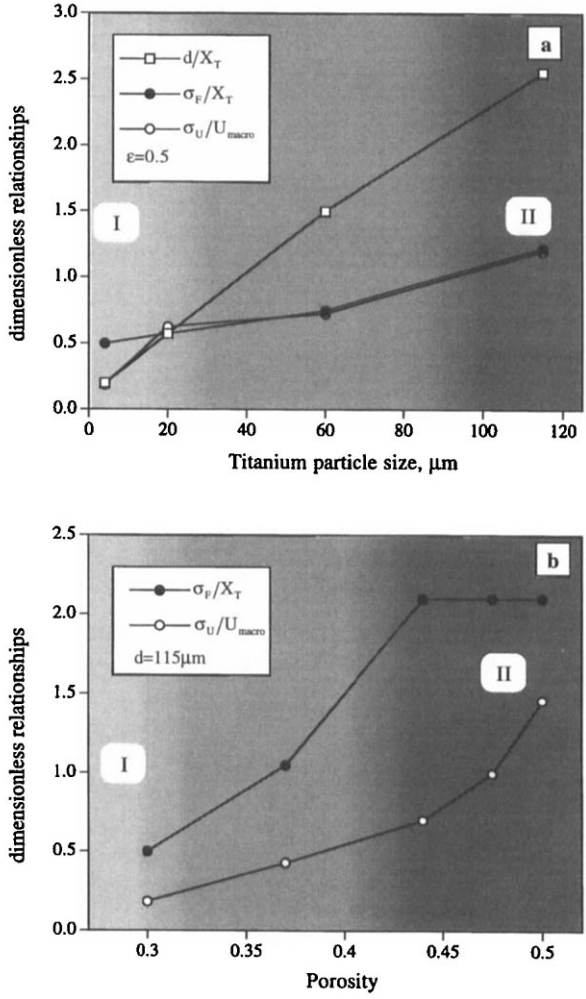

FIG. 75. Characteristic ratios of heterogeneity in the 5Ti-3Si system as functions of (a) titanium particle size; (b) initial sample porosity (Adapted from Mukasyan *et al.*, 1996).

bustion synthesis can be identified using a layer-by-layer analysis of quenched samples. In particle-foil experiments, the initial interaction between molten and solid reactants can be isolated, and the spreading rate of the liquid phase as well as features of the resulting product layer (e.g., phase composition, product grain size, layer thickness) identified. The dynamics of the phase composition and crystal structure ordering can be monitored continuously by TRXRD. Finally, microstructural analysis of the combustion wave provides important information about the local conditions which affect the synthesis process.

Each method described in this chapter elucidates some specific aspects of the structure-forming processes during combustion synthesis. These techniques have been developed primarily for combustion synthesis, where extreme reaction conditions such as short reaction times and steep thermal gradients exist. However, it should be noted that each technique also has limitations associated with it. In the particle-foil experiment, the foil temperature can be measured accurately, but the precise temperature of the particle in contact with the foil is difficult to determine. If a system follows a multistage reaction, where intermediates form and decompose in the postcombustion zone, quenching may affect the course of the reaction, and products not found in bulk samples may be present in the quenched sample. Finally, the TRXRD method does not detect amorphous, molten phases or solid solutions that may form during combustion synthesis, nor does it provide a direct visualization of the phases formed. Despite their shortcomings, these methods complement each other, and if applied to a given system, can lead to a reasonably complete description of the structure-forming processes.

For example, four microstructural models of the product formation process in solid-solid systems can be distinguished based on the results of the experimental methods discussed in this chapter. Brief descriptions of the models are presented in Fig. 76.

The first mechanism, *reaction-diffusion,* is based on the assumption that a layer of the solid product (or products) appears on the boundary between the two

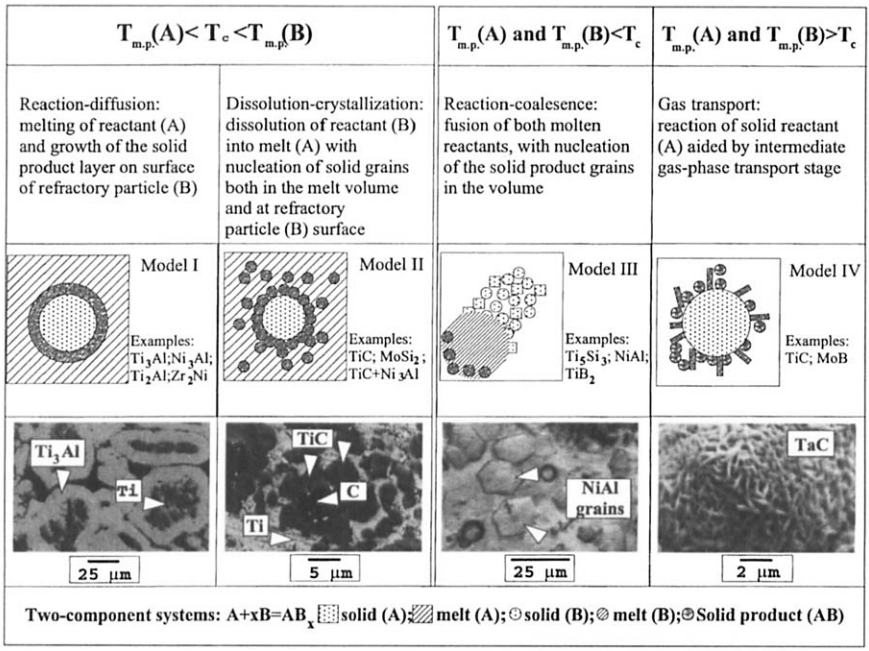

FIG. 76. Microstructural models of initial product.

reactants. This mechanism has been discussed thoroughly in the literature (e.g., Hardt and Phung, 1973; Aldushin and Khaikin, 1974; Kanury, 1992; Cao and Varma, 1994). It appears that this microstructural model applies mainly when intermetallic compounds are synthesized. In the synthesis of refractory ceramic materials, such as TiC, ZrC, etc., the carbides form separate grains of the initial product, which are difficult to pack into a continuous layer on the nonmelted reactant particle surface. The second model, *dissolution-crystallization,* represents the case where particle size of the nonmelted reactant is comparable to the initial product grain size (~0.1–1 μm), which is a common situation for most carbide and boride systems. This mechanism describes synthesis of polycrystalline ceramic materials or ceramic grain–metal matrix composites, depending on composition of the green mixture. When the combustion temperature is higher than melting points of both reactants, the *reaction coalescence* mechanism becomes dominant. Finally, when the temperature of combustion is lower than melting points of the reactants, *gas-transport* between solid particles plays a significant role in the initial product formation, as was shown for the Ta-C system (Merzhanov *et al.,* 1990b). In this case, an initial product with microstructure characteristic of gas phase deposition (lamellar and column crystals, whiskers) appears.

Note that even for the same reaction system, the combustion temperature T_c can be varied relative to the reactant melting points, by varying the initial temperature, dilution and stoichiometry. Thus different models may apply for the same system, depending on the experimental conditions. The examples listed in Fig. 76 correspond to the most common conditions, with no preheating or dilution.

Acknowledgments

We gratefully acknowledge financial support from the National Science Foundation (grants CTS 92-14009 and CTS 95-28941), including supplements for U.S.–Russia joint cooperative research, and NASA (NAG3-1644). Dr. Cynthia Kachelmyer contributed to early versions of this review, in particular, section VI.

Nomenclature

$A(T^*,\eta^*)$	Function; see Eq. (26)
b	Fraction of inert or product diluent
c_p	Heat capacity
d	Particle size

D	Characteristic length of the sample (e.g., pellet diameter)
D_{rc}	Diameter of the reaction cell; see Eq. (36)
D^*	Critical sample size
$\mathcal{D}$	Mass diffusivity
$f(d)$	Dependence of U on particle size (see Section IV,B)
$F(T)$	Dependence of U on temperature (see Section IV,B)
$F(y,t)$	Local combustion front profile
$\overline{F}(t)$	Average combustion front profile at time t (see Table XXII)
G	Forced gas velocity
G_i	Molar Gibbs free energy of component i
h	Convective heat transfer coefficient
H	Microhardness
ΔH_{fus}	Heat of fusion
$H_i(T)$	Enthalpy of component i
k_0	Preexponential constant for kinetics
k_f	Permeability coefficient, k/μ
L	Length of sample
Le	Lewis number, $\mathcal{D}/\alpha$
L_f	Filtration combustion parameter; see Eq. (55)
l_f	Length of filtration during combustion
MW_i	Molecular weight of component i
M_i	Reduced-metal intermediate or product i
$(MO_x)_i$	Metal oxide reactant
m	Mass
m_s	Mass of nonoxide phase (see Section I,B,3)
m_t	Total mass of the phase produced by the reaction (see Section I,B,3)
n_i	Number of moles of i
N_k	Number of components of type k
P_i	Product i
p	Gas pressure
$p(T)$	Probability of cell reaction; see Eq. (39)
p_0^{cr}	Critical gas pressure for full reaction
p_k	Partial pressure of gas phase component k
$\overline{p}$	Average gas pressure
q	Heat flux variable, $\lambda \cdot dT/dx$
Q	Heat of reaction
S	Surface area of sample
t	Time
T	Temperature
U	Combustion velocity
U_{macro}	Macroscopic combustion velocity (see Table XXII)
$\overline{\overline{U}}$	Average combustion velocity (see Table XXII)

V	Volume of sample
v_f	Velocity of gas filtration
v_T	Velocity of convective heat exchange front (see Section IV,3,a)
$W(\eta,T,p)$	Chemical reaction rate for gas–solid systems
x	Spatial coordinate in traveling wave frame; see Eq. (10)
x_T	Characteristic length of thermal relaxation in combustion wave, α/U
X	Spatial coordinate
X_i	Solid-phase reactant
y	Spatial coordinate
Y_i	Gas-phase reactant i
Z_i	Reducing-metal reactant
$(ZO_x)_i$	Oxide product i

Greek Letters

α_{st}	Stability parameter; see Eq. (46)
α	Thermal diffusivity
β	Stability parameter; see Eq. (40)
$\chi(d)$	Particle size distribution function (see Section IV,B)
δ	Thickness of product layer; see Eq. (35)
$\delta(x)$	Dirac delta function
ϵ_m	Emissivity
ϵ	Porosity
$\Phi_k(\eta,T)$	Heat release function for source or sink, k
$\phi(\eta,T)$	Reaction kinetic function
$\Gamma(z)$	Gamma function
γ	Stability parameter; see Eq. (40)
η	Reactant conversion
η^*	Reactant conversion controlling combustion front propagation
η_{ps}	Degree of phase separation (see Section I,B,3)
$\varphi(\eta)$	Kinetic dependence of reactant conversion
λ	Thermal conductivity
μ	Viscosity
ν_i	Stoichiometric coefficient of reactant i
π	Forced flux parameter, v_T/U (see Section IV,3,a)
ρ	Density
ρ_i	Amount of reactant i per unit sample volume
σ	Stefan–Boltzmann constant
σ_F	Dispersion of combustion front shape (see Table XXII)
σ_U	Dispersion of combustion front velocities (see Table XXII)
τ	Time step; see Eq. (39)

ω	Counter-current filtration parameter, U_k/v_f (see Section IV,1,b,1)
Ψ	Stability parameter; see Eq. (41)
ζ	Fraction of reactant melted; see Eq. (8)

Subscripts

0	Initial
a	Ambient value
c	Combustion
cool	Cooling
f	Filtration
i	Component *i*
k	Kinetic control
m	Melting point
max	Maximum
min	Minimum
ps	Phase separation
sc	Superconducting

Superscripts

ad	Adiabatic
cr	Critical
(g)	Gas-phase reactant or product
(l)	Liquid-phase reactant or product
(s)	Solid-phase reactant or product
*	Controlling combustion front propagation

References

Adachi, S., Wada, T., Mihara, T., Miyamoto, Y., Koizumi, M., and O. Yamada, Fabrication of titanium carbide ceramics by high-pressure self-combustion sintering of titanium powder and carbon fiber. *J. Am. Ceram. Soc.*, **72,** 805 (1989).

Adadurov, G. A., Borovinskaya, I. P., Gordopolov, Y. A., and Merzhanov, A. G., Technological fundamentals of SHS compacting. *J. Eng. Phys. Thermophys.*, **63,** 1075 (1992).

Advani, A. H., Thadhani, N. N., Grebe, H. A., Heaps, R., Coffin, C., and Kottke, T., Dynamic modeling of self propagating high temperature synthesis of titanium carbide ceramics. *Scripta Metall. Mater.*, **25,** 1447 (1991).

Agadzhanyan, N. N., and Dolukhanyan, S. K., Burning in the Zr+Nb+N+H system: Hydronitride synthesis. *Combust. Explos. Shock Waves,* **26,** 739 (1990).

Agrafiotis, C. C., Puszynski, J. A., and Hlavacek, V., Experimental study on the synthesis of titanium and tantalum nitrides in the self-propagating regime. *Combust. Sci. Tech.*, **76,** 187 (1991).

Akiyama, T., Isogai, H., and Yagi, J., Combustion synthesis of magnesium nickel. *Int. J. SHS,* **4,** 69 (1995).

Aldushin, A. P., New results in the theory of filtration combustion. *Combust. Flame,* **94,** 308 (1993).

Aldushin, A. P., Filtration combustion of metals. *In* "Thermal Wave Propagation in Heterogeneous Media (Russ.)." Nauka, Novosibirsk, 1988, p. 52.

Aldushin, A. P., and Khaikin, B. I., Combustion of mixtures forming condensed reaction products. *Combust. Explos. Shock Waves,* **10,** 273 (1974).

Aldushin, A. P., and Merzhanov, A. G., Filtration combustion theory: General approaches and results. *In* "Thermal Wave Propagation in Heterogeneous Media (Russ.)." Nauka, Novosibirsk, 1988, p. 9.

Aldushin, A. P., and Merzhanov, A. G., Gasless combustion with phase transformation. *Dokl. Phys. Chem.,* **236,** 973 (1978).

Aldushin, A. P., and Sepliarskii, B. S., Inversion of wave structure in porous medium during gas blow-through. *Phys. Dokl.,* **24,** 928 (1978a).

Aldushin, A. P., and Sepliarskii, B. S., Propagation of waves of exothermic reaction in porous medium during gas blow-through. *Phys. Dokl.,* **23,** 483 (1978b).

Aldushin, A. P., Matkowsky, B. J., Shkadinsky, K. G., Shkadinskaya, G. V., and Volpert, V. A., Combustion of porous samples with melting and flow of reactants. *Combust. Sci. Tech.,* **99,** 313 (1994a).

Aldushin, A. P., Matkowsky, B. J., and Volpert, V. A., Interaction of gasless and filtration combustion. *Combust. Sci. Tech.,* **99,** 75 (1994b).

Aldushin, A. P., Sepliarskii, B. S., and Shkadinskii, K. G., Theory of filtration combustion. *Combust. Explos. Shock Waves,* **16,** 33 (1980).

Aldushin, A. P., Lugovoi, V. D., Merzhanov, A. G., and Khaikin, B. I., Conditions of degeneration of steady combustion wave. *Phys. Dokl.,* **23,** 914 (1978).

Aldushin, A. P., Khaikin, B. I., and Shkadinskii, K. G., Effect of the inhomogeneity of the internal structure of the medium on the combustion of condensed mixtures, interacting through a layer of product. *Combust. Explos. Shock Waves,* **12,** 725 (1976a).

Aldushin, A. P., Merzhanov, A. G., and Sepliarskii, B. S., Theory of filtration combustion of metals. *Combust. Explos. Shock Waves,* **12,** 285 (1976b).

Aldushin, A. P., Ivleva, T. P., Merzhanov, A. G., Khaikin, B. I., and Shkadinskii, K. G., Combustion front propagation in porous exothermic metallic samples with oxidizer filtration. *In* Combustion Processes in Chemical Engineering and Metallurgy (Russ.) (A. G. Merzhanov, ed.). USSR Academy of Science, Chernogolovka, Russia, 1975, p. 245.

Aldushin, A. P., Merzhanov, A. G., and Khaikin, B. I., Conditions for the layer filtration combustion of porous metals. *Dokl. Phys. Chem.,* **215,** 295 (1974).

Aldushin, A. P., Martem'yanova, T. M., Merzhanov, A. G., Khaikin, B. I., and Shkadinskii, K. G., Propagation of the front of an exothermic reaction in condensed mixtures with the interaction of the components through a layer of high-melting product. *Combust. Explos. Shock Waves,* **8,** 159 (1972a).

Aldushin, A. P., Merzhanov, A. G., and Khaikin, B. I., Some features of combustion of condensed system with high-metal-point reaction products. *Dokl. Phys. Chem.,* **204,** 475 (1972b).

Aleksandrov, V. V., and Korchagin, M. A., Mechanism and macrokinetics of reactions accompanying the combustion of SHS systems. *Combust. Explos. Shock Waves,* **23,** 557 (1988).

Aleksandrov, V. V., Korchagin, M. A., and Boldyrev, V. V., Mechanism and macrokinetics of a reaction of components in a powder mixture. *Dokl. Phys. Chem.,* **292,** 114 (1987).

Aleksandrov, V. V., Gruzdev, V. A., and Kovalenko, Y. A., Thermal conductivity of certain aluminum-based SHS systems. *Combust. Explos. Shock Waves,* **21,** 93 (1985).

Alman, D. E., Reaction synthesis of Ni-36.8 wt% Al. *J. Mater. Sci. Lett.,* **13,** 483 (1994).

Andreev, K. K., "Thermal Decomposition and Combustion of Explosive Powders." Nauka, Moscow, 1966.

Andreev, V. A., Mal'tsev, N. M., and Seleznev, V. A., Study of the combustion of hafnium-boron mixtures by optical pyrometry. *Combust. Explos. Shock Waves,* **16,** 374 (1980).

Andrievski, R. A., and Baiman, I. F., Physical-mechanical properties of boride composites obtained by SHS compacting method. *Int. J. SHS,* **1,** 298 (1992).

Anselmi-Tamburini, U., and Munir, Z. A., The propagation of a solid-state combustion wave in Ni-Al foils. *J. Appl. Phys.,* **66,** 5039 (1989).

Astapchik, A. S., Podvoisky, E. P., Chebotko, I. S., Khusid, B. M., Merzhanov, A. G., and Khina, B. B., Stochastic model for a wavelike isothermal reaction in condensed heterogeneous systems. *Phys. Rev. E,* **47,** 1993 (1993).

Avakyan, P. B., Nersesyan, M. D., and Merzhanov, A. G., New Materials for electronic engineering. *Am. Ceram. Soc. Bull.,* **75,** 50 (1996).

Azatyan, T. S., Mal'tsev, V. M., Merzhanov, A. G., and Seleznev, V. A., Some principles in combustion of titanium-silicon mixtures. *Combust. Explos. Shock Waves,* **15,** 35 (1979).

Barzykin, V. V., Initiation of SHS processes. *Pure Appl. Chem.,* **64,** 909 (1992).

Boldyrev, V. V., Aleksandrov, V. V., Korchagin, M. A., Tolochko, B. P., Gusenko, S. N., Sokolov, A. S., Sheromov, M. A., and Lyakhov, N. Z., The study of dynamics of phase formation during nickel monoaluminade synthesis in the combustion regime. *Dokl. Akad. Nauk SSSR,* **259,** 722 (1981).

Booth, F., The theory of self-propagating exothermic reactions in solid systems. *Trans. Farad. Soc.,* **49,** 272 (1953).

Borovinskaya, I. P., Chemical classes of SHS processes and materials. *Pure Appl. Chem.,* **64,** 919 (1992).

Borovinskaya, I. P., Refractory compounds formation during combustion of heterogeneous condensed systems. *Proceedings of the Fourth All Union Symposium on Combustion and Explosion (Russian),* Moscow, 138 (1977).

Borovinskaya, I. P., and Loryan, V. E., Self-propagating high-temperature synthesis of titanium nitrides under high nitrogen pressures. *Sov. Powd. Metall.,* **11,** 851 (1978).

Borovinskaya, I. P., and Loryan, V. E., Self-propagating processes in the formation of solid solutions in the zirconium-nitrogen system. *Dokl. Phys. Chem.,* **231,** 1230 (1976).

Borovinskaya, I. P., and Pityulin, A. N., Combustion of hafnium in nitrogen. *Combust. Explos. Shock Waves,* **14,** 111 (1978).

Borovinskaya, I. P., Cantero, I., Estaire, L., Hernan, M. A., and Guzman, R., SHS Espana: An international experience. *Int. J. SHS,* **4,** 405 (1995).

Borovinskaya, I. P., Ivleva, T. I., Loryan, V. I., Merzhanov, A. G., and Shkadinskii, K. G., Autowave processes determined with an adsorption-diffusion mechanism of metal-gas interaction. *Int. J. SHS,* **2,** 227 (1993).

Borovinskaya, I. P., Merzhanov, A. G., Mukasyan, A. S., Rogachev, A. S., and Khusid, B. M., Macrokinetics of structure formation during infiltration combustion of titanium in nitrogen. *Dokl. Akad. Nauk SSSR,* **322,** 912 (1992a).

Borovinskaya, I. P., Ratnikov, V. I., and Vishnyakova, G. A., Some chemical aspects of powder SHS compacting. *J. Eng. Phys. Thermophys.,* **63,** 1059 (1992b).

Borovinskaya, I. P., Levashov, E. A., and Rogachev, A. S., "Physical-Chemical and Technological Base of Self-Propagating High-Temperature Synthesis, A Series of Lectures. MISiS Press, Moscow, 1991.

Borovinskaya, I. P., Merzhanov, A. G., Pityulin, A. N., and Shehtman, V. S., Self-propagating high-temperature synthesis of the tantalum nitride. *In* "Combustion Processes in Chemical Engineering and Metallurgy (Russ.)." (A. G. Merzhanov, ed.). USSR Academy of Science, Chernogolovka, Russia, 1975a, p. 113.

Borovinskaya, I. P., Vishnyakova, V. M., Maslov, V. M., and Mezhanov, A. G., On the possibility of the composite materials obtaining in combustion regime. *In* "Combustion Processes in Chemical Engineering and Metallurgy (Russ.)" (A. G. Merzhanov, ed.). USSR Academy of Science, Chernogolovka, Russia, 1975b, p. 141.

Borovinskaya, I. P., Merzhanov, A. G., Novikov, N. P., and Filonenko, A. K., Gasless combustion of mixtures of powdered transition metals with boron. *Combust. Explos. Shock Waves,* **10,** 2 (1974).

Borovinskaya, I. P., Merzhanov, A. G., Butakov, A. A., Rabin'kin, A. G., and Shehtman, V. S., Synthesis of tantalum mononotride. *Izvest. Bull.,* **9,** Certificate 264365, Patent 1311660 (1970).

Bowen, C. R., and Derby, B., Modelling of self-propagating high-temperature synthesis reactions. *In* Engineering Ceramics: Fabrication Science and Technology" (P. P. Thompson, ed.). The Institute of Metals, London, 1993, p. 29.

Brailsford, A. D., and Major, K. G., The thermal conductivity of aggregates of several phases, including porous materials. *Br. J. Appl. Phys.* **15,** 313 (1964).

Bratchikov, A. D., Merzhanov, A. G., Itin, V. I., Khachin, V. N., Dudarev, E. F., Gyunter, V. E., Maslov, V. M., and Chernov, D. B., Self-propagating high temperature synthesis of titanium nickelide. *Sov. Powd. Metall.,* **1,** 5 (1980).

Brezinsky, K., Brehm, J. A., Law, C. K., and Glassman, I., Supercritical combustion synthesis of titanium nitride. *Twenty-sixth Symposium (International) of Combustion.* The Combustion Institute, Pittsburgh, 1875 (1996).

Calcote, H. F., Felder, W., Keil, D. G., and Olson, D. B., A new flame process for synthesis of Si_3N_4 powders for advanced ceramics. *Twenty-third Symposium (International) on Combustion,* The Combustion Institute, Pittsburgh, 1739 (1990).

Cao, G., and Varma, A., A new expression for velocity of the combustion front during self-propagating high-temperature synthesis. *Combust. Sci. Tech.,* **102,** 181 (1994).

Chang, D. G., Shim, G. C., Won, C. W., and Chun, B.-S., Preparation of TiC powder by SHS (self-propagating high temperature synthesis). *J. Kor. Inst. Metals (Korean),* **29,** 626 (1991).

Chang, D. K., Won, C. W., Chun, B. S., and Shim, G. C., Purifying effects and product microstructure in the formation of TiC powder by the self-propagating high-temperature synthesis. *Metall. Mater. Trans. B,* **26B,** 176 (1995).

Chemical Engineering Progress, Process improves titanium diboride materials. **91,** 25 (1995).

Choi, Y., and Rhee, S.-W., Effect of aluminum addition on the combustion reaction of titanium and carbon to form TiC. *J. Mater. Sci.,* **28,** 6669 (1993).

Choi, Y., Mullins, M. E., Wijayatilleke, K., and Lee, J. K., Fabrication of metal matrix composites of TiC-Al through self-propagating synthesis reaction. *Metall. Trans. A,* **23A,** 2387 (1992).

Cooper, M. G., Mikic, B. B., and Yovanovich, M. M., Thermal contact conductance. *Int. J. Heat Mass Trans.,* **12,** 279 (1969).

Costantino, K., and Holt, J. B., High-pressure burning rate of silicon in nitrogen. *In* "Combustion and Plasma Synthesis" (Z. A. Munir and J. B. Holt, eds.). VCH Publishers, New York, 1990, p. 315.

Dandekar, H. W., Hlavacek, V., and Degreve, J., An explicit 3D finite-volume method for simulation of reactive flows using a hybrid moving adaptive grid. *Numer. Heat Trans., B,* **24,** 1 (1993).

Dandekar, H. W., Puszynski, J. A., and Hlavacek, V., Two-dimensional numerical study of cross-flow filtration combustion. *AIChE J.,* **36,** 1649 (1990).

Daniel, P. J., The theory of flame motion. *Proc. Roy. Soc.,* **126,** 393 (1930).

Davis, K., Brezinsky, K., and Glassman, I., Chemical equilibrium constants in the high-temperature formation of metallic nitrides. *Combust. Sci. Tech.,* **77,** 171 (1991).

DeAngelis, T. P., Advanced ceramic materials via reaction hot pressing. *Proceedings of the First US–Japanese Workshop on Combustion Synthesis,* Tokyo, Japan, 147 (1990).

DeAngelis, T. P., and Weiss, D. S., Advanced ceramics via SHS. *In* "Combustion and Plasma Synthesis of High-Temperature Materials" (Z. A. Munir and J. B. Holt, eds.). VCH Publishers, New York, 1990, p. 144.

Deevi, S. C., Diffusional reactions in the combustion synthesis of $MoSi_2$. *Mater. Sci. Eng.,* **A149,** 241 (1992).

Deevi, S. C., Structure of the combustion wave in the combustion synthesis of titanium carbides. *J. Mater. Sci.,* **26,** 2662 (1991).

Dolukhanyan, S. K., Hakobyan, H. G., and Aleksanyan, A. G., Combustion of metals in hydrogen and hydride production by SHS. *Int. J. SHS,* **1,** 530 (1992).

Dolukhanyan, S. K., Akopyan, A. G., and Merzhanov, A. G., Reaction of intermetallides based on zirconium and cobalt with hydrogen in combustion conditions. *Combust. Explos. Shock Waves,* **17,** 525 (1981).

Dolukhanyan, S. K., Nersesyan, M. D., Martirosyan, N. A., and Merzhanov, A. G., Using the SHS processes in the chemistry and technology of hydrides. *Izvestia AN SSSR, Neorganicheskie Materialy (Russ.),* **14,** 1581 (1978).

Dolukhanyan, S. K., Nersesyan, M. D., Nalbandyan, A. B., Borovinskaya, I. P., and Merzhanov, A. G., Combustion of the transition metals in the hydrogen. *Dokl. Akad. Nauk SSSR,* **231,** 675 (1976).

Dunmead, S. D., Munir, Z. A., and Holt, J. B., Temperature profile analysis of combustion in the Zr-B system using the Boddington-Laye method. *Int. J. SHS,* **1,** 22 (1992a).

Dunmead, S. D., Munir, Z. A., and Holt, J. B., Temperature profile analysis of combustion synthesis: I. Theory and background. *J. Am. Ceram. Soc.,* **75,** 175 (1992b).

Dunmead, S. D., Munir, Z. A., and Holt, J. B., Temperature profile analysis of combustion synthesis: II. Experimental observations. *J. Am. Ceram. Soc.,* **75,** 180 (1992c).

Dunmead, S. D., Holt, B. J., and Kingman, D. D., Simultaneous combustion synthesis and densification of AlN. *In* "Combustion and Plasma Synthesis of High-Temperature Materials" (Z. A. Munir and J. B. Holt, eds.). VCH Publishers, New York, 1990a, p. 186.

Dunmead, S. D., Holt, B. J., and Kingman, D. D., Combustion synthesis in the Ti-C-Ni-Al system. *In* "Combustion and Plasma Synthesis of High-Temperature Materials" (Z. A. Munir and J. B. Holt, eds.). VCH Publishers, New York, 1990b, p. 229.

Dutta, A., Self-propagating high-temperature synthesis (SHS)-cum-superplastic forging of Fe_3Al-Nb alloy. *Int. J. SHS,* **4,** 309 (1995).

Eslamloo-Grami, M., and Munir, Z. A., Effect of porosity on the combustion synthesis of titanium nitride. *J. Am. Ceram. Soc.,* **73,** 1235 (1990a).

Eslamloo-Grami, M., and Munir, Z. A., Effect of nitrogen pressure and diluent content on the combustion synthesis of titanium nitride. *J. Am. Ceram. Soc.,* **73,** 2222 (1990b).

Evans, T., and James, R., A study of the transformation of diamond to graphite. *Proc. Roy. Soc. A,* **277,** 260 (1964).

Fedorov, V. M., Gordopolov, Y. A., and Merzhanov, A. G., Explosive treatment of SHS end products (of high-temperature superconductors). *J. Eng. Phys. Thermophys.,* **63,** 1166 (1992).

Feng, A., and Munir, Z. A., Field-assisted self-propagating synthesis of SiC. *J. Appl. Phys.,* **76,** 1927 (1994).

Ferreira, A., Meyers, M. A., and Thadani, N. N., Dynamic compaction of titanium aluminides by explosively generated shock waves: Microstructure and mechanical properties. *Metall. Trans. A,* **23A,** 3251 (1992).

Filatov, V. M., and Naiborodenko, Y. S., Combustion mechanism for nickel-aluminum thermites. *Combust. Explos. Shock Waves,* **28,** 47 (1992).

Filatov, V. M., Naiborodenko, Y. S., and Ivanov, I. A., Combustion of low-gas systems with redox stages. *Combust. Explos. Shock Waves,* **24,** 472 (1988).

Filonenko, A. K., Non-stationary phenomena during the combustion of heterogeneous systems with refractory products. *In* "Combustion Processes in Chemical Engineering and Metallurgy (Russ.)" (A. G. Merzhanov, ed.). USSR Academy of Science, Chernogolovka, Russia, 1975, p. 258.

Fu, Z. Y., Wang, H., Wang, W. M., Yuan, R. Z., and Munir, Z. A., Process of study on self-propagating high-temperature synthesis of ceramic-metal composites. *Int. J. SHS,* **2,** 175 (1993a).

Fu, Z. Y., Wang, W. M., Wang, H., Yuan, R. Z., and Munir, Z. A., Fabrication of cermets by SHS-QP method. *Int. J. SHS,* **2,** 307 (1993b).

Glassman, I., "Combustion." Academic Press, New York, 1977.

Glassman, I., Davis, K. A., and Brezinsky, K., A gas-phase combustion synthesis process for non-oxide ceramics. *Twenty-fourth Symposium (International) on Combustion.* The Combustion Institute, 1877 (1992).

Goel, N. S., Geroc, J. S., and Lehmann, G., A simple model for heat conduction in heterogeneous materials and irregular boundaries. *Int. Comm. Heat Mass Transfer,* **19,** 519 (1992).

Gogotsi, G. A., Savada, V. P., and Khartionov, F. Y., Strength and crack resistance of ceramics. *Problemy Prochnosti (Russian),* **12,** 7 (1984).

Golubjatnikov, K. A., Stangle, G. C., and Sprigs, R. M., The economics of advanced self-propagating high-temperature synthesis materials fabrication. *Am. Ceram. Soc. Bull.,* **72,** 96 (1993).

Gordopolov, Y. A., and Merzhanov, A. G., Shock waves in SHS research. *Proceedings of the 13th International Colloquium on Dynamics of Explosion and Reactive Systems,* Nagoya, Japan (1991).

Gotman, I., Koczak, M. J., and Shtessel, E., Fabrication of Al matrix in situ composites via self-propagating synthesis. *Mater. Sci. Eng.,* **A187,** 189 (1994).

Grachev, V. A., Ivleva, T. I., and Borovinskaya, Filtration combustion in SHS reactor. *Int. J. SHS,* **4,** 252 (1995).

Grebe, H. A., Advani, A., Thadani, N. N., and Kottke, T., Combustion synthesis and subsequent explosive densification of titanium carbide ceramics. *Metall. Trans. A,* **23A,** 2365 (1992).

Grigor'ev, Y. M., Using the electrically heated wires for studying the kinetic of high temperature interaction in metal–gas system. *In* "Combustion Processes in Chemical Engineering and Metallurgy (Russ.)" (A. G. Merzhanov, ed.). USSR Academy of Science, Chernogolovka, Russia, 1975, p. 199.

Grigor'ev, Y. M., and Merzhanov, A. G., SHS coatings. *Int. J. SHS,* **1,** 600 (1992).

Hahn, Y.-D., and Song, I.-H., Microstructural characteristics of titanium aluminides synthesized by using the wave propagation mode. *Int. J. SHS,* **4,** 293 (1995).

Hakobian, H. G., and Dolukhanyan, S. K., Combustion process in the Mo-Al-Si system and synthesis of molybdenum alumocilicide. *Int. J. SHS,* **3,** 299 (1994).

Hardt, A. P., and Holsinger, R. W., Propagation of gasless reactions in solids—II. Experimental study of exothermic intermetallic reaction rates. *Combust. Flame,* **21,** 91 (1973).

Hardt, A. P., and Phung, P. V., Propagation of gasless reactions in solids—I. Analytical study of exothermic intermetallic reaction rates. *Combust. Flame,* **21,** 77 (1973).

Hernandez-Guerrero, A., Huque, Z., and Kanury, A. M., An experimental investigation of combustive synthesis of titanium carbide. *Combust. Sci. Tech.,* **81,** 115 (1992).

Hirao, K., Miyamoto, Y., and Koizumi, M., Combustion reaction characteristics at nitridation of silicon. *Adv. Ceramics,* **2,** 780 (1987).

Hlavacek, V., Combustion synthesis: A historical perspective. *Am. Ceram. Soc. Bull.,* **70,** 240 (1991).

Hlavacek, V., and Puszynski, J. A., Chemical engineering aspects of advanced ceramic materials. *Ind. Eng. Chem. Res.,* **35,** 349 (1996).

Ho-Yi, L., Hong-Yu, Y., Shu-Xia, M., and Sheng, Y., Combustion synthesis of titanium aluminides. *Int. J. SHS,* **1,** 447 (1992).

Hoke, D. A., Meyers, M. A., Meyer, L. W., and Gray III, G. T., Reaction synthesis: Dynamic compaction of titanium diboride. *Metall. Trans. A,* **23A,** 77 (1992).

Holt, J. B., and Dunmead, S. D., Self-heating synthesis of materials. *Annu. Rev. Mater. Sci.,* **21,** 305 (1991).

Holt, J. B., and Munir, Z. A., Combustion synthesis of titanium carbide: Theory and experiment. *J. Mater. Sci.,* **21,** 251 (1986).

Holt, J. B., Wong, J., Larson, E. M., Waide, P. A., Rupp, B., and Frahm, R., A new experimental approach to study solid combustion reaction using synchrotron radiation. *Proceedings of the First US–Japanese Workshop on Combustion Synthesis,* Tokyo, Japan, 107 (1990).

Holt, J. B., Kingman, D. D., and Bianchini, G. M., Kinetics of the combustion synthesis of TiB_2. *Mater. Sci. Eng.,* **71,** 321 (1985).

Howers, V. R., Graphitization of diamond. *Proc. Roy. Soc.,* **80,** 648 (1962).

Hunter, K. R., and Moore, J. J., The effect of gravity on the combustion synthesis of ceramic and ceramic-metal composites. *J. Mater. Syn. Proc.*, **2,** 355 (1994).

Huque, Z., and Kanury, A. M., A theoretical analysis of combustive synthesis of titanium carbide and a comparison of predictions with measurements. *Combust. Sci. Tech.*, **89,** 27 (1993).

Hwang, S., Ph.D. Dissertation, University of Notre Dame (1997).

Hwang, S., Mukasyan, A. S., Rogachev, A. S., and Varma, A., Combustion wave microstructure in gas-solid system: Experiments and theory. *Combust. Sci. Tech.*, **123,** 165 (1997).

Ikeda, S., Urabe, K., Koizumi, M., and Izawa, H., In-situ formation of SiC and SiC-C blocked solids by self-combustion synthesis. *In* "Combustion and Plasma Synthesis of High-Temperature Materials" (Z. A. Munir and J. B. Holt, eds.). VCH Publishers, New York, 1990, p. 151.

International Journal of SHS, SHS Bibliography, **5,** 303 (1996).

Itin, V. I., and Naiborodenko, Y. S., "High Temperature Synthesis of Intermetallic Compounds (Russ.)." Tomsk University Publishing, Tomsk, Russia, 1989.

Itin, V. I., Khachin, V. N., Gyunter, V. E., Bratchikov, A. D., and Chernov, D. B., Production of titanium nickelide by self-propagating high-temperature synthesis. *Porosh. Metall.*, **3,** 156 (1983).

Itin, V. I., Bratchikov, A. D., and Lepinskikh, A. V., Phase transition accompanying combustion of mixtures of copper and aluminum powders. *Combust. Explos. Shock Waves,* **17,** 506 (1981a).

Itin, V. I., Bratchikov, A. D., Merzhanov, A. G., and Maslov, V. M., Principles of self-propagating high-temperature synthesis of titanium compounds with elements of the iron group. *Combust. Sci. Tech.*, **17,** 293 (1981b).

Itin, V. I., Bratchikov, A. D., and Postnikova, L. N., Use of combustion and thermal explosion for the synthesis of intermetallic compounds and their alloys. *Sov. Powd. Metall.*, **19,** 315 (1980).

Itin, V. I., Khachin, V. N., Bratchikov, A. D., Gyunter, V. E., Dudarev, E. F., Monasevich, T. V., Chernov, D. B., Timonin, G. D., and Paperskii, A. P., Structure and properties of titanium nickelide materials made by self-propagating high-temperature synthesis. *Russ. Phys. J.*, **12,** 1631 (1977).

Ivleva, T. I., and Shkadinskii, K. G., "Mathematical modeling of two-dimensional problems in filtration combustion of condensed systems." *Proceedings of the Kinetics and Mechanisms of Physicochemical Processes,* Chernogolovka, Russia, 74 (1981).

Kachelmyer, C. R., and Varma, A., Combustion synthesis of niobium aluminide matrix composites. *Mater. Res. Soc. Symp.*, **350,** 33 (1994).

Kachelmyer, C. R., Rogachev, A. S., and Varma, A., Mechanistic and processing studies in combustion synthesis of niobium aluminides. *J. Mater. Res.* **10,** 2260 (1995).

Kachelmyer, C. R., Lebrat, J.-P., Varma, A., and McGinn, P. J., Combustion synthesis of intermetallic aluminides: Processing and mechanistic studies. *In* "Heat Transfer in Fire and Combustion Systems" (B. Farouk, M. P. Pinar Menguc, R. Viskanta, C. Presser, and S. Chellaiah, eds.). ASME, New York, 1993, p. 271.

Kachin, A. R., and Yukhvid, V. I., SHS of cast composite materials and pipes in the field of centrifugal forces. *Int. J. SHS,* **1,** 168 (1992).

Kaieda, Y., Nakamura, M., Otaguchi, M., and Oguro, N., Combustion synthesis of TiAl intermetallic compounds. *Proceedings of the First US–Japanese Workshop on Combustion Synthesis,* Tokyo, Japan, 207 (1990a).

Kaieda, Y., Otaguchi, M., and Oguro, N., Combustion synthesis of intermetallic compounds. *In* "Combustion and Plasma Synthesis of High-Temperature Materials" (Z. A. Munir and J. B. Holt, eds.). VCH Publishers, New York, 1990b, p. 106.

Kanamaru, N., and Odawara, O., Combustion synthesis of phosphides of aluminum, gallium and indium. *Int. J. SHS,* **3,** 305 (1994).

Kanury, A. M., A kinetic model for metal + nonmetal reactions. *Metall. Trans. A,* **23A,** 2349 (1992).

Kasat'skiy, N. G., Filatov, V. M., and Naiborodenko, Y. S., SHS in the low exothermic and high density aluminum systems. *In* "Self-Propagating High-Temperature Synthesis" (Ya. Maksimov, ed.). Tomsk, 1991, p. 63.

Kecskes, L. J., Niiler, A., and Kottke, T., Precursor morphology effects in combustion-synthesized and dynamically consolidated titanium carbide and titanium boride. *J. Am. Ceram. Soc.*, **76,** 2961 (1993).

Kecskes, L. J., Kottke, T., and Niiler, A., Microstructural properties of combustion-synthesized and dynamically consolidated titanium boride and titanium carbide. *J. Am. Ceram. Soc.*, **73,** 1274 (1990).

Khaikin, B. I., and Khudiaev, S. I., Nonuniqueness of combustion temperature and rate when competing reactions take place. *Phys. Dokl.*, **245,** 155 (1979).

Khaikin, B. I., and Merzhanov, A. G., Theory of thermal propagation of a chemical reaction front. *Combust. Explos. Shock Waves,* **2,** 22 (1966).

Kharatyan, S. L., and Nersisyan, H. H., Combustion synthesis of silicon carbide under oxidative activation conditions. *Int. J. SHS,* **3,** 17 (1994).

Khomenko, I. O., Mukasyan, A. S., Ponomarev, V. I., Borovinskaya, I. P., and Merzhanov, A. G., Dynamics of phase-forming processes in metal-gas system during combustion. *Combust. Flame,* **92,** 201 (1993).

Khusid, B. M., Khina, B. B., Kuang, V. Z., and Bashtovaya, E. A., Numerical investigation of quenching of the state of a material in a wave of SHS during a two-step reaction. *Combust. Explos. Shock Waves,* **28,** 389 (1992).

Kirdyashkin, A. I., Maksimov, Y. M., and Merzhanov, A. G., Effects of capillary flow on combustion in a gas-free system. *Combust. Explos. Shock Waves,* **17,** 591 (1981).

Koizumi, M., and Miyamoto, Y., Recent progress on combustion synthesis of high-performance material in Japan. *In* "Combustion and Plasma Synthesis of High-Temperature Materials" VCH Publishers, New York, 1990, p. 54.

Korchagin, M. A., and Aleksandrov, V. V., An electron-microscope study of the interaction of titanium with carbon. *Combust. Explos. Shock Waves,* **17,** 58 (1981).

Korchagin, M. A., and Podergin, V. A., Investigation of chemical transformations in the combustion of condensed system. *Fiz. Gor. Vzriva,* **15,** 325 (1979).

Kottke, T., Kecskes, L. J., and Niiler, A., Control of TiB_2 SHS reactions by inert dilutions and mechanical constraint. *AIChE J.*, **36,** 1581 (1990).

Kottke, T., and Niiler, A., "Thermal Conductivity Effects on SHS reactions," USA Ballistic Research Laboratory. Aberdeen Proving Ground, MD (1988).

Kumar, S., Self-propagating high-temperature synthesis of ceramic materials. Ph.D. Dissertation, State University of New York, Buffalo (1988).

Kumar, S., Agrafiotis, C., Puszynski, J., and Hlavacek, V., Heat transfer characteristics in combustion synthesis of ceramics. *AIChE Symp. Ser. 263,* **84,** 50 (1988a).

Kumar, S., Puszynski, J. A., and Hlavacek, V., Combustion characteristics of solid-solid systems experiments and modeling. *Proceedings of the International Symposium on Combustion and Plasma Synthesis of High Temperature Materials,* San Francisco (1988b).

Kuroki, H., and Yamaguchi, K., Combustion synthesis of Ti/Al intermetallic compounds and dimensional changes of mixed powder compacts during sintering. *Proceedings of the First US–Japanese Workshop on Combustion Synthesis,* Tokyo, Japan, 23 (1990).

Kvanin, V. L., Gorovoi, V. A., Balikhina, N. T., Borovinskaya, I. P., and Merzhanov, A. G., Investigation of the process of the forced SHS compaction of large-scale hard-alloy articles. *Int. J. SHS,* **2,** 56 (1993).

Lakshmikantha, M. G., and Sekhar, J. A., Influence of multi-dimensional oscillation combustion fronts on thermal profiles. *J. Mater. Sci.*, **28,** 6403 (1993).

Larson, E. M., Wong, J., Holt, J. B., Waide, P. A., Nutt, G., Rupp, B., and Terminello, L. J., A time-resolved diffraction study of the Ta-C Solid combustion system. *J. Mater. Res.*, **8,** 1533 (1993).

LaSalvia, J. C., and Meyers, M. A., Microstructure, properties, and mechanisms of TiC-Mo-Ni cermet produced by SHS. *Int. J. SHS,* **4,** 43 (1995).

LaSalvia, J. C., Meyers, M. A., and Kim, D. K., Combustion synthesis/dynamic densification of TiC-Ni cermets. *J. Mater. Syn. Proc.*, **2,** 255 (1994).

Lebrat, J.-P., and Varma, A., Self-propagating high-temperature synthesis of Ni_3Al. *Combust. Sci. Tech.*, **88,** 211 (1992a).

Lebrat, J.-P., and Varma, A., Some further studies in combustion synthesis of the $YBa_2Cu_3O_{7-x}$ superconductor. *Combust. Sci. Tech.*, **88,** 177 (1992b).

Lebrat, J.-P., and Varma, A., Combustion synthesis of the $YBa_2Cu_3O_{7-x}$ superconductor. *Physica C,* **184,** 220 (1991).

Lebrat, J.-P., Varma, A., and McGinn, P. J., Mechanistic studies in combustion synthesis of Ni_3Al and Ni_3Al-matrix composites. *J. Mater. Res.*, **9,** 1184 (1994).

Lebrat, J.-P., Varma, A., and Miller, A. E., Combustion synthesis of Ni_3Al and Ni_3Al–matrix composites. *Metall. Trans. A,* **23A,** 69 (1992).

Lee, W.-C., and Chung, S.-L., Self-propagating high-temperature synthesis of TiC powders. *Int. J. SHS,* **1,** 211 (1992).

Lee, W.-C., Hsu, K. C., and Chung, S.-L., Combustion synthesis of Ti-Al intermetallic materials. *Int. J. SHS,* **4,** 95 (1995).

Levashov, E. A., Vijushkov, B. V., Shtanskaya, E. V., Borovinskaya, I. P., Ohyanagi, M., Hosomi, S., and Koizumi, M., Regularities of structure and phase formation of SHS diamond-containing functional gradient materials: Operational characteristics of articles based on them. *Int. J. SHS,* **3,** 287 (1994).

Levashov, E. A., Borovinskaya, I. P., Rogachev, A. S., Koizumi, M., Ohyanagi, M., and Hosomi, S., SHS: A new method for production of diamond-containing ceramics. *Int. J. SHS,* **2,** 189 (1993).

Levashov, E. A., Bogatov, Y. V., and Milovidov, A. A., Macrokinetics and mechanism of the SVS-process in systems on a titanium-carbon base. *Combust. Explos. Shock Waves,* **27,** 83 (1991).

Li, H.-P., Processing Ti-B compounds by combustion synthesis. *Int. J. SHS,* **4,** 199 (1995).

Li, J., Zhou, M., and Wang, J., The study of microstructure of porous ceramic-lined pipes made by centrifugal SHS. *Proceedings of the 3rd International Symposium on Self-Propagating High-Temperature Synthesis (Book of Abstracts),* Wuhan, China, 48 (1995).

Li, J.-T., Xia, Y.-L., and Ge, C.-C., Combustion synthesis of magnesium nitride. *Int. J. SHS,* **3,** 225 (1994).

Lin, S.-C., Richardson, J. T., Luss, D., $YBa_{2Cu}3O_{6+x}$ synthesis using vertical self-propagating high-temperature synthesis. *Phys. C,* **233,** 281 (1994).

Luikov, A. V., Shashkov, A. G., Vasiliev, L. L., and Fraiman, Y. E., Thermal conductivity of porous systems. *Int. J. Heat Mass Trans.*, **11,** 117 (1968).

Makhviladze, G. M., and Novozilov, B. V., Two-dimensional stability of combustion of condensed systems. *Zhurn. Prikl. Mekhaniki I Tekhn. Fiziki,* **5,** 51 (1971).

Makino, A., and Law, C. K., SHS combustion characteristics of several ceramics and intermetallic compounds. *J. Am. Ceram. Soc.*, **77,** 778 (1994).

Maksimov, Y. M., Ziatdinov, M. K., Merzhanov, A. G., Raskolenko, L. G., and Lepakova, O. K., Combustion of vanadium-iron alloys in nitrogen. *Combust. Explos. Shock Waves,* **20,** 487 (1984).

Maksimov, Y. M., Ziatdinov, M. K. Raskolenko, A. G., and Lepakova, O. K., Interaction between vanadium and nitrogen in the combustion regime. *Combust. Explos. Shock Waves,* **15,** 420 (1979).

Maksimov, E. I., Merzhanov, A. G., and Shkiro, V. M., Gasless compositions as a simple model for the combustion of nonvolatile condensed systems. *Combust. Explos. Shock Waves,* **1,** 15 (1965).

Mallard, E., and Le Chatelier, H. L., Combustion des melanges gazeux explosifs. *Ann. Mines,* **4,** 274 (1883).

Mamyan, S. S., and Vershinnikov, V. I., Specific features of combustion of SHS systems containing magnesium as a reductant. *Int. J. SHS,* **1,** 392 (1992).

Margolis, S. B., A new route of chaos in gasless combustion. *Combust. Sci. Tech.*, **88,** 223 (1992).

Margolis, S. B., An asymptotic theory of heterogeneous condensed combustion. *Combust. Sci. Tech.*, **43,** 197 (1985).

Margolis, S. B., An asymptotic theory of condensed two-phase flame propagation. *SIAM J. Appl. Math.*, **43,** 351 (1983).

Martirosyan, N. A., Dolukhanyan, S. K., and Merzhanov, A. G., Nonuniqueness of stable regimes during combustion of powder mixture of Zr and C in hydrogen. *Fizika Fizika Goreniia i Vzryva,* **5,** 39 (1983).

Martynenko, V. M., and Borovinskaya, I. P., Some characteristic features of the combustion in system niobium–carbon. *In* "Combustion Processes in Chemical Engineering and Metallurgy (Russ.)" (A. G. Merzhanov, ed.). USSR Academy of Science, Chernogolovka, Russia, 1975, p. 127.

Maslov, V. M., Voyuev, S. I., Borovinskaya, I. P., and Merzhanov, A. G., The role of inert-diluent dispersion in gasless combustion. *Combust. Explos. Shock Waves,* **26,** 441 (1990).

Maslov, V. M., Borovinskaya, I. P., and Ziatdinov, M. K., Combustion of the systems niobium–aluminium and niobium–germanium. *Combust. Explos. Shock Waves,* **15,** 41 (1979).

Maslov, V. M., Borovinskaya, I. P., and Merzhanov, A. G., Problem of the mechanism of gasless combustion. *Combust. Explos. Shock Waves,* **12,** 631 (1976).

Mason, W., and Wheeler, R. V., The uniform movement during the propagation of flame. *J. Chem. Soc.,* **CXI,** 1044 (1917).

Matkowsky, B. J., and Sivashinsky, G. I., Propagation of a pulsating reaction front in solid fuel combustion. *SIAM J. Appl. Math.,* **35,** 465 (1978).

Matsuzaki, Y., Fujioka, J., Minakata, S., and Miyamoto, Y., Fabrication of $MoSi_2$-SiC/TiAl functional gradient materials by gas-pressure combustion sintering process. *Proceedings of the 1st Int. Symposium on Functionally Gradient Materials,* Tokyo, 263 (1990).

Maupin, H. E., and Rawers, J. C., Metal-intermetallic composites formed by reaction-sintering elemental powders. *J. Mater. Sci. Lett.,* **12,** 540 (1993).

Mei, B., Wang, W., Yuan, R., and Fu, Z., Study of TiC/Ni_3Al composites prepared by combustion synthesis. *Int. J. SHS,* **3,** 79 (1994).

Mei, B., Yuan, R., and Duan, X., Investigation of Ni_3Al-matrix composites strengthened by TiC. *J. Mater. Res.,* **8,** 2830 (1993).

Mei, B., Yuan, R., and Duan, X., Self-propagating high-temperature synthesis of MoB_2. *Int. J. SHS,* **1,** 421 (1992).

Merzhanov, A. G., History of and new developments in SHS. *Ceram. Int.* **21,** 371 (1995).

Merzhanov, A. G., Combustion processes that synthesize materials. Paper presented at AMPT'93 International Conference on Advances in Materials and Processing Technology, Dublin, Ireland (1993a).

Merzhanov, A. G., Theory and practice of SHS: Worldwide state of the art and the newest results. *Int. J. SHS,* **2,** 113 (1993b).

Merzhanov, A. G., Self-propagating high-temperature synthesis and powder metallurgy: Unity of goals and competition of principles. *In* "Particulate Materials and Processes: Advances in Powder Metallurgy and Particulate Materials." Metal Powder and Industries Federation, Princeton, NJ, 1992, p. 341.

Merzhanov, A. G., Advanced SHS ceramics: Today and tomorrow morning. Invited paper presented at International Symposium devoted to the 100th Anniversary of Ceramic Society of Japan, Yokohma (1991).

Merzhanov, A. G., Self-propagating high-temperature synthesis: Twenty years of search and findings. *In* "Combustion and Plasma Synthesis of High-Temperature Materials" (Z. A. Munir and J. B. Holt, eds.). VCH Publishers, New York, 1990a, p. 1.

Merzhanov, A. G., Self-propagating high-temperature synthesis of ceramic (oxide) superconductors. *In* "Ceramic Transactions: Superconductivity and Ceramic Superconductors" (K. M. Nair and E. A. Giess, eds.). American Ceramic Society, Westerville, OH, 1990b, p. 519.

Merzhanov, A. G., Self-propagating high-temperature synthesis. *In* "Current Topics in Physical Chemistry (Russ.)" (Ya. M. Kolotyrkin, ed.). Khimiya, Moscow, 1983, p. 8.

Merzhanov, A. G., SHS-process: Combustion theory and practice. *Archivum Combustionis,* **1,** 24 (1981).

Merzhanov, A. G., New elementary models of the second kind. *Dokl. Phys. Chem.,* **223,** 430 (1977).

Merzhanov, A. G., and Borovinskaya, I. P., Self-propagating high-temperature synthesis of refractory inorganic compounds. *Dokl. Chem.,* **204,** 429 (1972).

Merzhanov, A. G., and Khaikin, B. I., Theory of combustion waves in homogeneous. *Prog. Energy Combust. Sci.,* **14,** 1 (1988).

Merzhanov, A. G., and Rogachev, A. S., Structural macrokinetics of SHS processes. *Pure Appl. Chem.,* **64,** 941 (1992).

Merzhanov, A. G., and Yukhvid, V. I., The self-propagating high temperature synthesis in the field of centrifugal forces. *Proceedings of the First US–Japanese Workshop on Combustion Synthesis,* Tokyo, Japan, 1 (1990).

Merzhanov, A. G., Borovinskaya, I. P., Khomenko, I. O., Mukasyan, A. S., Ponomarev, V. I., Rogachev, A. S., and Shkiro, V. M., Dynamics of phase formation during SHS processes. *Ann. Chimie,* **20,** 123 (1995).

Merzhanov, A. G., Borovinskaya, I. P., Ponomarev, V. I., Khomenko, I. O., Zanevskii, Y. V., Chernenko, S. P., Smykov, L. P., and Cheremukhina, G. A., Dynamic x-ray study on phase formation in the course of SHS. *Phys. Dokl.,* **328,** 11 (1993).

Merzhanov, A. G., Rogachev, A. S., Mukasyan, A. S., and Khusid, B. M., Macrokinetics of structural transformation during the gasless combustion of a titanium and carbon powder mixture. *Combust. Explos. Shock Waves,* **26,** 92 (1990a).

Merzhanov, A. G., Rogachev, A. S., Mukasyan, A. S., Khusid, B. M., Borovinskaya, I. P., and Khina, B. B., The role of gas-phase transport in combustion of tantalum–carbon system. *J. Eng. Phys. Thermophys.,* **59,** 809 (1990b).

Merzhanov, A. G., Borovinskaya, I. P., Yukhvid, V. I., and Ratnikov, V. I., New production methods of high temperature materials based on combustion. *In* "Scientific Principles of Material Science." Nauka, Moscow, 1981, p. 193.

Merzhanov, A. G., Yukhvid, V. I., and Borovinskaya, I. P., Self-propagating high-temperature synthesis of cast inorganic refractory compounds. *Dokl. Chem.,* **255,** 503 (1980).

Merzhanov, A. G., Borovinskaya, I. P., and Volodin, Y. E., Combustion of porous metallic samples in nitrogen. *Dokl. Phys. Chem.,* **206,** 833 (1972).

Merzhanov, A. G., Shkiro, V. M., and Borovinskaya, I. P., Synthesis of refractory inorganic compounds. *Izvest. Bull.* **10,** Certificate 255221. (1971). (See also French Patent 2088668, 1972; U.S. Patent 3726643, 1973; U.K. Patent 1321084, 1974; Japanese Patent 1098839, 1982.)

Meyers, M. A., Yu, L.-H., and Vecchio, K. S., Shock synthesis of silicides—II. Thermodynamics and kinetics. *Acta Metall. Mater.,* **42,** 715 (1994).

Meyers, M. A., LaSalvia, J. C., Meyer, L. W., Hoke, D., and Niiler, A., Reaction Synthesis/Dynamic Compuction of Titanium Carbide and Titanium Diboride. *J. de Physique IV (Colloque),* **1,** 123 (1991).

Michelson, V. A., *In* "Collected Works (Russ.)." Novyi Agronom, Moscow, 1930, vol. 1, p. 56.

Miyamoto, Y., Tanihata, K., Matsuzaki, Y., and Ma, X., HIP in SHS technology. *Int. J. SHS,* **1,** 147 (1992).

Miyamoto, Y., Nakanishi, H., Tanaka, I., Okamoto, T., and Yamada, O., Processing study for the functionally gradient material TiC-Ni by the gas-pressure combustion sintering. *Proceedings of the First US–Japanese Workshop on Combustion Synthesis,* Tokyo, Japan, 173 (1990b).

Miyamoto, Y., Takahura, T., Tanihata, K., Tanaka, I., Yamada, O., Saito, M., and Takahashi, H., Processing study for TiB_2-Ni FGM by gas-pressure combustion sintering. *Proceedings of the 1st International Symposium on FGMs,* Tokyo, Japan, 169 (1990b).

Miyamoto, Y., Koizumi, M., and Yamada, O., High-pressure self-combustion sintering for ceramics. *J. Am. Ceram. Soc.*, **67,** C224 (1984).

Molodetskaya, I. E., Pisarskii, V. P., and Ulanova, O. O., Effect of the parameters of the starting Zn-S mixture on the structure of ZnS synthesized in a combustion wave. *Combust. Explos. Shock Waves,* **28,** 385 (1992).

Molokov, I. V., and Mukasyan, A. S., Explosive treatment of SHS gas–solid systems. *Int. J. SHS,* **1,** 155 (1992).

Moore, J. J., Combustion synthesis of ceramic-metal composite materials in microgravity. *Proceedings of the Third International Microgravity Workshop,* Cleveland, OH, 165 (1995).

Moore, J. J., and Feng, H. J., Combustion synthesis of advanced materials. *Prog. Mater. Sci.,* **39,** 243 (1995).

Moore, J. J., Feng, H. J., Hunter, K. R., and Wirth, D. G., *Proceedings of the Second International Microgravity Combustion Workshop,* Cleveland, OH, 157 (1992).

Muchnik, S. V., Formation of nickel phosphides under combustion conditions. *Izv. Akad. Nauk SSSR, Nearg. Mater.,* **20,** 158 (1984).

Muchnik, S. V., Lomnitskaya, Y. F., Chernogorenko, V. B., and Lynchak, K. A., Interaction under combustion conditions in copper-zirconium-phosphorus mixtures. *Sov. Powd. Metall.,* **32,** 865 (1993).

Mukasyan, A. S., Structure- and phase-formation of nitrides in SHS processes. D.Sc. Dissertation, Institute of Structural Macrokinetics, Russian Academy of Science (1994).

Mukasyan, A. S., Characteristics and mechanism of silicon and boron combustion in nitrogen." Ph.D. Dissertation, Institute of Chemical Physics, USSR Academy of Science (1986).

Mukasyan, A. S., and Borovinskaya, I. P., Structure formation in SHS nitrides. *Int. J. SHS,* **1,** 55 (1992).

Mukasyan, A. S., Blinov, M. Y., Borovinskaya, I. P., and Merzhanov, A. G., Some preparation aspects of nitrogen ceramics by direct SHS methods. *Proceedings of the International Conference Engineering Ceramics,* Smolenice Castle, Czechoslovakia, 161 (1989).

Mukasyan, A. S., Khomenko, I. O., and Ponomarev, V. I., About nonuniqueness of combustion modes in the heterogeneous systems. *Combust. Sci. Tech.,* **128,** 215 (1977a).

Mukasyan, A. S., Pelekh, A. E., Varma, A., and Rogachev, A. S., The effects of gravity on combustion synthesis in heterogeneous gasless systems. *AIAA J,* **35,** 1 (1997b).

Mukasyan, A. S., Hwang, S., Rogachev, A. S., Sytchev, A. E., Merzhanov, A. G., and Varma, A., Combustion wave microstructure in heterogeneous gasless systems. *Combust. Sci. Tech.,* **115,** 335 (1996).

Mukasyan, A. S., Merzhanov, A. G., Martynenko, V. M., Borovinskaya, I. P., and Blinov, M. Y., Mechanism and principles of silicon combustion in nitrogen. *Combust. Explos. Shock Waves,* **22,** 534 (1986).

Munir, Z. A., and Anselmi-Tamburini, U., Self-propagating exothermic reactions: The synthesis of high-temperature materials by combustion. *Mater. Sci. Reports,* **3,** 277 (1989).

Munir, Z. A., and Holt, J. B., The combustion synthesis of refractory nitrides. Part 1: Theoretical analysis. *J. Mater. Sci.,* **22,** 710 (1987).

Munir, Z. A., and Lai, W., The SHS diagram for TiC. *Combust. Sci. Tech.,* **128,** 215 (1977a).

Munir, Z. A., and Sata, N., SHS diagrams: Theoretical analysis and experimental observations. *Int. J. SHS,* **1,** 355 (1992).

Naiborodenko, Y. S., and Itin, V. I., Gasless combustion of mixtures of metal powders. I Mechanism and details. *Combust. Explos. Shock Waves,* **11,** 293 (1975a).

Naiborodenko, Y. S., and Itin, V. I., Gasless combustion of mixtures of metal powders. II Effect of mixture composition of the combustion rate and the phase composition of the products. *Combust. Explos. Shock Waves,* **11,** 626 (1975b).

Naiborodenko, Y. S., Lavrenchuk, G. V., and Filatov, V. M., Self-propagating high-temperature synthesis of aluminides. *Sov. Powd. Metall.,* **21,** 909 (1982).

Naiborodenko, Y. S., Itin, V. I., and Savitskii, K. V., Reactions at phase boundaries and their effects on the sintering process—I. Exothermic effects in powder sintering. *Sov. Powd. Metall.*, **7,** 562 (1970).

Naiborodenko, Y. S., Itin, V. I., and Savitskii, K. V., Exothermic effects during sintering of a mixture of nickel and aluminium powders. *Sov. Phys. J.*, **11,** 19 (1968).

Nekrasov, E. A., Tkachenko, V. N., and Zakirov, A. E., Diffusive combustion of multicomponent gasless systems forming multi-phase peroducts. *Combust. Sci. Tech.*, **91,** 207 (1993).

Nekrasov, E. A., Smolyakov, V. K., and Maksimov, Y. M., Mathematical model for the titanium–carbon system combustion. *Combust. Explos. Shock Waves,* **17,** 513 (1981).

Nekrasov, E. A., Maksimov, Y. M., Ziatdinov, M. K., and Shteinberg, A. S., Effect of capillary spreading on combustion-wave propagation in gas-free system. *Combust. Explos. Shock Waves,* **5,** 575 (1978).

Niiler, A., Kecskes, L. J., and Kottke, T., Consolidation of combustion synthesised materials by explosive compaction," *Proceedings of the First US–Japanese Workshop on Combustion Synthesis,* Tokyo, Japan, 53 (1990).

Nishida, T., and Urabe, K., TiC ceramic prepared by SHS/HIP processing. *Int. J. SHS,* **1,** 566 (1992).

Novikov, N. P., Borovinskaya, I. P., and Merzhanov, A. G., Dependence of the product composition and combustion wave as a function of the green mixture composition in the metal–boron systems. *Fizika Gorenia I Vzriva,* 201 (1974).

Novozilov, B. V., Non-linear SHS phenomena: Experiments, theory, numerical modeling. *Pure Appl. Chem.,* **64,** 955 (1992).

Novozilov, B. V., The rate of propagation of the front of an exothermic reaction in a condensed phase. *Phys. Dokl.,* **141,** 836 (1961).

Odawara, O., SHS technology for large composite pipes. *Int. J. SHS,* **1,** 160 (1992).

Odawara, O., Long ceramic-lined pipes produced by a centrifugal-thermite process." *J. Am. Ceram. Soc.,* **73,** 629 (1990).

Odawara, O., Method for providing ceramic lining to a hollow body by thermite reaction." U.S. Patent 4363832 (1982).

Odawara, O., and Ikeuchi, J., Ceramic composite pipes produced by a centrifugal-exothermic process. *J. Am. Ceram. Soc.,* **69,** C80 (1986).

Odawara, O., Mori, K., Tanji, A., and Yoda, S., Thermite reaction in a short-time microgravity environment. *J. Mater. Syn. Process.* **1,** 203 (1993).

Ohyanagi, M., Koizumi, M., Tanihata, K., Miyamoto, Y., Yamada, O., Matsubara, I., and Yamashitaa, H., Production of superconducting NbN thin plate and wire by the self-propagating high-temperature synthesis method. *J. Mater. Sci. Lett.,* **12,** 500 (1993).

Okolovich, E. V., Merzhanov, A. G., Khaikin, B. I., and Shkadinskii, K. G., Propagation of the combustion zone in melting condensed mixtures. *Combust. Explos. Shock Waves,* **13,** 264 (1977).

Orru', R., Simoncini, B., Virdis, P. F., and Cao, G., Further studies on a centrifugal SHS process for coating preparation and structure formation in thermite reactions. *Int. J. SHS,* **4,** 137 (1995).

Osipov, E. Y., Levashov, Y. A., Chernyshev, V. N., Merzhanov, A. G., and Borovinskaya, I. P., Prospects for simultaneous use of vacuum-performed SHS processes and various hot rolling techniques for production of semifinished and finished items of ceramometallic or intermetallic composites. *Int. J. SHS,* **1,** 314 (1992).

Padyukov, K. L., and Levashov, E. A., Self-propagating high-temperature synthesis: a new method for production of diamond-containing materials. *Diamond Related Mater.,* **2,** 207 (1993).

Padyukov, K. L., Kost, A. G., Levashov, E. A., Borovinskaya, I. P., and Bogatov, Y. V., Production regularities, structure, and properties of diamond-containing and composite materials. *Int. J. SHS,* **1,** 443 (1992a).

Padyukov, K. L., Levashov, E. A., Borovinskaya, I. P., and Kost, A. G., Specific features of the behavior of synthetic diamond in a self-propagating high-temperature synthesis (SHS) combustion wave. *J. Eng. Phys. Thermophys.,* **63,** 1107 (1992b).

Padyukov, K. L., Levashov, E. A., Kost, A. G., and Borovinskaya, I. P., SHS: A new fabrication method for diamond-containing ceramics. *Indust. Diamond Rev.*, **5,** 255 (1992c).

Pampuch, R., Stobierski, L., Lis, J., and Raczka, M., Solid combustion synthesis of β SiC powders. *Mater. Res. Bull.*, **22,** 1225 (1987).

Pampuch, R., Stobierski, L., and Lis, J., Synthesis of sinterable β-SiC Powders by solid combustion method. *J. Am. Ceram. Soc.*, **72,** 1434 (1989).

Petrovskii, V. Y., Gorvits, E. I., Borovinskaya, I. P., and Martinenko, V. M., SHS silicon nitride: An attractive powder for dielectric ceramic production. *In* "Problems of Technological Combustion." Chernogolovka, 5 (1981).

Philpot, K. A., Munir, Z. A., and Holt, J. B., An investigation of the synthesis of nickel aluminides through gasless combustion. *J. Mater. Sci.*, **22,** 159 (1987).

Pityulin, A. N., Sytschev, A. E., Rogachev, A. S., and Merzhanov, A. G., One-stage production of functionally gradient materials of the metal-hard alloy type by SHS-compaction. *Proceedings of the 3rd International Symposium on Structural and Functional Gradient Materials (Book of Abstracts)*, Lausanne, Switzerland, 25 (1994).

Pityulin, A. N., Bogatov, Y. V., and Rogachev, A. S., Gradient hard alloys. *Int. J. SHS,* **1,** 111 (1992).

Pityulin, A. N., Shcherbakov, V. A., Borovinskaya, I. P., and Merzhanov, A. G., Laws and mechanism of diffusional surface burning of metals. *Combust. Explos. Shock Waves,* **15,** 432 (1979).

Podlesov, V. V., Radugin, A. V., Stolin, A. M., and Merzhanov, A. G., Technological basis of SHS extrusion. *J. Eng. Phys. Thermophys.*, **63,** 1065 (1992a).

Podlesov, V. V., Stolin, A. M., and Merzhanov, A. G., SHS extrusion of electrode materials and their application for electric-spark alloying of steel surfaces. *J. Eng. Phys. Thermophys.*, **63,** 1156 (1992b).

Prausnitz, J. M., Lichtenthaler, R. N., and de Azevedo, E. G., "Molecular Thermodynamics of Fluid-Phase Equilibria." Prentice-Hall, Englewood Cliffs, NJ, 1986.

Puszynski, J., Degreve, J., and Hlavachek, V., Modeling of exothermic solid-solid noncatalytic reactions. *Ind. Engng Chem. Res.*, **26,** 1424 (1987).

Rabin, B. H., and Wright, R. N., Microstructure and properties of iron aluminides produced from elemental powders. *Int. J. SHS,* **1,** 305 (1992).

Rabin, B. H., and Wright, R. N., Synthesis of iron aluminides from elemental powders: reaction mechanisms and densification behavior." *Metall. Trans. A,* **22A,** 277 (1991).

Rabin, B. H., Korth, G. E., and Williamson, R. L., Fabrication of TiC-Al_2O_3 composites by combustion synthesis and subsequent dynamic consolidation. *Int. J. SHS,* **1,** 336 (1992a).

Rabin, B. H., Wright, R. N., Knibloe, J. R., Raman, R. V., and Rale, S. V., Reaction processing of iron aluminides. *Mater. Sci. Eng.*, **A153,** 706 (1992b).

Rabin, B. H., Bose, A., and German, R. M., Combustion synthesis of nickel aluminides. *In* "Combustion and Plasma Synthesis of High-Temperature Materials" (Z. A. Munir and J. B. Holt, eds.). VCH Publishers, New York, 1990, p. 114.

Raman, R. V., Rele, S. V., Poland, S., LaSalvia, J., Meyers, M. A., and Niiler, A. R., The one-step synthesis of dense titanium-carbide tiles. *J. Metals,* **47,** 23 (1995).

Rawers, J. C., Wrzesinski, W. R., Roub, E. K., and Brown, R. R., TiAl-SiC composites prepared by high temperature synthesis. *Mater. Sci. Tech.*, **6,** 187 (1990).

Rice, R. W., Microstructural aspects of fabricating bodies by self-propagating synthesis. *J. Mater. Sci.*, **26,** 6533 (1991).

Rice, R. W., Richardson, G. Y., Kunetz, J. M., Schroeter, T., and McDonough, W. J., Effects of self-propagating synthesis reactant compact character on ignition, propagation and microstructure. *Adv. Ceramic Mater.*, **2,** 222 (1987).

Rice, R. W., McDonough, W. J., Richardson, G. Y., Kunetz, J. M., Schroeter, T., Hot-rolling of ceramics using self-propagating synthesis. *Ceram. Eng. Sci. Proc.*, **7,** 751 (1986).

Rogachev, A. S., D.Sc. Dissertation, Institue of Structural Macrokinetics, Russian Academy of Science (1995).

Rogachev, A. S., Shugaev, V. A., Khomenko, I. A., Varma, A., and Kachelmyer, C., On the mechanism of structure formation during combustion synthesis of titanium silicides. *Combust. Sci. Tech.*, **109,** 53 (1995).

Rogachev, A. S., Khomenko, I. O., Varma, A., Merzhanov, A. G., and Ponomarev, V. I., The mechanism of self-propagating high-temperature synthesis of nickel aluminides, Part II: Crystal structure formation in a combustion wave. *Int. J. SHS,* **3,** 239 (1994a).

Rogachev, A. S., Shugaev, V. A., Kachelmyer, C. R., and Varma, A., Mechanisms of structure formation during combustion synthesis of materials. *Chem. Eng. Sci.,* **49,** 4949 (1994b).

Rogachev, A. S., Varma, A., and Merzhanov, A. G., The mechanism of self-propagating high-temperature synthesis of nickel aluminides, Part I: Formation of the product microstructure in a combustion wave. *Int. J. SHS,* **2,** 25 (1993).

Rogachev, A. S., Shkiro, V. M., Chausskaya, I. D., and Shvetsov, M. V., Gasless combustion in titanium–carbon–nickel system. *Combust. Explos. Shock Waves,* **24,** 720 (1988).

Rogachev, A. S., Mukasyan, A. S., and Merzhanov, A. G., Structural transitions in the gasless combustion of titanium-carbon and titanium boron systems. *Dokl. Phys. Chem.,* **297,** 1240 (1987).

Rozenkranz, R., Frommeyer, G., and Smarsly, W., Microstructures and properties of high melting point intermetallic Ti_5Si_3 and $TiSi_2$ compounds. *Mater. Sci. Eng.,* **A152,** 288 (1992).

Saidi, A., Chrysanthou, A., Wood, J. V., and Kellie, J. L. F., Characteristics of the combustion synthesis of TiC and Fe-TiC composites. *J. Mater. Sci.,* **29,** 4993 (1994).

Samsonov, G. V., "Refractory Transition Metal Compounds; High Temperature Cermets. Academic Press, New York, 1964.

Samsonov, G. V., and Vinitskii, I. M., Handbook of Refractory Compounds. IFI/Plenum, New York, 1980.

Sarkisyan, A. R., Dolukhanyan, S. K., and Borovinskaya, I. P., Self-propagating high-temperature synthesis of transition metal silicides. *Sov. Powd. Metall.,* **17,** 424 (1978).

Sata, N., SHS-FGM studies on the combustion synthesis of fine composites. *Int. J. SHS,* **1,** 590 (1992).

Sata, N., Nagata, K., Yanagisawa, N., Asano, O., Sanada, N., Hirano, T., and Teraki, J., Research and development on functionally gradient materials by using a SHS process. *Proceedings of the First US–Japanese Workshop on Combustion Synthesis,* Tokyo, Japan, 139 (1990a).

Sata, N., Sanada, N., Hirano, T., and Niino, M., Fabrication of a functionally gradient material by using a self-propagating reaction process. *In* "Combustion and Plasma Synthesis of High-Temperature Materials" (Z. A. Munir and J. B. Holt, eds.). VCH Publishers, New York, 1990b, p. 195.

Semenov, N. N., Zur theorie des verbrennungsprozesses. *Zhur. Fiz. B.,* **42,** 571 (1929).

Shah, D. M., Berczik, D., Anton, D. L., and Hecht, R., Appraisal of other silicides as structural materials. *Mater. Sci. Eng.,* **A155,** 45 (1992).

Sharipova, N. S., Ermolaev, V. N., and Kahn, C. G., Study by electron microscopy, of processes occurring at boundary between Cr_2O_3 and Al. *Combust. Explos. Shock Waves,* **28,** 151 (1992).

Shcherbakov, V. A., Gryadunov, A. N., and Shteinberg, A. S., Macrokinetics of the process of SHS compaction. *J. Eng. Phys. Thermophys.,* **63,** 1111 (1992).

Shcherbakov, V. A., and Pityulin, A. N., Unique features of combustion of the system Ti-C-B. *Combust. Explos. Shock Waves,* **19,** 631 (1983).

Shingu, P. H., Ishihara, K. N., Ghonome, F., Hayakawa, T., Abe, M., and Taguchi, K., Solid state synthesis of TiAl by use of pseudo HIP. *Proceedings of the First US–Japanese Workshop on Combustion Synthesis,* Tokyo, Japan, 65 (1990).

Shirayev, A. A., Yuranov, I., and Kashireninov, O., Thermodynamics of high speed combustion processes: Some particular features. *Proceedings of the Joint meeting of the Russian and Japanese Combustion Section,* Chernogolovka, Russia, 158 (1993).

Shishkina, T. N., Podlesov, V. V., and Stolin, A. M., Microstructure and properties of extruded SHS materials. *J. Eng. Phys. Thermophys.,* **63,** 1082 (1992).

Shkadinskii, K. G., Shkadiskaya, G. V., Matkowsky, B. J., and Volpert, V. A., Combustion synthesis of a porous layer. *Combust. Sci. Tech.*, **88,** 247 (1992a).

Shkadinskii, K. G., Shkadiskaya, G. V., Matkowsky, B. J., and Volpert, V. A., Self-compaction or expansion in combustion synthesis of porous materials. *Combust. Sci. Tech.*, **88,** 271 (1992b).

Shkadinskii, K. G., Khaikin, B. I., and Merzhanov, A. G., Propagation of a pulsating exothermic reaction front in the condensed phase. *Combust. Explos. Shock Waves,* 15 (1971).

Shkiro, V. M., and Borovinskaya, I. P., Capillary flow of liquid metal during combustion of titanium mixtures with carbon. *Combust. Explos. Shock Waves,* **12,** 828 (1976).

Shkiro, V. M., and Borovinskaya, I. P., Study of the titanium and carbon mixtures combustion. *In* "Combustion Processes in Chemical Engineering and Metallurgy (Russ.)" (A. G. Merzhanov, ed.). USSR Academy of Science, Chernogolovka, Russia, 1975, p. 253.

Shkiro, V. M., Nersisyan, G. A., Borovinskaya, I. P., Merzhanov, A. G., and Shekhtman, V. S., Preparation of tantalum carbides by self-propagating high-temperature synthesis. *Sov. Powd. Metall.*, **18,** 227 (1979).

Shkiro, V. M., Nersisyan, G. A., and Borovinskaya, I. P., Principles of combustion of tantalum–carbon mixtures. *Combust. Explos. Shock Waves,* **14,** 455 (1978).

SHS Bibliography, *Int. J. SHS,* **5,** 309 (1996).

Shteinberg, A. S., Scherbakov, V. A., Martynov, V. V., Mukhoyan, M. Z., and Merzhanov, A. G., Self-propagating high-temperature synthesis of high-porosity materials under zero-g conditions. *Phys. Dokl.*, **36,** 385 (1991).

Shtessel, E. A., Kurylev, M. V., and Merzhanov, A. G., Features of self-propagating processes in the reaction of aluminum with iodine. *Dokl. Phys. Chem.*, **288,** 529 (1986).

Shugaev, V. A., Rogachev, A. S., and Ponomarev, V. I., A model for structure formation in SHS systems. *Int. J. SHS,* **1,** 72 (1992a).

Shugaev, V. A., Rogachev, A. S., Ponomarev, V. I., and Merzhanov, A. G., Structurization of products from the interaction of boron with niobium when subjected to rapid heating. *Dokl. Phys. Chem.*, **314,** 348 (1992b).

Skibska, M., Szulc, A., Mukasyan, A. S., and Rogachev, A. S., Microstructural peculiarities of silicon nitride formation under high nitrogen pressures. Part I: The influence of initial Si particle size distribution on Si_3N_4 SHS morphology. *Int. J. SHS,* **2,** 39 (1993a).

Skibska, M., Szulc, A., Mukasyan, A. S., Shugaev, V. A., and Shiryaev, A. A., Microstructural peculiarities of silicon nitride formation under high nitrogen pressures. Part II: The effect of nitrogen pressure on SHS Si_3N_4 morphology and phase composition. *Int. J. SHS,* **2,** 247 (1993b).

Storms, E. K., "The Refractory Carbides." Academic Press, New York, 1967.

Strutt, A. J., Vecchio, K. S., Yu, L.-H., and Meyers, M. A., Shock synthesis of nickel aluminides. *AIP Conf. Proc.*, **309,** 1259 (1994).

Subrahmanyam, J., Combustion synthesis of $MoSi_2$-Mo_5Si_3 composites. *J. Mater. Res.*, **9,** 2620 (1994).

Subrahmanyam, J., Vijaykumar, M., and Ranganath, S., Thermochemistry of self propagating high temperature synthesis of titanium diboride composites. *Metals Mater. Processes,* **1,** 105 (1989).

Tabachenko, A. N., and Kryuchkova, G. G., Self-propagating high-temperature synthesis of composite materials. The melting compounds (TiC, TiB_2)—intermetallides, their structure and properties. *J. Eng. Phys. Thermophys.*, **65,** 1026 (1993).

Taneoka, Y., Odawara, O., and Kaieda, Y., Combustion synthesis of the titanium–aluminum–boron system. *J. Am. Ceram. Soc.*, **72,** 1047 (1989).

Tanihata, K., Miyamoto, Y., Matsushita, K., Ma, X., Kawasaki, A., Watanabe, R., and Hirano, K., Fabrication of Cr_3C_2/Ni functionally gradient materials by gas-pressure combustion sintering. *Proceedings of the 2nd. Int. Symp. on FGMs,* San Francisco (1992).

Thadani, N. N., Shock-induced chemical reactions and synthesis of materials. *Prog. Mater. Sci.*, **37,** 117 (1993).

Trambukis, J., and Munir, Z. A., Effect of particle dispersion on the mechanism of combustion synthesis of titanium silicide. *J. Am. Ceram. Soc.*, **73,** 1240 (1990).

Urabe, K., Miyamoto, Y., Koizumi, M., and Ikawa, H., Microstructure of TiB_2 sintered by the self-combustion method. *In* "Combustion and Plasma Synthesis of High-Temperature Materials" (Z. A. Munir and J. B. Holt, eds.). VCH Publishers, New York, 1990, p. 281.

Vadchenko, S. G., Gordopolov, A. Y., and Mukasyan, A. S., The role of gas- and solid-phase conduction mechanisms in propagation of heterogeneous combustion wave. *Phys. Dokl.*, **42,** 288 (1997).

Vadchenko, S. G., Merzhanov, A. G., Mukasyan, A. S., and Sytchev, A. E., Influence of uniaxial loading on the macrokinetics of gasless systems combustion. *Phys. Dokl.*, **337,** 618 (1994).

Vadchenko, S. G., Bulaev, A. M., Gal'chenko, Y. A., and Merzhanov, A. G., Interaction mechanism in laminar bimetal nickel-titanium and nickel-aluminium systems. *Combust. Explos. Shock Waves,* **23,** 706 (1987).

Vadchenko, S. G., Grigoriev, Y. M., and Merzhanov, A. G., The kinetics of high-temperature tantalum nitriding. *Bull. Akad. Nauk SSSR, Metals,* **5,** 223 (1980).

Vadchenko, S. G., Grigoriev, Y. M., and Merzhanov, A. G., Investigation of the mechanism of the ignition and combustion of the system Ti+C, Zr+C, by an electrothermographic method. *Combust. Explos. Shock Waves,* **12,** 606 (1976).

Varma, A., and Lebrat, J.-P., Combustion synthesis of advanced materials. *Chem. Eng. Sci.*, **47,** 2179 (1992).

Vecchio, K. S., Yu, L.-H., and Meyers, M. A., Shock synthesis of silicides—I. Experimentation and microstructural evolution. *Acta Metall. Mater.*, **42,** 701 (1994).

Vecchio, K. S., LaSalvia, J. C., Meyers, M. A., and Gray, G. T., Microstructural characterization of self-propagating high-temperature synthesis: Dynamically compacted and hot-pressed titanium carbides. *Metall. Trans. A,* **23A,** 87 (1992).

Volpe, B. M., and Evstigneev, V. V., Structure formation in the SHS-system titanium–aluminium–carbon. *Combust. Explos. Shock Waves,* **28,** 173 (1992).

Walton, J. D., and Poulos, N. E., Cermets from thermite reactions. *J. Am. Ceram. Soc.*, **42,** 40 (1959).

Wang, L., Wixom, M. R., and Tompson, L. T., Structural and mechanical properties of TiB_2 and TiC prepared by self-propagating high-temperature synthesis/dynamic compaction. *J. Mater. Sci.,* **29,** 534 (1994a).

Wang, L. L., Munir, Z. A., and Holt, J. B., The combustion synthesis of copper aluminides. *Metall. Mater. Trans. B,* **21B,** 567 (1990).

Wang, W., Mei, B., Fu, Z., and Yuan, R., Self-propagating high-temperature synthesis and densification of intermetallic compound-matrix composites (IMCs). *Int. J. SHS,* **2,** 183 (1993).

Wang, Z., Ge, C., and Chen, L., Fabrication of TiB_2-Cu composites and functionally gradient materials by GPCS. *Int. J. SHS,* **3,** 85 (1994b).

Wenning, L. A., Lebrat, J.-P., and Varma, A., Some observations on unstable self-propagating high-temperature synthesis of nickel aluminides. *J. Mater. Syn. Proc.,* **2,** 125 (1994).

Wiley, J. B., and Kaner, R. B., Rapid solid-state precursor synthesis of materials. *Science,* **255,** 1093 (1992).

Williams, F. A., "Combustion Theory." Addison-Wesley, Reading, MA, 1965.

Wong, J., Larson, E. M., and Holt, J. B., Time-resolved X-ray diffraction study of solid combustion reaction. *Science,* **249,** 1406 (1990).

Work, S. J., Yu, L. H., Thadhani, N. N., Meyers, M. A., Graham, R. A., and Hammetter, W. F., Shock-induced chemical synthesis of intermetallic compounds. *In* "Combustion and Plasma Synthesis of High-Temperature Materials" (Z. A. Munir and J. B. Holt, eds.). VCH Publishers, New York, 1990, p. 133.

Xiangfeng, M., Tanihata, K., and Miyamoto, Y., Gas-pressure combustion sintering and properties of Cr_3C_2 ceramic and its composite with TiC. *J. Ceram. Soc. Japan,* **100,** 605 (1992).

Yamada, O., Fabrication of fully dense composite materials by SHS under pressurized reactive-gas atmosphere. *J. Soc. Mater. Sci. Japan,* **43,** 1059 (1994).

Yamada, O., Miyamoto, Y., and Koizumi, M., High-pressure self-combustion sintering of titanium carbide. *J. Am. Ceram. Soc.,* **70,** C206 (1987).

Yamada, O., Miyamoto, Y., and Koizumi, M., Self-propagating high-temperature synthesis of the SiC. *J. Mater. Res.,* **1,** 275 (1986).

Yamada, O., Miyamoto, Y., and Koizumi, M., High pressure self-combustion sintering of silicon carbide. *Am. Ceram. Soc. Bull.,* **64,** 319 (1985).

Yanagisawa, N., Asano, O., Sata, N., and Sanada, N., Synthesis and properties of TiB_2-TiNi composite materials by SHS process. *Proceedings of the First US–Japanese Workshop on Combustion Synthesis,* Tokyo, Japan, 157 (1990).

Yi,. H. C., and Moore, J. J., The combustion synthesis of Ni-Ti shape memory alloys. *J. Metals,* **42,** 31 (1990).

Yi,. H. C., and Moore, J. J., Combustion synthesis of TiNi intermetallic compounds. Part 1: Determination of heat of fusion of TiNi and heat capacity of liquid TiNi. *J. Mater. Sci.,* **24,** 3449 (1989).

Yi,. H. C., Varma, A., Rogachev, A. S., and McGinn, P. J., Gravity-induced microstructural nonuniformities during combustion synthesis of intermetallic-ceramic composite materials. *Ind. Eng. Chem. Res.,* **35,** 2982 (1996).

Yukhvid, V. I., Modifications of SHS processes. *Pure Appl. Chem.,* **64,** 977 (1992).

Yukhvid, V. I., Kachin, A. R., and Zakharov, G. V., Centrifugal SHS surfacing of the refractory inorganic materials. *Int. J. SHS,* **3,** 321 (1994).

Yukhvid, V. I., Borovinskaya, I. P., and Merzhanov, A. G., Influence of pressure on the laws governing the combustion of molten heterogeneous systems. *Combust. Explos. Shock Waves,* **19,** 277 (1983).

Zavitsanos, P. D., Gebhardt, J. J., and Gatti, A., The use of self-propagating high-temperature synthesis of high-density titanium diboride. *In* "Combustion and Plasma Synthesis of High-Temperature Materials" (Z. A. Munir and J. B. Holt, eds.). VCH Publishers, New York, 1990, p. 170.

Zeldovich, Y. B., Theory for the limit of the quiet flame propagation. *J. Exper. Theor. Phys.,* **11,** 159 (1941).

Zeldovich, Y. B., and Frank-Kamenetskii, D. A., The theory of thermal propagation of flames. *Zh. Fiz. Khim.,* **12,** 100 (1938).

Zeldovich, Y. B., Barenblatt, G. I., Librovich, V. B., and Makhviladze, G. M., "Mathematic Theory of Combustion and Explosions" (D. H. McNeil, trans.). Consultant Bureau, New York, 1985.

Zenin, A. A., Merzhanov, A. G., and Nersisyan, G. A., Thermal wave structure in SHS processes (by the example of boride synthesis). *Combust. Explos. Shock Waves,* **17,** 63 (1981).

Zenin, A. A., Merzhanov, A. G., and Nersisyan, G. A., Structure of the heat wave in some self-propagating high-temperature processes. *Dokl. Phys. Chem.,* **250,** 83 (1980).

Zhang, X., Yin, W., and Guo, J., Exploration of combustion synthesis of TiNi intermetallic compound. *Int. J. SHS,* **4,** 301 (1995).